BATTERY DUAL STATE ESTIMATION

STRATEGY FOR TRACTION APPLICATION

IMPACT OF CHARGE PROFILE ON BATTERY FAST CHARGING AGING AND DUAL STATE ESTIMATION STRATEGY FOR TRACTION APPLICATIONS

BY

JOSIMAR DA SILVA DUQUE, MBA, B. Eng. Mechanical

A THESIS

SUBMITTED TO THE DEPARTMENT OF MECHANICAL ENGINEERING

AND THE SCHOOL OF GRADUATE STUDIES OF MCMASTER

UNIVERSITY IN PARTIAL FULFILMENT OF THE REQUIREMENTS FOR

THE DEGREE OF MASTER OF APPLIED SCIENCE

Master of Applied Science (2021)   McMaster University

(Mechanical Engineering)   Hamilton, Ontario, Canada

TITLE: Impact of Charge Profile on Battery Fast Charging

                    Aging and Dual State Estimation Strategy for Traction

                    Applications

AUTHOR: Josimar da Silva Duque

                    MBA, B. Eng. Mechanical

SUPERVISOR: Dr. Ali Emadi

NUMBER OF PAGES: xx, 162

To my family and friends, for all your support and trust.

Abstract

The fast-growing electric vehicles (EVs) market demands huge efforts from car manufacturers to develop and improve their current products' systems. A fast charge of the battery pack is one of the challenges encountered due to the battery limitations regarding behaviour and additional degradation when exposed to such a rough situation. In addition, the outcome of a study performed on a battery does not apply to others, especially if their chemistries are different. Hence, extensive testing is required to understand the influence of design decisions on the particular energy storage device to be implemented. Due to batteries' nonlinear behaviour that is highly dependent on external variables such as temperature, the dynamic load and aging, another defying task is the widely studied state of charge (SOC) estimation, commonly considered one of the most significant functions in a battery management system (BMS).

This thesis presents an extensive battery fast charging aging test study equipped with promising current charging profiles from published literature to minimize aging. Four charging protocols are carefully designed to charge the cell from 10 to 80% SOC within fifteen minutes and have their performances discussed. A dual state estimation algorithm is modelled to estimate the SOC with the assistance of a capacity state of health (SOHcap) estimation. Finally, the dual state estimation model is validated with the fast charging aging test data.

Acknowledgement

I would like to thank all people who showed their generosity and patience and say that without their help, I am not certain I would be able to accomplish this journey. First, to my good friend Daniel Barroso for the trust and faith in my competence, your indication for the program was indispensable. To my supervisor Dr. Ali Emadi, who gave me this one lifetime opportunity to study and grow as a professional in one of the best education institutions in the world, no word can retribute such kindness and consideration you always treated me.

Thank you to Dr. Phillip Kollmeyer for the mentoring and countless meetings sharing your wisdom and knowledge contributing to the presented thesis. Your patience and guidance influenced what I know in the Transportation Electrification field to this day.

To Dr. Saeid Habibi and Cam Fisher, thank you for providing the Battery Laboratory facility in Centre for Mechatronics and Hybrid Technologies at McMaster Automotive Resource Centre, where the tests performed impacted the accomplishment of this work.

Finally, a thank you to my good friends Fabricio Machado and Lucas Bruck and all other fellow students for the opportunity to be a part of this welcoming team that is always prompt to support each other.

Nomenclature

BC	Boost Charging
BCNP	Boost Charging with Negative Pulse
BCR	Boost Charging with Rest
BEVs	Battery Electric Vehicles
BMS	Battery Management System
CC	Constant Current
CCCCCV	Constant Current Constant Current Constant Voltage
CCCV	Constant Current Constant Voltage
CCCVCCCV	Constant Current Constant Voltage Constant Current Constant Voltage
CC-CVNP	Constant Current Constant Voltage with Negative Pulse
CD	Cold Derating
CI	Current Interrupt
CKF	Cubature Kalman Filter
CP	Constant Power
CPCV	Constant Power Constant Voltage
CTCV	Constant Temperature Constant Voltage
CVCCCV	Constant Voltage Constant Current Constant Voltage
DOE	Design of Experiment
DST	Dynamic Stress Test

EKF	Extended Kalman Filter
EKF/SVSF	Dual State Estimation Algorithm
EOL	End-of-Life
FUDRLS	Fast Upper-triangular and Diagonal Recursive Least Squares
GA	Genetic Algorithm
UKF	Unscented Kalman Filter
LCD	Linear Current Decay
MCC	Multistage Constant Current
MCH	Multistage Constant Heating
NE	Negative Electrode
NRI-CF	Normalized Resistance Increase - Capacity Fading Relationship
OPR	Overpotential Reserve
PC	Pulse Charging
PE	Positive Electrode
PSO	Particle Swarm Optimization
RTLS	Recursive Total Least Squares
SEI	Solid Electrolyte Interphase
SOC	State of Charge
SOGA	Single Objective Genetic Algorithm
SOH	State of Health
SOHcap	Capacity State of Health
SRC	Sinusoidal Ripple Current

SVSF   Smooth Variable Structure Filter

SVSF-VBL Smooth Variable Structure Filter with Variable Boundary Layer

UKF   Unscented Kalman Filter

UVP   Universal Voltage Protocol

VCD   Varying Current Decay

VFPC   Variable Frequency Pulse Charging

Content

List of Figures

List of Tables

Chapter 1

Introduction

1.1 Background and Motivation

The high output voltage and energy density place Lithium-ion battery as the principal means of rechargeable energy storage for portable devices. Recently, the demand for a faster charging time of batteries applied to these mobile devices such as electronics, electric vehicles, power tools, and even military equipment has been given increasing attention [1]. That is mainly driven by the electrification of transportation estimated to have battery electric vehicles (BEVs) representing about 60% of the automobile market by 2050 [2].

The acceptance of battery electric vehicles BEVs by potential customers is linked to the improvement of the battery's ability to compete with internal combustion engine vehicles (ICEs) concerning the charging time and the range anxiety, which is related to the driver's fear of having the battery depleted during his journey [3],[4],[5],[6]. Improving the battery charging time of a BEV to be equivalent to the refuelling time of an ICE would require a charging power of least 400kW [7]. Nevertheless, reaching such a high power is a challenge due to physical

constraints from the battery itself, charge stations and the electric grid infrastructure.

The BEV fleet available today is increasing fast, with new models surging from both the well-established car manufacturers and smaller players getting into the market. These new models' charging times, Table 1.1, are still not competitive with ICE vehicles and are dependent on the charge station power used and the battery pack size it carries. In addition, the fast charging (FC) time accounts for the first about 80% of the battery pack capacity and does not cover the other twenty percent of the remaining capacity that can last even longer than the FC.

Table 1.1: Battery electric vehicle fast charging times [8].

Vehicle	Battery Capacity [KWh]	Fast Charging Time [Min]
2019 CHEVROLET BOLT	60	**30**
2019 AUDI E-TRON	95	**60**
2019 BMW I3	42.2	**50**
2019 HONDA CLARITY EV	25.5	**30**
2019 HYUNDAI IONIQ EV	28	**33**
2019 HYUNDAI KONA EV	64	**75**
2019 JAGUAR I-PACE	90	**55**
2019 KIA SOUL EV	27	**46**
2019 KIA NIRO EV	64	**75**
2019 NISSAN LEAF	40	**60**
2019 NISSAN LEAF PLUS	64	**45**
2019 VOLKSWAGEN E-GOLF	35.8	**60**

Note: Charging time based on a level 3 50kW DC charge station.

Along with the charging time challenge, companies face other problems in composing an attractive and reliable product. States estimation of the energy storage system is one of them. That is because the batteries behave differently depending on external variables such as temperature gradient, current load and their state of health (SOH). The battery management system is responsible for providing crucial information through measurements and software for the control and protection of the storage unit. State of charge (SOC) and state of health are two estimations within the set BMS provides. SOC is the ratio of current flow integrated by the battery rated capacity, whereas SOH is the ratio of the metric used, capacity or impedance, for an aged battery and a new one [3].

The growing interest in fast-charging from industry has required the necessity of better understanding the charging process limits and the consequences different approaches bring to the battery life. The strong impact charging profile has on battery life, the pursuit for fast charging minimizing the large gap in time between the internal combustion vehicle refuel and electric vehicle charging, and the importance of providing a consistent state of charge estimation at the different stages of the battery life has motivated this work. Therefore, this thesis brings a fast charging aging study with promising current charging profiles from published literature and a dual state estimation strategy accounting for the capacity state of health (SOHcap) and state of charge (SOC).

1.2 Research Contributions

The work performed in the course of this thesis brings a vast data set with valuable information pertaining to battery aging prepared to be easily employed in the development of state of charge, health and power algorithms. Programs with the test schedules are written for the battery cycler and can be straightforwardly modified to continue the investigation of the influence fast charging profiles have on batteries.

To complete this work, new cabling of the channels for the purchased battery tester was built, and the battery laboratory facility improved with new cable trays installed. Also, fixtures for sixteen purchased cylindrical cell holders were built, contributing to future studies eliminating the need to assemble new fixtures and weld them on every cell's terminals tested. These efforts will benefit future researchers with ready to be used equipment.

1.3 Thesis Outline

This thesis contains a combination of experiments and modelling and is organized into seven chapters:

Chapter 1 addresses the motivation and contributions to future works.

Chapter 2 provides a review of battery charging methodologies and their influence on degradation minimization through the outcomes of their use in the literature.

Chapter 3 introduces a review of state estimation algorithms applied in the battery state of charge and state of health.

Chapter 4 describes the fast charging aging test design of experiment created with the four protocols designed to prevent battery aging. It also exposes the motivation of the features considered in their design.

Chapter 5 presents an overview of the dual state estimation modelling development with the strategies adopted in the model's conception.

Chapter 6 reveals the outcomes of the fast charging aging test to date with an analysis of the influence each designed charging profile had on capacity retention, battery temperature, internal resistance, and open circuit voltage curve drift across the battery life cycle. In a second part, the dual state estimation algorithm designed in Chapter 5 is validated with a series of simulations encompassing the SOC estimation robustness to sensor error simulating nine cases for a new and aged battery, robustness to initial SOC error, and SOC and SOH estimation over the battery life cycle.

Chapter 7 summarizes the work with a discussion about the outcomes of both experimental and simulation work, with the recommendation of future work to enrich the current analysis.

Chapter 2

Battery Charging Methodologies to Minimize Aging: State of the Art

The growing interest in fast-charging from industry has required the necessity of better understanding the charging process limits and the consequences different approaches bring to the battery life. The battery management system (BMS) is the most expensive system of an electric battery vehicle [9]; thus, extra attention shall be laid on its integrity.

Battery degradation occurs independently if the device is being utilized or not. The degradation magnitude is dictated by a combination of the way the battery is solicited and external factors such as temperature. For instance, positive and negative electrodes present different degradation mechanisms [10] and are responsible for the majority of the battery aging phenomena [2]. These mechanisms are originally caused by mechanical or chemical reactions inside the battery that can induce changes in the structure and chemical composition of the electrodes and electrolytes.

The battery charging methodology presents itself as extremely important in the battery's performance to minimize aging phenomenons. As demonstrated in

[11], charging current and voltage can distinctively affect different lithium-ion batteries' cycle life. Additionally, in general, high charging current has more impact on cell life than discharging currents. Therefore, this chapter brings a review of the charging profiles, Figure 2.1, studied in the literature aiming at battery aging minimization.
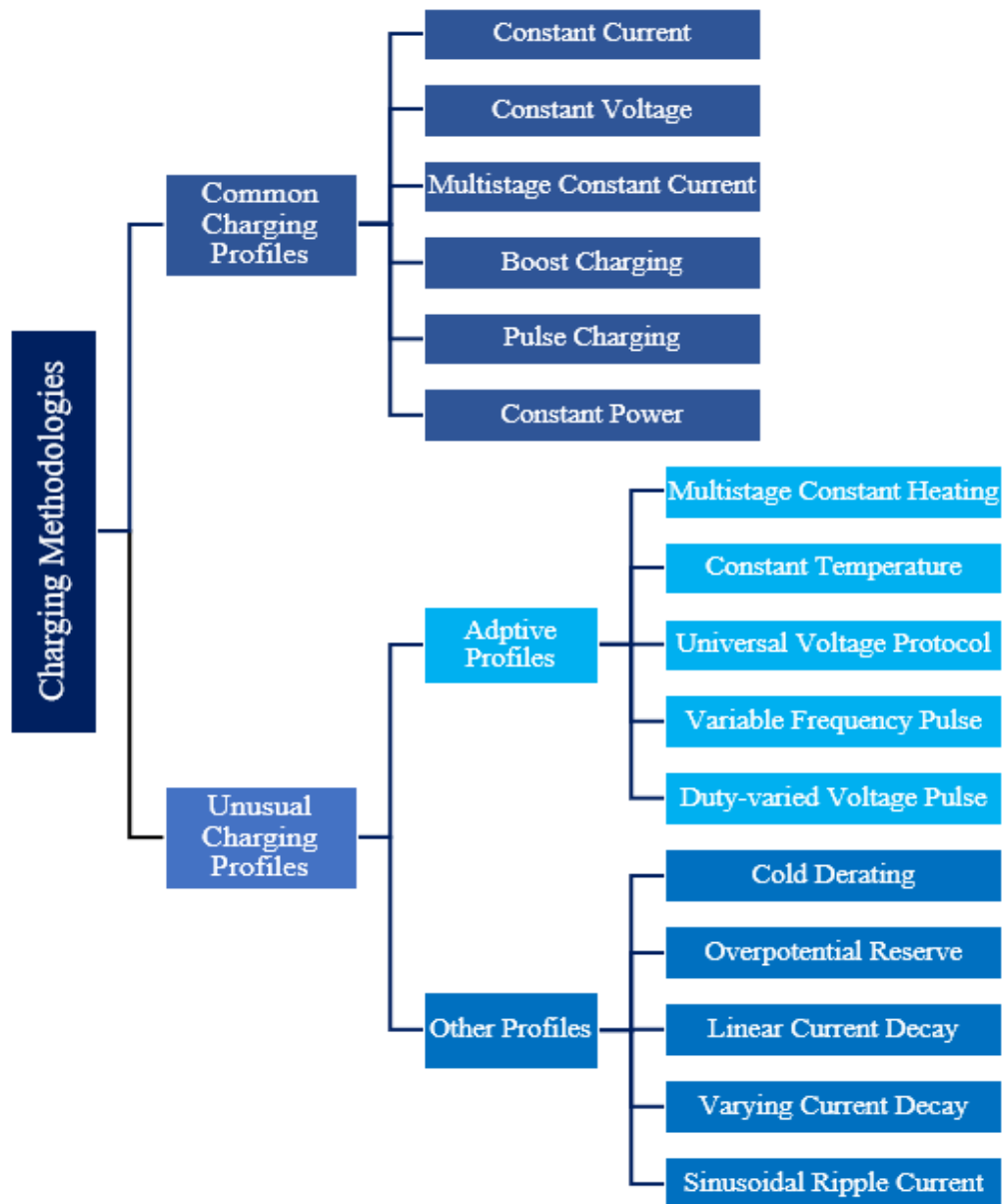
Figure 2.1: Battery charging methodologies.

2.1 Constant Voltage Protocol

The constant voltage (CV) is a charging profile that maintains the potential V_{ch} steady, usually at the value of the maximum battery voltage V_{max}, while the current drops due to the internal impedance increase up to a higher state-of-charge, Figure 2.2. It is mainly employed as the last phase of charging protocols to take the cell's capacity utilization to its highest. Nevertheless, the algorithm can also be applied as a one-phase charging profile from the beginning or incorporated between other phases to build different charging strategies.

2.1.1   Constant Voltage in the Literature

The CV used to charge the battery from depleted condition to fully charged causes a faster degradation rate due to its high initial currents [12]. The experiment brought in [13] depicted the almost two times faster charging with the CV protocol of charge voltage V_{ch} equals to battery maximum voltage V_{max} compared to the standard constant current constant voltage (CCCV) that could keep a nearly linear aging in the capacity up to about the cycle 180 when the degradation is enhanced, and the end of life (EoF) takes place just past the 200th cycle. However, the speed turned to be more detrimental to the 1.1Ah Sony US18500 battery than the CCCV that kept similar behaviour until EoF a little over 300 cycles. [12] work likewise experimented with the constant voltage protocol in 1.4Ah Sony US18650 cell, stating that the charging time from 0 to 80% was almost twice as fast as the CCCV; however, the battery used did not reveal a drastic capacity fade of the cell submitted

to CV. Instead, the batteries aged 7.3% and 9.5% with the standard and CV charging, respectively, after a hundred and fifty cycles.

2.2 Constant Current Protocol

This type of protocol consists of applying an unchanged current until the end of charging or up to the following profile to form a charging strategy. Combining it with a following constant voltage (CV) phase forms the constant current constant voltage (CCCV) profile, the most prevalent method for charging a battery [13], [14]. The constant current (CC) charging alone is applied when there is no need in charging the cell to its total capacity; this is because when the growing voltage hits the maximum voltage specified by the manufacturer or the maximum voltage of the designed protocol, the battery still has not reestablished all the lithium-ions back to the anode. Consequently, charging profiles with decaying current must be applied at the end of charging protocols to charge the battery to its full capacity.

The CCCV charging profile, Figure 2.2, also serves as a reference when comparing the effectiveness of other designed charging protocols and works as described: first, the charging current I_{chg} is kept constant at a specified C-rate until the rising voltage reaches a pre-defined value V_{max}, then the second phase, the CV, the charging voltage V_{ch} remains constant to the point the dropping current hits a defined limit I_{end} or the time passes a maximum pre-set value t_{chg}.
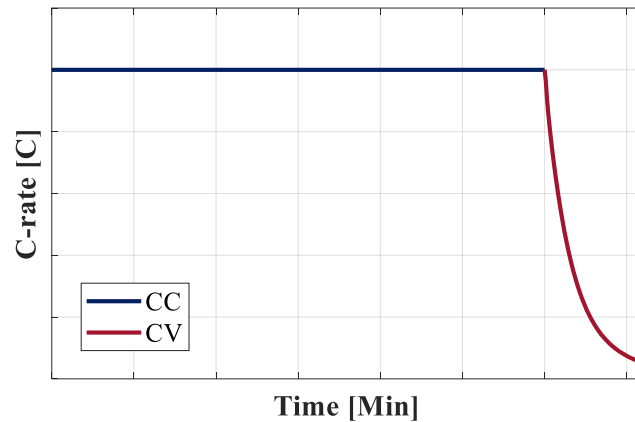
Figure 2.2: Illustrative chart of constant current constant voltage protocol.

2.2.1   Constant Current in the Literature

The work in [11] showed the difference in capacity retention an aging test can result in three different cells with similar characteristics. Through CCCV protocols with absolute ampere values of 1A, 3A and 5A constant current phase, a strategy claimed by the authors to submit the cells to comparable current density and electrode stress, they demonstrated the 1.25Ah Sanyo UR18650SA and 1.1Ah Sony US18650VT1 cells that shared the same cathode and anode materials, diverged regarding the number of cycles at the end of life (80% SOH). Sony's cell reached around 1000 cycles using the three protocols. In contrast, the Sanyo's got 900, 700 and 500 cycles with 1A (0.9C), 3A (2.7C) and 5A (4.5C) CCCV, respectively. The third cell, a 1.1Ah A123 APR18650M1A, had the best outcome concerning cycle life among the CCCV protocols. It lost just 3% of its capacity when submitted to 1A (0.9C) CCCV protocol after one thousand two hundred cycles and 5% with the 3A (2.7VC) CCCV one. With the current increased to 5A (4.5C), the A123 cell behaved like Sanyo's cell, having just 600 cycles achieved with 80% capacity

retention. These results indicate the current increase caused lithium plating, intensifying the cell degradation massively.

2.3 Multistage Constant Current Protocol

The multistage constant current profile is a variant of the CC protocol. It consists of constant current steps of different C-rates increasing, decreasing or randomly shaped to attend to design requirements, Figure 2.3. This protocol works similarly to the CC; however, transitions are set to occur at values of voltages lower than the V_{max}, either triggerd by the pre-defined voltages or time spent on each particular phase (step). Equally to CC charging, the MCC also has to count on a decaying current profile at the end of its schedule to charge the battery to its full capacity utilization, a CV phase, for example.
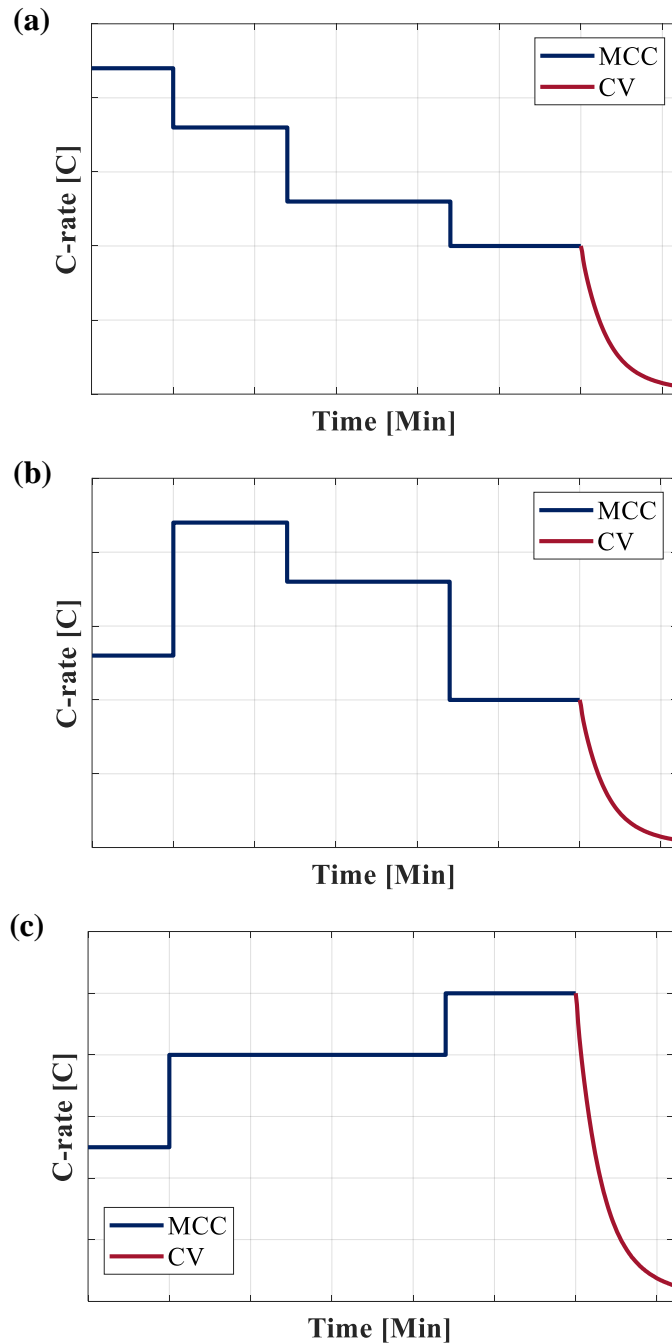
Figure 2.3: Illustration of multistage constant current protocols followed by a CV phase: (a) decreasing MCC, (b) increasing MCC, and (c) random MCC.

The application of the MCC protocol is not limited to the early stages of charging strategies. The protocol can replace the CV charging method by applying

a monotonically decreasing C-rate of the periods to reach a higher state of charge of the cell [11]. When used that way, it is designed to follow the CV charging as close as possible with the necessary number of stages to reach the desired capacity. It begins with a current I_1 switching to the next period of lower C-rate, defined in the design, when the terminal voltage hits the V_{max}. Once the final current I_{end} phase (lowest pre-set current step) runs and the V_{max} is reached, the charging is terminated. Timewise, it is inferior to CV charging if both implemented to charge up to the same SOC, but it has the advantage of simpler implementation as the need for voltage controlling through software and hardware is eliminated [11].
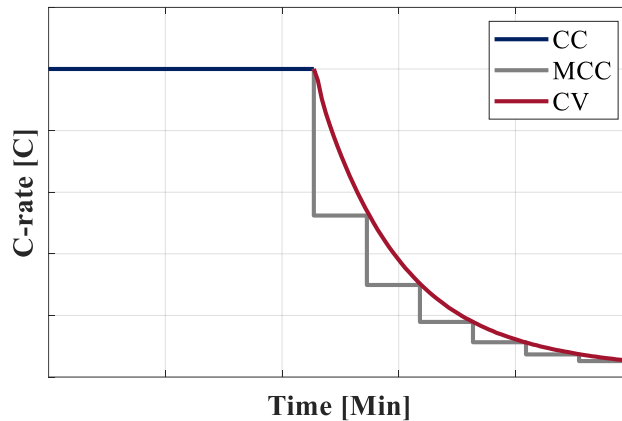
Figure 2.4: Illustrative comparison of constant voltage and multistage constant current protocol in charging strategies.

2.3.1   Multistage Constant Current in the Literature

Authors have studied the advantages and how to extract the best from MCC. In [15], an algorithm using Particle Swarm Optimization (PSO) with a fuzzy logic control to maximize battery charging time and cycle life was proposed. The same strategy was employed in [16] work that reduced the charging time by half while

improving the battery lifespan; however, with the expense of 12% less capacity charged each cycle from MCC capability to reach higher SOC. Taguchi method approach was used in [17] to search for an optimal five stages MCC charging pattern and obtain claimed benefits from the charging method such as energy transfer improvement, cycle life increase and faster charging [18].

A comparison of multistage constant current, constant current constant voltage and pulse charging is depicted in [19]. MCC profile outperforms the other two profiles in an overall analysis of charging time, efficiency, control complexity, implementation complexity and cycle life. Employing a consecutive orthogonal array [20] could optimize multistage constant current capable of charging the battery to 95% SOC while improving the efficiency by one percent compared to the CCCV charging. The study also showed that the designed charging protocol increased the battery lifespan by 57% at seventy percent capacity retention.

2.4 Boost Charging Protocol

Boost Charging (BC) derivates from the CCCV protocol with an extra constant voltage phase implemented at the beginning of charging, making it a faster charging algorithm [13]. It comprises a brief first phase of high dropping current input into the battery because of applied V_{boost} that is terminated by the time t_{boost}, followed by a CCCV protocol of lower currents, Figure 2.5 (b). According to [13], if the resulting current from the CV applied somehow surpasses the battery limit, the CV boost phase can be replaced by a CC or a CCCV to limit it, forming a CCCCCV and a CCCVCCCV or (CCCV)^2, respectively. The values of V_{boost},

t_{boost} and I_{boost} are arbitrary and shall respect battery specifications not to bring further damage to it.
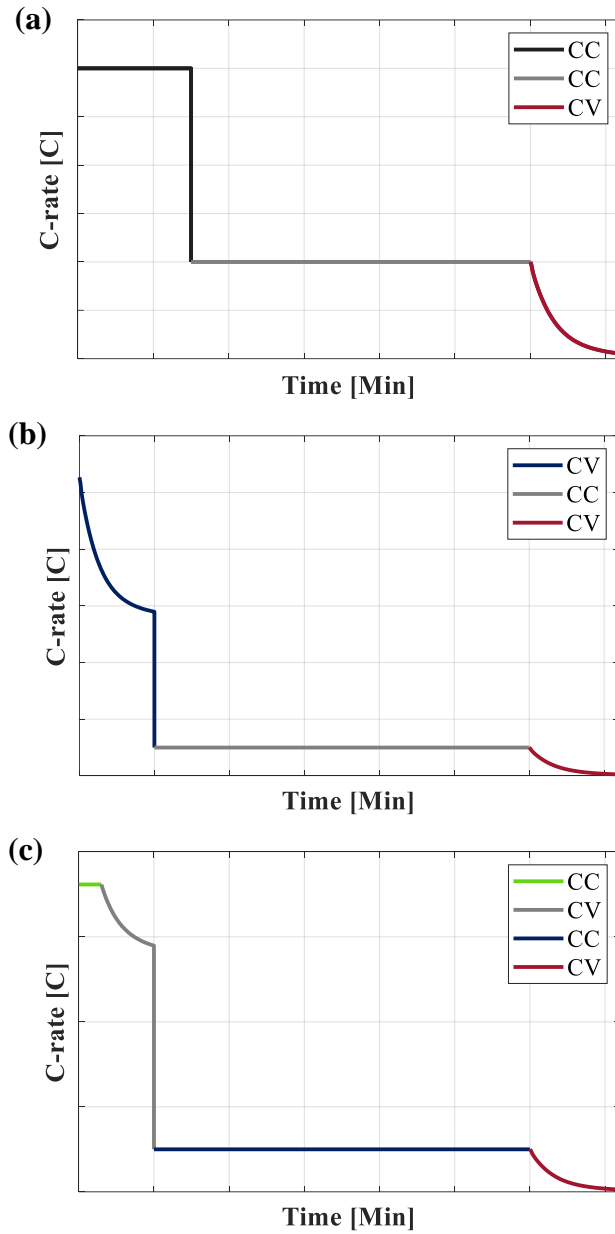
Figure 2.5: Illustrative curves of boost charging protocols: (a) CCCCCV, (b) CVCCCV and (C) CCCVCCCV.

2.4.1   Boost Charging in the Literature

BC is said to decrease the time of the charging process with no further degradation to the battery due to lower chances of lithium plating occurrence at a low state of charge [11]. The protocol results from [13] using Sony US18500 cylindrical cells exhibited a similar aging rate compared to the standard 1C CCCV charging, even with the five minutes initial CV phase with V_{boost} of 4.3V, 100mV higher than the battery maximum voltage, to enhance the charging speed.

In [13], they submitted a prismatic Philips LP423048 Li-ion battery to two variants of the BC protocol with 4.5C I_{boost}: a CCCCCV of 4.4V V_{boost_max} and a $(CCCV)^2$ of 4.3V V_{boost_max}. In this comparison, the $(CCCV)^2$ depicted a slightly better curve when contrasted with the standard 1C CCCV, indicating the high initial currents can be applied with no extra damage to the battery. In addition, the result suggests that the currents at higher SOC have more influence on aging as for the CCCV protocols, the decreasing CV phase initiated at a higher SOC compared to the two other BC protocols. Nevertheless, the CCCCCV protocol had the highest aging rate of the three, probably caused mainly by the higher voltage achieved in the boost phase.

The boost phase in charging concerning the beginning of the period was observed in [11] research. The CC boost phase counted with either five or six minutes duration, depending on the cell, charging 40% of their capacity. They based their designed protocols on the previous research [13], also taking the V_{boost_max} above the V_{max} but by 50mV. Out of the three profiles with boost interval starting

at 0, 10 and 20% SOC, the last presented the best result in both Sanyo UR18650SA 1.25Ah and an A123 APR18650M1A 1.1Ah cells. Yet, the high current BC protocols were found to be detrimental to the batteries as the charging time is about in the middle of 1C and 3C CCCV protocols, but with similar aging of the 3C one. The authors inferred that the results might be a cause of the greater changes in the anode volume or the higher internal resistances that lead to lithium plating at earlier stages of SOC, and further investigation was required to better understand the real cause. Denominated in [21] as a multistage fast charging technique, a boost charging protocol CCCCCV type capable of charging the tested cell in twenty minutes was proposed. Their extensive test showed similar capacity retention compared to the standard charging protocol recommended by the cell's supplier of charging time almost three times slower, indicating no further degradation occurred to the cell.

2.5 Pulse Charging Protocol

Presenting as a more dynamic charging strategy, pulse charging (PC) appears in the literature claiming benefits to battery life. As a characteristic, this profile has sudden changes in the current amplitude applied into the storage device, forming periodic waves. It consists in decreasing the charging current I_{high} to a lower current I_{low}, To a rest period (no current flow), or even change the direction of amperage discharging the cell for a brief period (configuring an alternate current profile), Figure 2.6. It is over either after a specified period or when the terminal voltage exceeds a pre-defined value as in other charging methodologies.
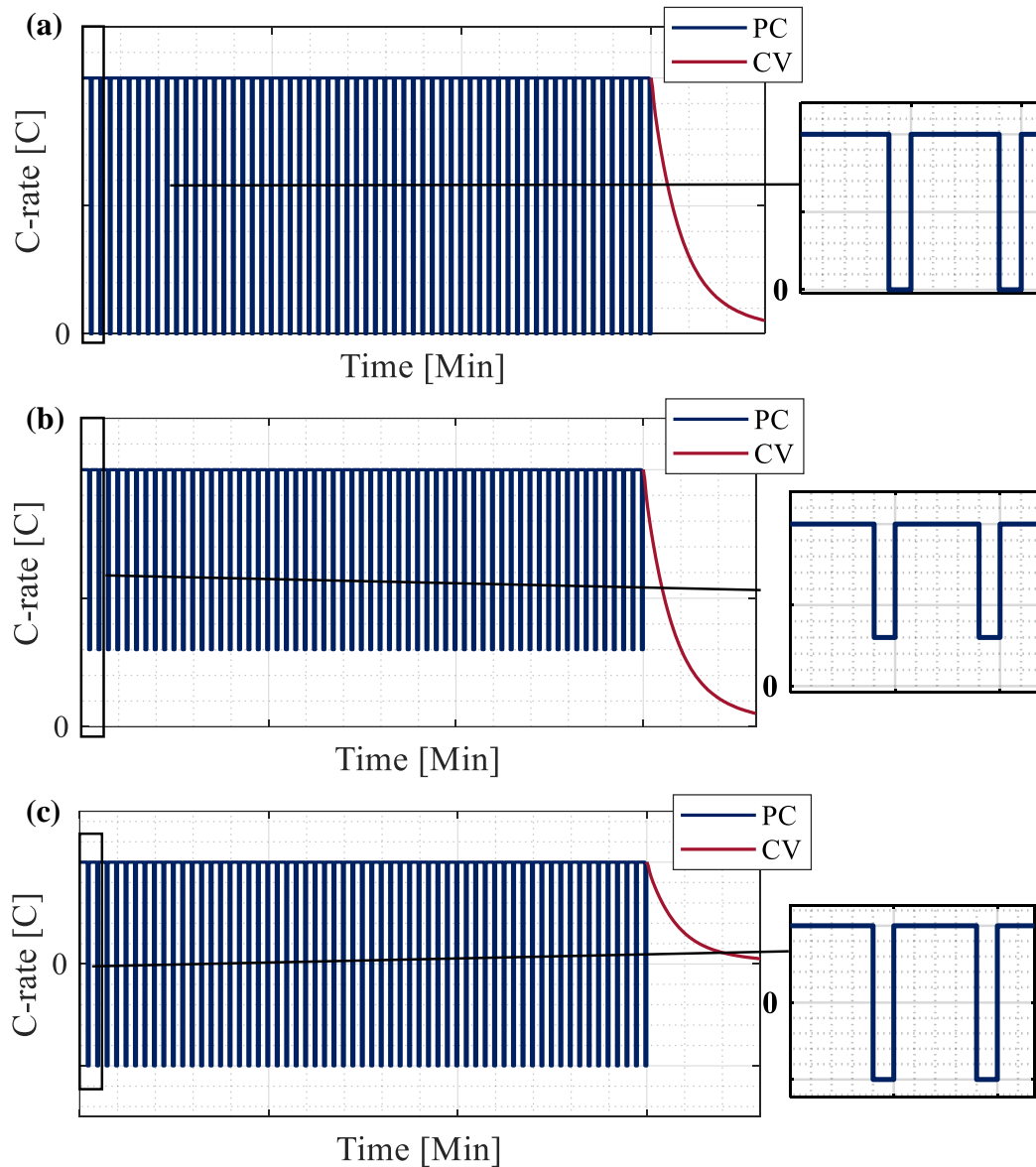
Figure 2.6: Illustrative of pulse protocols followed by CV phase: (a) PC with rest, (b) PC with positive lower current, and (c) PC with negative lower current.

The PC also serves as a final charging phase replacing the CV charging to take the cell towards its full capacity as the MCC, Figure 2.7. As there is no need for voltage control as with CV and variable amperage amplitudes like in MMC, it offers a lower implementation cost. The PC phase starts after the terminal voltage

reaches a pre-defined voltage V_{switch} that is lower than the maximum voltage V_{max}.

The pulse current I_{high} works just like when used in the main charging phase;

however, the pauses obey a minimum pause duration $t_{\min\_pause}$ and a pre-defined

voltage V_{float} lower than V_{max}. When a pulse is ceased, a rest period starts, and

voltage drops towards V_{float}. The rest period lasts until the two requirements,

terminal voltage hits V_{float} and $t_{\min\_pause}$ are met. The charging process comes to

a halt when the cell voltage takes more than a maximum period $t_{\max\_pause}$ to reach

V_{float}. Due to no clamp of the voltage at the pulses, V_{float} shall be reasonably lower

than V_{max} so the cell voltage does not surpass too much V_{max} when the pulse is

applied. The closer V_{float} is to V_{max} more capacity utilization of the cell is achieved.

Nevertheless, the strategy comes with more degradation of the battery because of

higher voltages of the terminal during the pulses [11].
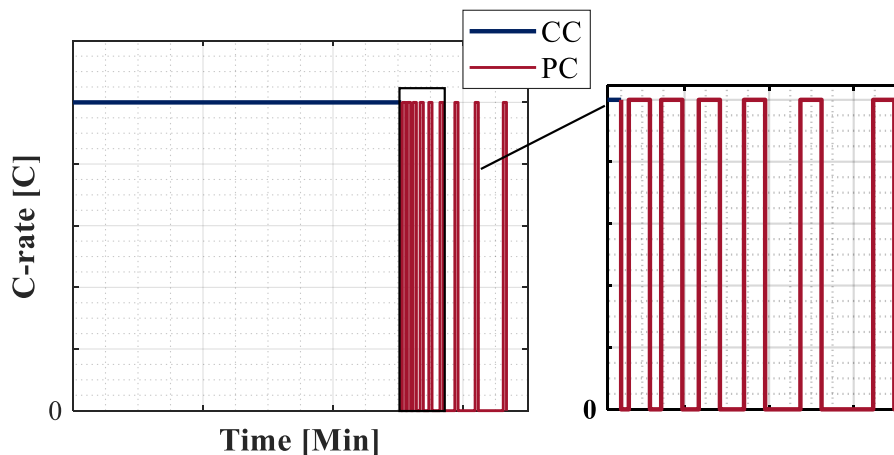
Figure 2.7: Illustrative curve of Constant Current Pulse Charging protocol.

Apart from being used in fast charging phases and as the last phase of a

charging protocol, the PC is used alternatively to other methods to preheat batteries

in lower temperature environments and recuperates the cell kinetic, improving its performance [22].

2.5.1   Pulse Charging in the Literature

Lithium-ion diffusion speed in the electrode is a crucial factor when charging a Li-ion cell [23]. With higher rate charging, concentration polarization is more susceptible and causes a faster increase in the voltage towards the upper limit. Pulse charging is claimed to ease this concentration polarization, enabling a higher power transfer rate, speeding up battery charging. Tests to verify these statements were performed on Sony US18650S 900 mAh cells by [23]. They concluded that the cells submitted to pulse charging presented higher active material utilization, engendering a higher discharging capacity and increased battery lifespan. The study also analyzed tests performed with scanning electron microscopy (SEM) and X-ray diffraction (XRD) that showed better inhibition of passive film growth on the anode and superior stability of the cathode material.

Variations of Pulse charging profile have been investigated. In [24], various charging protocols such as CC, CCCV and the named by the authors "constant current-constant voltage with negative pulse (CC-CVNP)" were employed on Lithium-ion EIG 7 Ah LiFePO4-based cells to study the influence frequency, period and amplitude of negative pulse (NP) on cell aging. The CC-CVNP protocols were designed to approach negative pulse and rest period at the same protocol, example shown in Figure 2.8. Results showed that protocols with the same amount of time spent on negative pulses spread in more extended periods along

charging bring more positive effects than the smaller periods applied at a higher frequency. Moreover, the lower amplitude of NP lasting longer versus higher amplitude in a briefer period resulting in the same amount of ampere-hours taken out of the battery during these pulses also leads to the assumption that the longer time spent on a single negative pulse has more to offer for battery's life than the pulse amplitude.
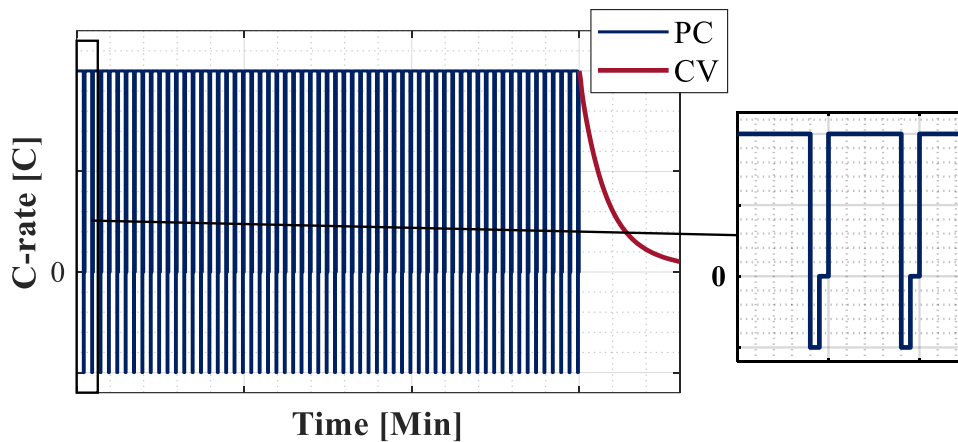
Figure 2.8: Illustrative image of constant current-constant voltage with negative pulse (CC-CVNP), based on [24].

The same EIG 7Ah high power cell was studied posteriorly to [24] work. Expecting better active material utilization and the possible effect of Li-ion diffusion on the electrolyte/active material particles interface through a decreased diffusion resistance using very low frequency (mHz), [25] investigated the negative pulse impact in fast charging. They designed and performed aging tests with eight different charging protocols, two with negative pulses and rest period incorporated, reaching a rate of up to 4C. After 1700 cycles, the results revealed that both strategies with negative pulses had better capacity retention than the constant

current constant voltage one. Plus, even when compared against the multistage constant current constant voltage protocols of lower mean current, these two protocols had higher capacity retention. The study also brought better numbers favouring the negative pulse protocols concerning ohmic resistance, charge transfer resistance, passivation resistance, and diffusion resistance, contributing to the acceleration of Li+ ions diffusion through the active materials.

The pulse frequency was studied in [11] with two different cells, a Sanyo UR18650SA 1.25Ah and an A123 APR18650M1A 1.1 Ah. Using a 50% duty cycle $(t_{I_{high}}/t_{cyle})$, meaning half the time the current is at the higher amperage, the designed protocols had 5A (4C Sanyo and 4.5C A123) as I_{high} and 1A 5A (0.8C Sanyo and 0.9C A123) as I_{low}, forming a 3A 5A (2.4C Sanyo and 2.7C A123) mean current profile. The authors designed 1 Hz and 25 Hz PC protocols to investigate further the findings form [26] that stated different impacts on cells performance above and below ~10 Hz cycle PC. The test outcome confirmed the expectations with a slightly better performance of the 25Hz protocol over the 1Hz one for Sanyo's cell. However, for the A123 cell, the result was a negligible difference in the capacity fade of the PC protocols and the 3A CCCV one.

The use of pulse charging in place of constant voltage protocols as the last phase of the charging methodology was also tested in [11]. They revealed that the PC charges the batteries up to different SOC with the same algorithm, 82%, 92% and 98% for the three cells tested. Additionally, the PC phase takes longer than the usual CV period. Lastly, they demonstrated the protocols, even surpassing the V_{max}

by around 70mV did not degrade the cell as much as the CCCV with V_{ch} set 50mV above V_{max}, also tested in the research, staying with a similar performance of the standard CCCV of the same CC current amplitude.

2.6 Constant Power Protocol

Constant Power (CP) bases on the current I_{ch} following its relationship with voltage V_{ch} ($P_{ch} = V_{ch} * I_{ch}$) to result in the constant power P_{ch} input into the battery. CP charging is then characterized as a protocol that starts with a high current that decays along with time until the increasing voltage hits the V_{max} [27], Figure 2.9.
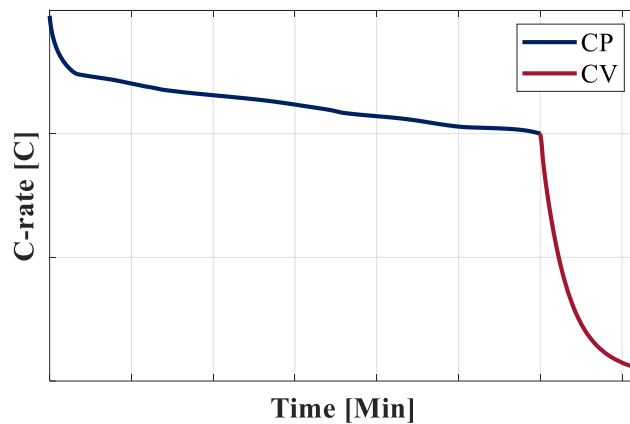
Figure 2.9: Illustrative curve of Constant Power protocol.

2.6.1   Constant Power in the Literature

The constant current protocol followed by a CV (CPCV) was evaluated against CCCV and MCCCV protocols in the [27] studies. They submitted the cells to 0.5C current mean up to cycle one hundred and increased the mean current to 1C until the cells end-of-life. Interestingly, the CP charging had a slightly higher

capacity fading up to the C-rate rise, with the numbers inverting and favouring CP past cycle two-hundredth.

2.7 Unusual Charging Protocols

2.7.1   Adaptive Charging Protocols

More complex charging protocols involving temperature control, function of voltage or internal resistance are proposed in the literature. Using a genetic algorithm, a multistage constant heating (MCH) strategy was developed in [14]. The study accomplished to reduce by 9% the charging time while maintaining the cell temperature lower than the conventional CCCV approach depending on the environment temperature tested. In the same line, [28] proposed the constant temperature constant voltage (CTCV) adjustable to both cell and environment temperature. They accomplished to reproduce different scenarios of cooling and confirmed the designed CTCV algorithm could improve the charging time by 20% while maintaining the maximum temperature similar to the 1C CCCV profile.

A universal voltage protocol (UVP) was developed and tested in [29] study to adapt to cell aging and be employed on cells of the same design regardless of the number of cycles. The protocol dictates a voltage path resulting in a nonlinear current profile that starts low with a high ascending slope at the early SOC stages, reaching its peak around 15% SOC, and then a descending curve up to the charging end, Figure 2.10.
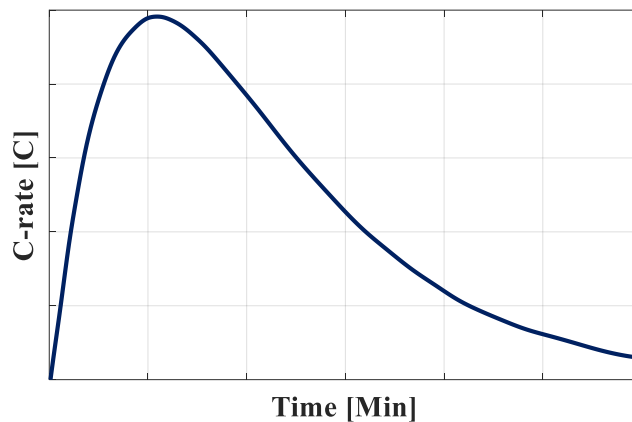
Figure 2.10: Illustrative curve of the Universal Voltage Protocol, adapted from [29].

Aging tests were conducted with UVP and 2C CCCV protocols of similar charging time and proved to effectively maintain the charging efficiency across tests and improve the battery life cycles by more than 3.5 times the 2C CCCV protocol.

A method formed of a periodic flow of three phases, the search mode, the charge mode, and the full charge detect mode resulting in a variable frequency pulse charging of fixed voltage amplitude (4.2V), was developed and proposed in [30]. The study showed an improvement of 10% in charging time of the variable frequency pulse charging (VFPC) when compared to pulse charging of fixed frequency. A 14% faster charging was achieved with the duty-varied voltage pulse-charging (DVVPC) in comparison to the CCCV protocol in [31]. Additionally, the charge efficiency was improved by 3.4% in the comparison.

In [32], they introduced an impedance tracking method to detect lithium plating offline and online through the impedance differential and be used as a trigger to decrease the charging current amplitude in fast charging. With the

requirement of a brief pause of 0.5s on every SOC percentage, both methods induce the charging profiles to be a multistage pulse charging protocol of variable duty. The work compared the profiles originated from the two 1C PC with the same rest period. The offline and online protocols reached 1.75 and 3.5 times the lifespan PC algorithm provided but at the expense of increasing 20% the charging time.

2.7.2   Other Charging Protocols

Cold derating (CD) algorithm was explored in [33], Figure 2.11. It starts with a low increasing current lasting the first SOCs followed by a CC phase up to the end of the charging or a next phase to charge the battery completely. The protocol is said to prevent the start of lithium plating since the kinetics is inferior at low SOCs, and the high charging load launched right away in the charging process would favour the degradation mechanism [33]. The overpotential reserve (OPR) protocol, Figure 2.11, on the other hand, has a high constant current start followed by a nonlinear diminishing current following the curve of the open-circuit potential of the negative electrode. The strategy is driven by the assumption that the negative overpotential in the electrolyte/negative electrode interface shall not surpass the overpotential dictated by the negative electrode open-circuit potential to avoid the lithium plating trigger [34].

(a)

(b)
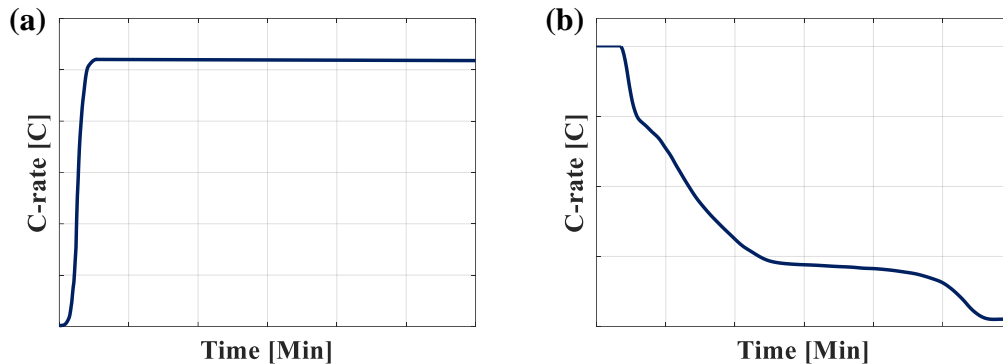
Figure 2.11: Illustrative image of (a) pure Cold Derating and (b) Overpotential reserve superimposed on a 1C constant current protocol, adapted from [33].

Cold derating (CD), overpotential reserve (OPR), alternating current (AC) of 2.5Hz frequency and 50% duty cycle, and a current interrupt (CI) 90% duty cycle, these last two configuring pulse charging protocols, were approached in designed charging profiles based on strong physical theories to mitigate degradation in [33]. All four neutral mean current protocols and fourteen combinations made with them selected using statistical analysis to reduce the number of experiments preserving the significance level of the results were superimposed on a 1C constant current profile. As a benchmark, four cells were tested with pure 1C CC protocols forming twenty-two experiments in total. The aging tests comprised charging the batteries from 0 to 80% SOC with no CV phase to balance the electrodes. The novel had some surprising outcomes, such as the poor performance of the CD protocol that had its end-of-life earlier than any profile tested and the best being profiles with all four algorithms applied together, depicting more than double the CD method lifespan. Other conclusions were that the OPR show itself as the most effective in preserving the cell aging as the best results came from profiles containing the

method. Moreover, making a rank out of the four pure superimposed charging profiles, the best was the OPR, followed by AC, CI, and CD.

The linear current decay (LCD) protocol was explored in [35] and asserted to charge the battery 2.5 times faster than the constant current profile. The protocol that follows the equation $I_{ch}(t) = I_0 - kt$, where I_0 and k are arbitrary values for initial current and slope of the diminisinh curve, respectively, was later analyzed in [12] and considered a not worthy approach to fast charging due to some downsides such as the inability of the algorithm to take the battery to its full capacity utilization and a lower lifespan. To overcome LCD limitations, they proposed an algorithm so-called varying current decay (VCD) that was able to charge the battery to about 98% capacity, the same capacity as its contestants CCCV and CV profiles. The algorithm comprised a first 3.57C CC short phase up to the point the cell hit a cut-off voltage followed by the varying current decay dictated by the equation $I_{ch}(t) = (I_0 - k_1 t^{\frac{1}{2}})/(k_2 t^{\frac{1}{2}} + k_3 t)$. The comparison showed the proposed protocol was able to charge the battery from 0 to 80% SOC about fifteen percent faster than the CV methods and still have a slower capacity fade after 150 cycles.

A study conducted in [36] compared the proposed sinusoidal ripple current (SRC) and CCCV concerning capacity charged, efficiency, temperature rise, charging time and cycle life. The latest two were improved around 17% and 16% compared to the standard CCCV, respectively. The work also matched PC with rest period to SRC, indicating in their findings that both protocols presented a similar

performance on the frequencies tested, except for the cycle life not performed in PC profile.

2.8 Concluding Remarks

The literature shows controversy in the consensus of an optimal charging protocol to prevent the battery from aging. It also exposes the particular behaviour to charging algorithms of each energy storage device that can not be freely extended to others due to design characteristics that influence different phenomena, such as the stress in electrodes and temperature gradient. Moreover, most of the research focuses on the "standard" temperature of 25 degrees Celsius, contrary to the EV market that concentrates in North America, Europe and China, cold regions of the planet. Hence, there should be more effort to understand the influence of charging protocols to overcome the conditions and obstacles faced in these markets effectively. Nevertheless, considering the results presented, pulse charging protocols show an overall good outcome in most of the studies it is implemented and should be considered a candidate for battery aging minimization.

Chapter 3

Battery State of Charge and Health

Estimation: State of the Art

The growing market of electrified vehicles requires efforts from car manufacturers to build robust systems to deal with all types of situations their products will face in customers' hands. A major system of electrified vehicles is the energy storage unit [37]. The complexity of batteries lies in their nonlinear behaviour that is highly dependent on external components such as temperature and dynamic load required from it. For a good estimation of these behaviours, the battery management system relies on estimation algorithms that inform the states of the storage unit, such: State of charge (SOC), state of health (SOH), and state of power (SOP). Widely studied in the industry and academia, SOC estimation is commonly considered one of the most significant functions in a BMS [38]. Still, SOH is attracting more interest because of its importance in the automotive application for supporting a more consistent SOC and SOP estimation.

State estimation is characterized by the indirect extraction of hidden states from uncertain and inaccurate measurements [39]. The literature contains many techniques to estimate the states and parameters of linear and nonlinear systems.

Generally, the accuracy of these methods is directly related to their complexity. Electrochemical models, for instance, provide the lowest errors yet with the cost of being the most computationally expensive [38]. Open circuit voltage based models offer the lowest implementation difficulty along with a good result; however, their applications are limited to the usage of the device it is implemented. Figure 3.1 illustrates the normalized range of errors and implementation complexity of the SOC estimation methods where the top of the chart means a higher degree.
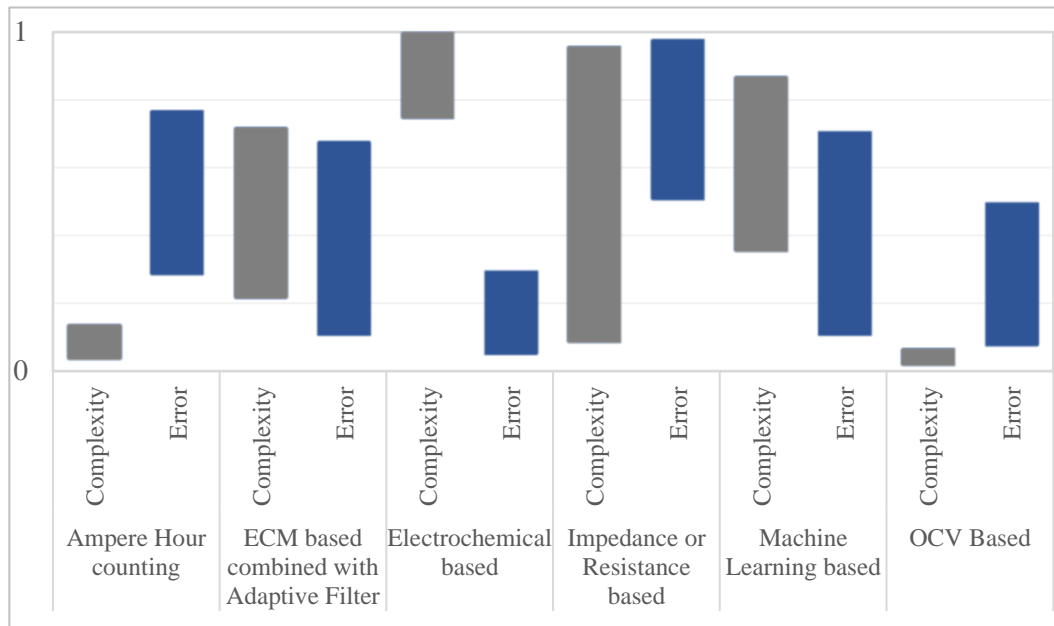
Figure 3.1: Normalized range of the complexity and error for battery SOC estimation methods, adapted from [38].

This chapter explores some of the states of charge and health methods studied in the literature that could contribute to a reliable BMS design. Machine learning techniques are not addressed in this work. However, a great review of the method applied to battery state of charge and health estimation is found in [40].

3.1 Battery State of Charge Estimation Methods

Described as the battery's available capacity concerning its rated capacity [3], [41], hence, expressed in percentage, the state of charge estimation plays a key whole in the BMS. An accurate SOC estimation is a complex assignment given not only by the fact that direct measurement of the parameter is not possible with the device being used, but batteries of different chemistries have divergence in behaviour, present different features as they age and are temperature-dependent, and the diversity of applications they are submitted. The concept is directly related to range anxiety, and much effort has been put into it for a reliable estimation [42], [43], [44], [45], [46], [47], by the employment of a variety of estimation methods as shown in Figure 3.2 and Table 3.1, and reviewed in the following topics.
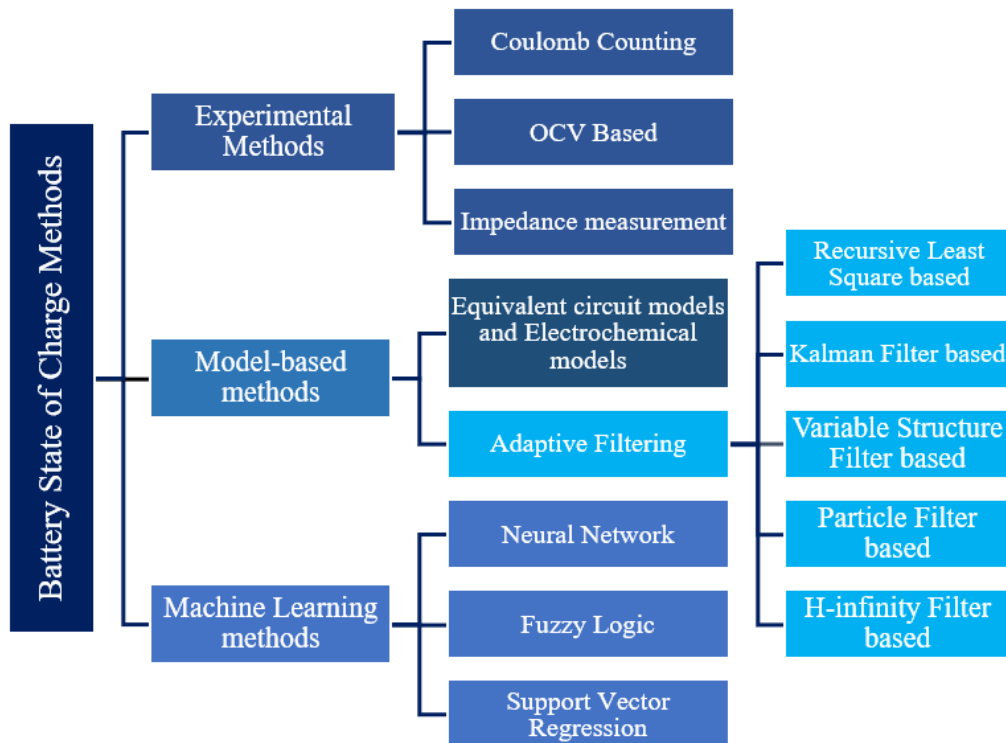
Figure 3.2: State of charge estimation methods.

Table 3.1: Battery SOC estimation methods results.

Work	Method	Data Profile	Error [%]
[42]*	EKF	UDDS	0.15 (RMSE)
	UKF		0.12 (RMSE)
	CKF		0.11 (RMSE)
[46]	EKF	BJDC	1.5 (RMSE)
	UKF		1.3 (RMSE)
[48]	AEKF	UDDS	~1.0 (RMSE)
[49]	EKF	UDDS	3.2 (Mean)
	AEKF		1.0 (Mean)
[50]	UKF	DST	3.1 (RMSE)
[51]**	SVSF	UDDS	2.4 (RMSE)
	EKF		2.7 (RMSE)
[52]	EKF	UDDS	4.7 (RMSE)
	SVSF		3.6 (RMSE)
	VBL-SVSF		2.6 (RMSE)

*80% initial SOC offset
**15% initial SOC offset

3.1.1   Coulomb Counting

Coulomb counting is a widely used method for state of charging estimation that involves integrating the current flow through the battery in a time interval. Hence, error in current measurement is one of the sources that could make the method inaccurate. Additionally, it is highly dependent on an accurate initial SOC and battery capacity, as demonstrated in the following equation 3.1.

$$SOC = SOC(t_0) + \int_{t_0}^{t} \frac{\eta \cdot i(t)}{C_n} dt \qquad 3.1$$

where $SOC(t_0)$ is the initial SOC, η is the Coulombic efficiency, $i(t)$ stands for the current at instant t, and C_n is the nominal capacity of the batter.

According to [53], besides the uncertainty of the battery's nominal capacity dictated by battery state of health and the initial SOC, current integration thought time, current measurement, and timing oscillator would also affect the SOC estimation with coulomb counting. [38] adds the self-discharging as an error input into the method. With all cons, it is computationally inexpensive for its low complexity [38].
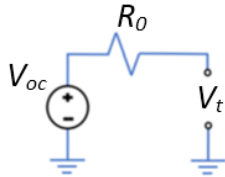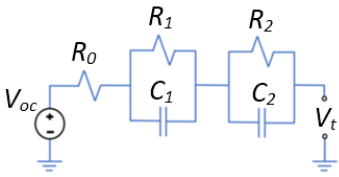
3.1.2   Open Circuit Voltage (OCV) Based

This SOC estimation method involves measuring the battery voltage in an open-circuit state (no load) and posteriorly transforming the voltage to SOC through the SOC-OCV relationship curve acquired with extensive testing at different temperatures and states of health [38]. This is because the SOC-OCV relationship changes over temperature [54], [55] and cycle life [56]. The method presents some obstacles that make it unfeasible in certain conditions once it needs a rest period of about three for the battery relaxation, as exhibited in [57] and when applied on batteries with flat SOC-OVC curves as produced by $LiFePO_4$ battery type demonstrated in [58]. However, in electric vehicles, this method can be employed whenever the system is powered up, which would give a reasonably close SOC value of the pack if the rest period for battery relaxation has not reached the OCV state. Furthermore, the technique requires low computational effort [59].

3.1.3   Equivalent Circuit Model (ECM)

ECM based SOC estimation is currently the most used SOC estimation method in online applications [59], [60]. The model lies on arrangements of resistances and capacitances, such as the most common internal resistance (Rint) model [61] and n-resistor-capacitor (*n*RC) models [62], Table 3.2, to capture the battery dynamics under charge/discharge current. With the model, the OVC can be estimated and posteriorly, the SOC-OCV relationship is applied to acquire the battery state of charge. [38] refers to a second tactic that utilizes a predefined SOC to calculate the cell terminal voltage that is matched with the measurement. This approach entails the use of other SOC estimation algorithms such as Extended Kalman Filter (EKF) to calculate the final SOC.

Table 3.2: Equivalent Circuit Models example.

ECM	Schematic	Equation
Rint [61]		$Vt_k = V_{ocv,k} - R_0 I_k$
Second-order R-2RC [63]		$V_{1,k+1} = 1 - \frac{\Delta t}{R_1 C_1} V_{1,k} + \frac{\Delta t}{C_1} I_k$ $V_{2,k+1} = 1 - \frac{\Delta t}{R_2 C_2} V_{1,k} + \frac{\Delta t}{C_2} I_k$ $Vt_k = V_{ocv,k} - V_{1,k} - V_{2,k} - R_0 I_k$

3.1.4   Electrochemical Model

Because of the capability of modelling the lithium diffusion in the electrolyte and electrodes, electrochemical models have been broadly studied in the literature [9]. The method's approach is a set of partial differential equations [60] to simulate the mass transfer, the thermodynamics and the chemical dynamics of the battery [38]. Although it has a higher accuracy when compared to ECM models, it also requires a more robust computational capacity and has parameters that are generally not given by the battery producer [60].

3.1.5   Kalman Filter based

The method was first introduced in 1960 as a new approach to linear filtering [64] but not referred to as "Kalman filter" (KF) at the time. KF has been extensively studied and appears as the most utilized state estimation method [65], [66]. The method works in a predictor-corrector mode. The prediction phase, also named *a priori*, uses a model to predict the current state, then *a posteriori* phase refines the states through a gain calculated with the *a priori* covariance estimate $P_{k|k-1}$ and the measurement covariance S_k.

When weel-defined, KF provides the most accurate estimation for a linear system with Gaussian white noise [66]. The method is characterized by the process and measurement noise that directly influences the stability and performance of the estimation. Its tuning is obtained through the covariance matrices, where the measurement noise "R" can be simply attained with the sensor used in the

experiment. In contrast, the process noise covariance "Q" has to be attributed by trial and error.

Kalman filter has many variants like the most spread extended Kalman filter (EKF), unscented Kalman filter (UKF) [67], cubature Kalman Filter (CKF) [68], quadrature Kalman filter [69], adaptive extended and unscented Kalman filters [70], [71], created for nonlinear systems estimation as the original algorithm is limited to linear systems. These extensions have been vastly studied in the literature for SOC estimation. [72] used hardware in the loop to validate the battery SOC estimation of a 2nd R-2RC model coupled with EKF. [46] used a Beijing Driving Cycle (BJDC) to validate a cubature Kalman Filter showing its superiority in Battery SOC estimation over the EKF algorithm. [48] developed a 1st order R-RC model with an adaptive extended Kalman filter (AEKF) for battery SOC estimation reaching RMSE under 1% for UDDS and a maximum error of 2%. An AEKF was also developed in [49] and compared with the standard version EKF. However, differently from [48], this work combined a 2nd order R-2RC ECM with the algorithms to estimate the battery SOC ran in the federal urban driving schedule. The results exhibited 3.2% and 1% mean SOC error for the EKF and AEKF, respectively.

A UKF was employed with a simple R model for SOC estimation in [50]. The algorithm gave a reasonably good estimation given the limited battery model and the flat OCV-SOC curve from the LiFeO4 battery, under 3% RMSE, for all cases tested with an initial SOC offset. The work in [42] compared the SOC estimation

performance of the EKF, CKF and sigma-point Kalman filter (SPKF) for a 1st order

R-RC ECM. The study concluded that EKF has the poorest convergence results to

true value when an offset is applied to the initial SOC and the highest RMSE. SPKF

showed similar SOC RMSE and computation time to the CKF; however,

convergence time was close to EKF. CKF was considered the fittest regarding the

trade-off it offers with respect to the computation time and estimation accuracy of

around 0.1% RMSE for the UDDS drive cycle. EKF and UKF had their

performance matched in the battery SOC estimation under CC discharge and CC

charge/discharge cycles in [45] work. UKF presented lower errors in both

scenarios.

3.1.5.1   Extended Kalman Filter (EKF)

Created from KF, the extended Kalman filter addresses nonlinear systems

[39]. The standard Kalman filter discussed previously assumes the linear form

shown in equations 3.2 and 3.3

$$\hat{x}_{k|k-1} = F\hat{x}_{k-1|k-1} + Gu_{k-1} + w_{k-1} \qquad\qquad 3.2$$

$$\hat{z}_{k|k-1} = Hx_{k|k-1} + v_{k-1} \qquad\qquad 3.3$$

Where $\hat{x}_{k|k-1}$ stands for the state estimate, F is the system matrix, G is the input matrix,

u_{k-1} the input, $\hat{z}_{k|k-1}$, the measurement estimate, H is the output matrix and, the

w_{k-1} and v_{k-1} are the system and measurement noise, respectively.

The battery SOC estimation configures a nonlinear system; therefore, KF

cannot address it. For that matter, the extended Kalman filter should be employed

instead. The method works very similarly to the KF, except for the fact that the

system matrix F and the output matrix H are time-varying based on the state estimate

[73]. For the computation of the functions f and h they must be linearized after their

Jacobian's as demonstrated in equations 3.4 and 3.5 [45]. This linearization around

the state estimate makes EKF sub-optimal and creates uncertainties that could lead

to the instability of the filter [74], limiting the use of the filter in several real world

applications [75].

$$F_{k-1} = \frac{\partial f}{\partial x}\bigg|_{\hat{x}_{k-1|k-1}, u_{k-1}} \qquad 3.4$$

$$H_k = \frac{\partial h}{\partial x}\bigg|_{\hat{x}_{k|k-1}, u_k} \qquad 3.5$$

The EKF process is illustrated in Table 3.3 where the state estimate $\hat{x}_{k|k-1}$,

the measurement vector $\hat{z}_{k|k-1}$ and covariance estimate $P_{k|k-1}$ are computed in the

prediction step. Posteriorly, in the second step, the gain K_k, the refinement of the

predicted state estimate $\hat{x}_{k|k-1}$ and covariance estimate $P_{k|k-1}$ are processed.

Table 3.3: Extended Kalman filter algorithm.

Prediction (*A priori*)	
State estimate	$\hat{x}_{k|k-1} = f(\hat{x}_{k-1|k-1}, u_{k-1}, w_{k-1})$
Measurement vector	$\hat{z}_{k|k-1} = h(\hat{x}_{k|k-1}, u_k, v_k)$
Covariance estimate	$P_{k|k-1} = F_{k-1}P_{k-1|k-1}F_{k-1}^T + Q_{k-1}$
Correction (*A posteriori*)	
Kalman gain	$K_k = P_{k|k-1}H_k^T(H_kP_{k|k-1}H_k^T + R_k)^{-1}$
State estimate	$\hat{x}_{k|k} = \hat{x}_{k|k-1} + K_{SVSF_k}(z_k - h(\hat{x}_{k|k-1}))$
Covariance estimate	$P_{k|k} = P_{k|k-1} - K_kH_kP_{k|k-1}$

3.1.5.2   Unscented Kalman Filter (UKF)

The UKF is another variant of KF employed in nonlinear systems. UKF is a type of sigma point Kalman filter (SPKF) among other UKF variants like the general, simplex, and spherical unscented [39], [76]. Instead of linearizing the state space equations through the Taylor-series expansion, SPKF approaches the linearization by a weighted statistical linear regression producing a few numbers designated as sigma points [76]. Subsequently, these sigma points are used to determine the *a posteriori* estimate for the probability distribution.

UKF works similarly to Monte Carlo methods, except that it employs a much smaller number of points to estimate the mean and covariance of the system [39].

In UKF, a minimal number of points around the mean are selected utilizing a deterministic sampling strategy called unscented transform (UT). This tactic makes the UKF more accurate than EKF that has errors introduced into the mean and covariance through the linearization [42]. A schematic of the difference between the linearization and UT is illustrated in Figure 3.3.
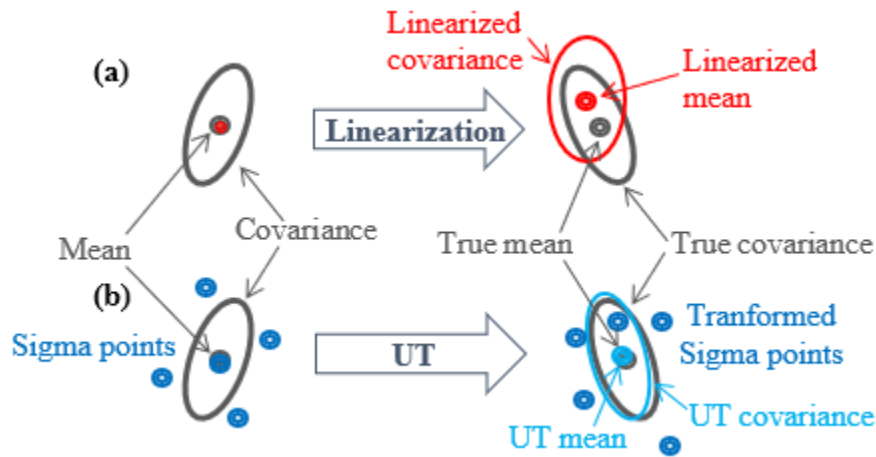
Figure 3.3: EKF Linearization (a) and UKF unscented transform (b), adapted from [74].

As in the KF and EKF, UKF also works in a predictor-correction way and has as a first step the calculation of the sigma points shown in equation 3.6 [39].

$$\begin{cases} \mathcal{X}^0_{k-1|k-1} = \bar{x}_{k-1|k-1} & i = 0 \\ \mathcal{X}^i_{k-1|k-1} = \bar{x}_{k-1|k-1} + (\gamma\sqrt{P_{k-1|k-1}})_i & i = 1, \dots, n \\ \mathcal{X}^{i+n}_{k-1|k-1} = \bar{x}_{k-1|k-1} - (\gamma\sqrt{P_{k-1|k-1}})_i & i = 1, \dots, n \end{cases} \qquad 3.6$$

where the $x_{k-1|k-1}$ is an n-dimensional state, $\bar{x}_{k-1|k-1}$ is an approximated mean, $P_{k-1|k-1}$ is an approximated covariance. The parameter γ is $\sqrt{n+k}$.

The weight coefficients are computed next with the scaling factor k, equation 3.7.

$$\begin{cases} w_0 = k/(n+k), & i = 0 \\ w_i = 1/2(n+k), & i = 1, \dots, 2n \end{cases} \qquad 3.7$$

The rest of the method process is described in the following Table 3.4 [39].

Table 3.4: Unscented Kalman filter algorithm.

Prediction (*A priori*)	
State model sigma point propagation	$\mathcal{X}^i_{k\|k-1} = f(\mathcal{X}^i_{k-1\|k-1})$
State mean	$\hat{x}_{k\|k-1} = \sum_{i=0}^{2n} w_i\, \mathcal{X}^i_{k\|k-1}$
State error covariance	$P_{k\|k-1} = \sum_{i=0}^{2n} w_i\, [\mathcal{X}^i_{k\|k-1} - \hat{x}_{k\|k-1}][\mathcal{X}^i_{k\|k-1} - \hat{x}_{k\|k-1}]^T$
Measurement sigma point propagation	$\Upsilon^i_{k\|k-1} = h(\mathcal{X}^i_{k\|k-1})$
Measurement mean	$\hat{y}_{k\|k-1} = \sum_{i=0}^{2n} w_i\, \Upsilon^i_{k\|k-1}$
Correction (*A posteriori*)	
Measurement covariance	$P_{yy,k\|k-1} = \sum_{i=0}^{2n} w_i\, [\Upsilon^i_{k\|k-1} - \hat{y}_{k\|k-1}][\Upsilon^i_{k\|k-1} - \hat{y}_{k\|k-1}]^T$
Cross-covariance	$P_{xy,k\|k-1} = \sum_{i=0}^{2n} w_i\, [\mathcal{X}^i_{k\|k-1} - \hat{x}_{k\|k-1}][\Upsilon^i_{k\|k-1} - \hat{y}_{k\|k-1}]^T$
Kalman gain	$K_k = P_{xy,k\|k-1} P_{yy,k\|k-1}^T$
State estimate	$\hat{x}_{k\|k} = \hat{x}_{k\|k-1} + K_k(z_k - \hat{y}_{k\|k-1})$
Covariance estimate	$P_{k\|k} = P_{k\|k-1} - K_k P_{yy,k\|k-1} k_k^T$

3.1.6   Variable Structure Filter-based

In 2003, Saeid Habibi introduced the variable structure filter (VSF) concept developed for linear applications [65]. Later in 2006, the author proposed a new formulation of the methods named extended variable structure filter (EVSF) to estimate nonlinear systems [77]. In the subsequent year, the smooth variable structure filter (SVSF) concept was introduced in [78] to eliminate the chattering effect that can reduce the estimation efficiency [39].

The algorithm has been implemented and benchmarked against other estimation techniques applied for SOC estimation. SVSF and EKF were applied in six different battery models, a combined model, a simple model, zero-state and one-state hysteresis models, and enhanced self-correcting models of two and four states to benchmark their accuracy in the SOC estimation [79]. The work showed through UDDS cycle that enhanced self-correcting model (four-state) delivered the best terminal voltage among all six models and concluded that SVSF provides superior estimation accuracy than EKF when combined with the same battery model.

In [51], SVSF was implemented for SOC estimation along with a fast upper-triangular and diagonal recursive least squares (FUDRLS) and recursive total least squares (RTLS) algorithms, processing parameter identification and capacity, respectively, and benchmarked against a dual extended Kalman filter model. The simulations demonstrated that the model offered a slightly higher SOC estimation precision than the DEKF and stated to be computationally more efficient. The algorithm had its robustness tested in [80]. The work approach was based on an

offline parameter estimation by a genetic algorithm (GA) of a new and aged cell providing just one set of a first-order R-RC ECM for the entire SOC range. Providing the limited ECM model, SVSF could quickly converge to the true value, initial SOC set in 80 and 50% for the new and aged cell, respectively, in the mix of UDDS, HWFET, and US06, up to about 50% SOC when it diverged. A higher-order ECM and sets of parameters for different SOC levels would probably solve the issue.

A new variant of the SVSF was presented, namely SVSF with a variable boundary layer (SVSF-VBL) [66]. Its capability was later explored in [52] against the SVSF and EKF in estimating a simulated vehicle's battery SOC and terminal voltage in AVL CRUISE software. SVSF-VBL outperformed the two other estimators, with EKF offering the least reliable estimation.

3.1.6.1   Variable Structure Filter (VSF)

The VSF is a state estimation strategy that can be employed in linear systems. The method, which operates in a predictor-corrector mode, works with a gain that directs the state towards the true value switching it back and forth, resulting in a discontinuous corrective action within an existence space β of unknown width, Figure 3.4. Different from the Kalman filter, the strategy eases the trial error tuning [65]. The concept aims at the stability and convergence of the state in high modelling uncertainties where Kalman filter-based algorithms may have the estimation compromised [39].

The estimation process is given in Table 3.5 [65]. Where, as a first step, the state estimate prediction $\hat{x}_{k|k-1}$ is calculated by means of the system matrix Φ, the previous a posteriori state $\hat{x}_{k-1|k-1}$, the control matrix G, and the input/control vector u_{k-1}. The measurement estimate and error are computed terminating the prediction phase. In the method correction phase the VSF gain is computed with the equation described in Table 3.5. Where the H^+ stands for the pseudoinverse of the output matrix, the Υ is the constant diagonal gain matrix with elements ≤ 1, $\circ$ is the Schur product, V_{max} and W_{max} are the measurement and system noise upper bounds, respectively. $\tilde{\xi}_{max}$, $\tilde{\delta}_{max}$, and $\widetilde{H}_{max}$ indicate the upper bounds for uncertainties. Finally, the state updated $\hat{x}_{k|k}$ is calculated.

Table 3.5: Variable structure filter algorithm.

Prediction (*A priori*)	
State estimate	$\hat{x}_{k|k-1} = \Phi\hat{x}_{k-1|k-1} + Gu_{k-1}$
Measurement estimate	$\hat{z}_{k|k-1} = Hx_{k|k-1}$
Measurement error	$e_{z_{k|k-1}} = z_k - \hat{z}_{k|k-1}$
Correction (*A posteriori*)	
VSF gain	$\begin{aligned} K_{VSF} = \Phi^{-1}H^+(\|&|H\Phi|_{ABS}\{\Upsilon|H^+|_{ABS}|e_{z_{k|k-1}}|_{ABS} \\ &+ |\Phi^{-1}H^+\tilde{\xi}_{max}z_k|_{ABS} + [|H^+|_{ABS} \\ &+ |\Phi^{-1}H^+|_{ABS}(\tilde{\xi}_{max}+I)]V_{max} \\ &+ |\Phi^{-1}H^+\tilde{\delta}_{max}u_k|_{ABS} + (|\Phi^{-1}|_{ABS} \\ &+ |\Phi^{-1}H^+\widetilde{H}_{max}|_{ABS})W_{max}\}|_{ABS} \\ &\circ S_{gn}(e_{z_{k|k-1}}) \end{aligned}$
Estimate update	$\hat{x}_{k|k} = \hat{x}_{k|k-1} + K_{VSF}$

3.1.6.2   Smooth Variable Structure Filter (SVSF)

The SVSF surged as an improved version of the VSF that can be employed in nonlinear systems [39]. The method is considered to be robust to model uncertainties [66], providing some features described as follows [78]: SVSF performance is improved when the upper bounds are well defined, offering the robustness from the variable structure control concept; the trial and error tuning is alleviated due to the possibility of recognizing the uncertainty source and specifying a bound to it; it has a second performance indicator other filters such Kalman-based, and particle filters are not elaborated with that can measure the degree of modelling uncertainty.

In the strategy concept, the estimated state is directed to the existence space β that varies over time and contains the true state trajectory. The state estimation is then forced to remain within β generating a discontinuous corrective action of high-frequency, chattering effect, bringing degradation to the estimation [39]. To overcome this detrimental effect, a smooth function called smooth boundary layer Ψ, illustrated in Figure 3.4 (b), of known width can be incorporated into the gain depicted in Table 3.6 through a saturation function equation 3.8. However, the state smoothing is only provided if $\Psi>\beta$, otherwise the chattering effect persists within the existence space β [78]. The filter convergence is dictated by the value of γ (diagonal gain, coefficient matrix) that is set to be between zero and one.
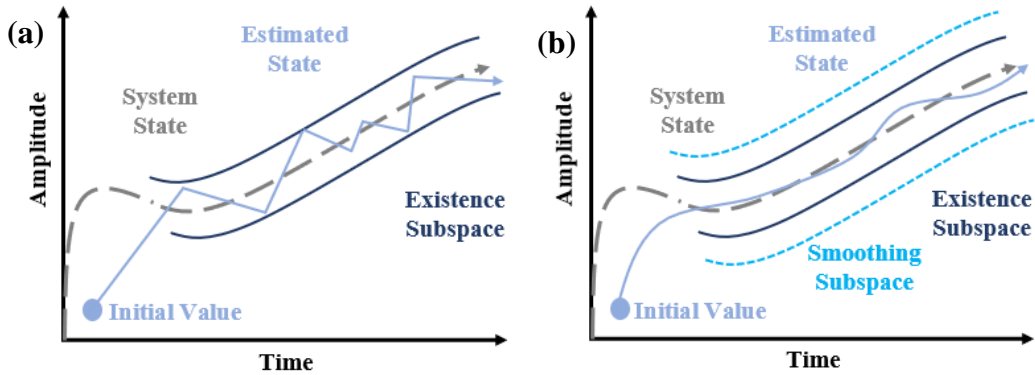
Figure 3.4: VSF (a) and SVSF (b) state estimation concepts, adapted from [78].

$$sat(\psi_i^{-1} e_{z_{k|k-1}}) = \begin{cases} 1, & e_{z_{k|k-1}}/\psi_i > 1 \\ e_{z_{k|k-1}}/\psi_i & -1 \leq e_{z_{k|k-1}}/\psi_i \leq 1 \\ -1, & e_{z_{k|k-1}}/\psi_i \leq -1 \end{cases} \qquad 3.8$$

SVSF process presented in Table 3.6 [78] starts with the nonlinear function composed of a posteriori states estimate $\hat{x}_{k-1|k-1}$ of previous step and the input vector u_{k-1} to obtain the prediction of the state estimate $\hat{x}_{k|k-1}$. Measurement estimate and error are calculated as in VSF. The correction phase counts on the SVSF gain obtained using the predicted measurement error $e_{z_{k|k-1}}$, a prosteriori error $e_{z_{k-1|k-1}}$ from last step and, the smooth boundary layer Ψ and coefficient matrix γ tuned for chattering effect diminishing and ensure stability, respectively. Finally, measurement estimate and error are computed for the next step calculation.

Table 3.6: Smooth variable structure filter algorithm.

Prediction (*A priori*)	
State estimate	$\hat{x}_{k|k-1} = f(\hat{x}_{k-1|k-1}, u_{k-1})$
Measurement estimate	$\hat{z}_{k|k-1} = Hx_{k|k-1}$
Measurement error	$e_{z_{k|k-1}} = z_k - \hat{z}_{k|k-1}$
Correction (*A posteriori*)	
SVSF gain	$K_{SVSF_k} = H^+ diag\left[\left(\left|e_{z_{k|k-1}}\right| + \gamma \left|e_{z_{k-1|k-1}}\right|\right) \circ sat(\psi^{-1} e_{z_{k|k-1}})\right] diag(e_{z_{k|k-1}})^{-1}$
Estimate update	$\hat{x}_{k|k} = \hat{x}_{k|k-1} + K_{SVSF_k} e_{z_{k|k-1}}$
Measurement estimate	$\hat{z}_{k|k} = H_k \hat{x}_{k|k}$
Measurement error	$e_{z_{k|k}} = z_k - \hat{z}_{k|k}$

3.1.6.3 Smooth Variable Structure Filter with Variable Boundary Layer (SVSF-VBL)

The standard SVSF considers a constant smooth boundary layer set based on the knowledge of the system covering the model uncertainties and the upper limit of measurement noise [39]. This approach can lead to a conservative choice of the boundary layer preventing the algorithm from reaching optimal estimation. The SVSF-VBL was proposed in [66] to address this conservative boundary setting through a partial derivative of the *a posteriori* covariance matrix concerning the smooth boundary layer, equation 3.9, to obtain the time-varying smooth boundary

layer ψ_k , leading to an optimal state estimation as in the Kalman filter. The ψ_k is

denoted as the upper and lower optimal boundery layers depicted in Figure 3.5.

$$\frac{\partial(trace[P_{k|k}])}{\partial\psi} = 0 \hspace{3cm} 3.9$$
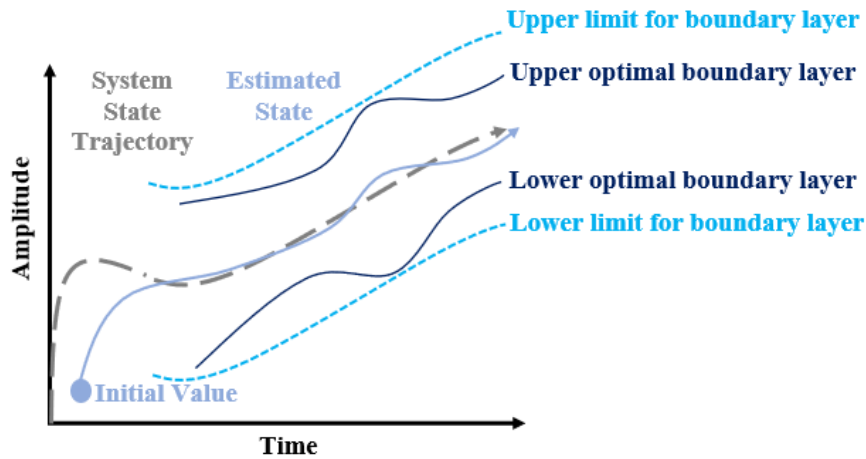
Figure 3.5: SVSF-VBL well-defined case, adapted from [66].

The method offers an optimal state estimation from KF and the robustness

imposed by the SVSF algorithm through a saturation function illustrated in Figure

3.6 that verifies the width of the time-varying smooth boundary layer ψ_k against

the constant smooth boundary layer, here referred to as Upper and lower limit for

boundary layer ψ_{lim}, employed in the standard SVSF. Note in Figure 3.5 the ψ_k

amplitude varies over time in relation to the system state trajectory and remains

within upper and lower ψ_{lim}. This scenario means the model had the case well-

designed not presenting any fault that requires the standard SVSF gain to take over

to maintain stability.
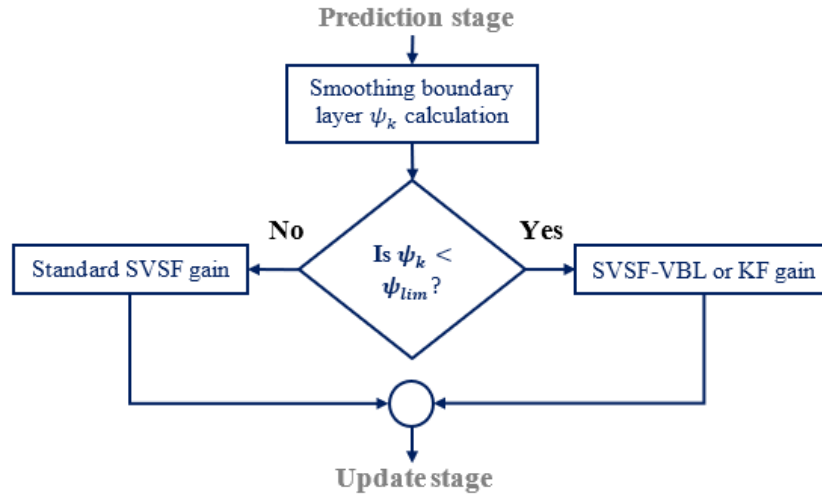
Figure 3.6: Summary of the SVSF-VBL strategy for state estimation stability, adapted from [66].

The algorithm process has the exact prediction stage calculations found in the EKF when treating a nonlinear system with the state estimate and covariance matrix. The correction phase of the method begins with the calculation of the smooth boundary layer according to the combined error and the measurement/measurement covariance S_k that is illustrated as $(H_k P_{k|k-1} H_k^T + R_k)^{-1}$, Table 3.7. At this point, the saturation function, equation 3.10, is applied to verify the gain to be used at the step. Posteriorly, the state and covariance estimates are updated.

$$sat(Gain) = \begin{cases} SVSF - VBL\ gain, & \psi_k < \psi_{lim} \\ Standard\ SVSF\ gain, & \psi_k \geq \psi_{lim} \end{cases} \qquad 3.10$$

Table 3.7: SVSF with variable boundary layer algorithm.

Prediction (*A priori*)	
State estimate	$\hat{x}_{k|k-1} = f(\hat{x}_{k-1|k-1}, u_{k-1}, w_{k-1})$
Measurement estimate	$\hat{z}_{k|k-1} = Hx_{k|k-1}$
Measurement error	$e_{z_{k|k-1}} = z_k - \hat{z}_{k|k-1}$
Covariance estimate	$P_{k|k-1} = F_{k-1}P_{k-1|k-1}F_{k-1}^T + Q_{k-1}$
Correction (*A posteriori*)	
Combined error	$E_k = \left|e_{z_{k|k-1}}\right| + \gamma \left|e_{z_{k-1|k-1}}\right|$
Smoothing boundary layer	$\psi_k = (E_k^{-1}HP_{k|k-1}H^T(H_kP_{k|k-1}H_k^T + R_k)^{-1})^{-1}$
VBL gain	$K_{VBL_k} = H^{-1}E_k\psi_k^{-1}$
Estimate update	$\hat{x}_{k|k} = \hat{x}_{k|k-1} + K_{VBL_k}e_{z_{k|k-1}}$
Covariance estimate	$P_{k|k} = (I - K_kH_k)P_{k|k-1}(I - K_kH_k)^T(K_kR_kK_k^T)$
Measurement estimate	$\hat{z}_{k|k} = H_kx_{k|k}$
Measurement error	$e_{z_{k|k}} = z_k - \hat{z}_{k|k}$

3.1.7   Particle Filter (PF)

Particle filter is employed to estimate states of nonlinear systems with non-Gaussian noise distribution [39], [81]. The approximation of the probability density function or nonlinear characteristics is achieved by applying the Monte Carlo

technique with a random set of particles [81]. That makes PF a method that works in a global approach, which brings a higher computational cost, making the method impractical for certain online applications. Nevertheless, it has attracted more attention in the past decade due to improvements in computational power [39].

3.1.8   H∞ Filter

The H-infinity filter theory was introduced in [82]. The technique is a robust filter that is not affected by the process and measurement noises at specific conditions. However, its performance might be impacted by battery aging and temperature [81]. Contrarily to Kalman based filters, H∞ filter can handle nonzero mean uncertainties.

3.2 Battery State of Health Estimation Methods

To ensure a safe operation and provide accurate information about the battery states of electric vehicles, battery management systems (BMSs) are required. One of the challenges BMS faces is delivering the battery state of health (SOH) that is essential for energy management and vehicle performance. SOH estimation uses some indicators to describe the state, and two of the most used are the battery capacity and the internal resistance [83]. While the capacity is related to the energy stored in the battery and the vehicle's driving range, the internal resistance impacts the power delivered by the storage system. Along the time, internal resistance increases and capacity decreases. For vehicle purposes, the end of life (EoF) is

considered when the energy storage unit delivers 80% of its initial capacity [3], [84], [85].

According to [37], there are basically three SOH estimation methods: Experimental methods, Model-based methods (including adaptive filtering) and Machine Learning methods. Figure 3.7 displays the model-based methods explored in this section and others not surveyed but worth mentioning.
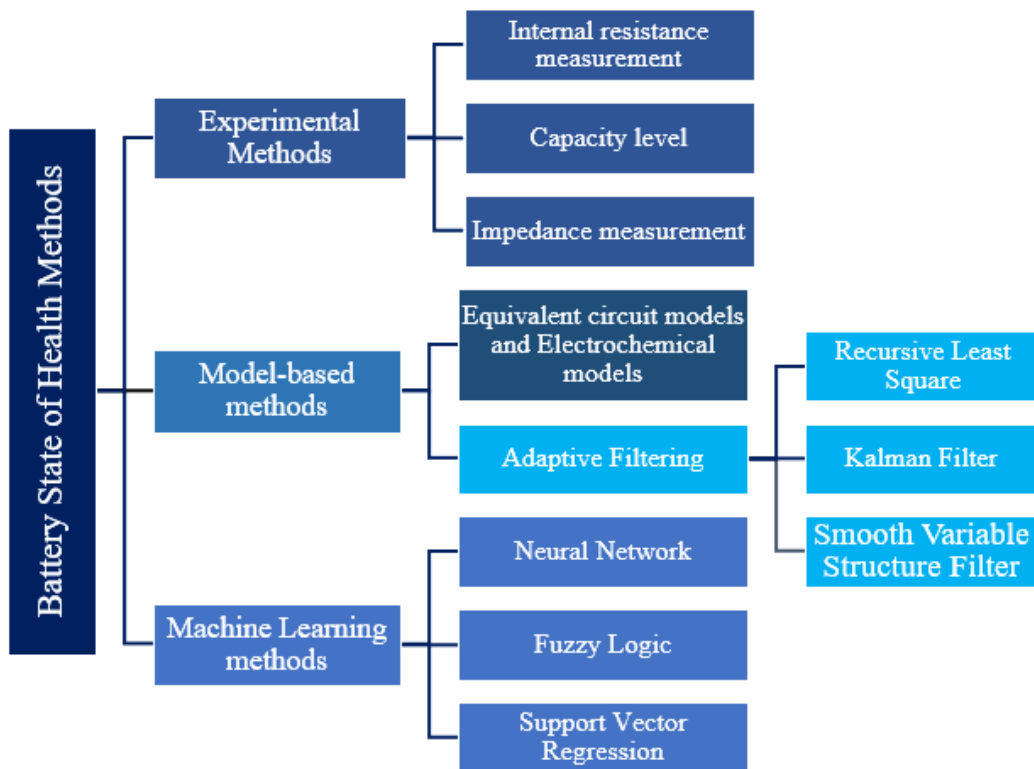
Figure 3.7: State of health estimation methods.

3.2.1   Recursive Least Square based Methods

Recursive least square based algorithms to estimate battery parameters have been vastly studied in the literature [86], [87], [88], [89]. Approaching the parameter estimation with the method has advantages like only one tuning

parameter to be dealt with, the forgetting factor λ that is typically between 0.95 and 1 [86], [90], and its low computational complexity [89].

A combination of the RLS outfitted with multiple fixed forgetting factors optimized by particle swarm optimization (PSO) was proposed and compared to an RLS optimized by a single objective genetic algorithm (SOGA) and a third RLS optimized by multi-objective genetic algorithm for parameter estimation in [87]. The proposed model obtained success over the two others presenting lower OCV mean square error. In [89], a square-root recursive least squares (SR-RLS) was employed to provide the battery parameters estimation for SOC estimation estimated by an SVSF algorithm. In [91], an adaptive forgetting factor recursive least square (AFFRLS) method was proposed to identify the ECM parameters and feed the online voltage predictor mode. The method presented superiority compared with forgetting factor recursive least square (FFRLS) and variable forgetting factor recursive least square (VFFRLS) in terms of precision and time processing.

3.2.1.1   Recursive Least Square

RLS parameter estimation uses a recursive implementation and is represented by the regressed form shown in equation 3.11.

$$y_k = \theta^T \varphi_k \qquad\qquad 3.11$$

where y_k is the measured voltage, θ^T stands for the desired parameters to be estimated, and φ_k is the regressor comprised of known parameters.

The set of equations composing the algorithm is displayed as described and demonstrated in Table 3.8. First, a Kalman gain is calculated with the previous

covariance matrix P_{k-1} and the forgetting factor λ. A second step is the update o the covariance matrix, and finally, the estimate update is computed.

Table 3.8: Recursive least square algorithm.

Kalman gain	$K_k = P_{k-1}\varphi_k(\lambda + \varphi_k^T P_{k-1}\varphi_k)^{-1}$
Covariance matrix	$P_k = \dfrac{1}{\lambda}(I - K_k\varphi_k^T)P_{k-1}$
Estimate update	$\hat{\theta}_k = \hat{\theta}_{k-1} + K_k(y_k - \hat{\theta}_{k-1}^T \varphi_k)$

3.2.2   Kalman Filter Based Methods

As mentioned in topic 3.1.5, Kalman filter is extensively employed for SOC estimation in the literature. Likewise, it is vastly employed in parameter estimation [37]. [92] imployed a dual extended Kalman filter (DEKF) algorithm to estimate the battery parameters parallelly with the states. The work revealed that using the DEKF improved the SOC estimation as the battery aged compared with a plain EKF without parameter update. Nevertheless, admitted the algorithm needed improvements for real-world application. Another approach was carried with an adaptive extended Kalman filter (MAEKF) created to estimate the SOC of aged cells in [70]. The author showed the method was able to estimate the battery SOC with a maximum of 4% error in a constant current discharge, while an EKF model had an error close to 30%. However, the method requires a constant current

discharge to update the ECM model, making it unfeasible in the automotive application.

A dual adaptive extended Kalman filter is proposed and matched with a recursive least square extended Kalman filter (RLS-EKF) model and a simple EKF under the dynamic stress test (DST) conditions and Beijing Dynamic Pressure Test Conditions (BJDST) [93]. The developed algorithm improved the SOC estimation compared to the other two in both conditions tested, and the work demonstrated joint model could enhance the estimation by three times compared to a single model. Recently, an improved extended Kalman filter (IEKF) equipped with concepts from noise adaptation, a fading filter and linear-nonlinear filtering was developed in [94]. In [95], a double extended Kalman filter for SOC and parameter estimation was presented and validated through a new and aged battery submitted to UDDS drive cycles. The authors compared the influence of neglecting the battery capacity, parameters and SOC-OCV curve update in the SOC estimation and concluded the last impacted the most.

3.2.3   Smooth Variable Structure Filter

The Smooth variable filter is applicable in SOH estimation as Kalman filter variants. In [96], a chattering indicator was proposed to address the health regarding the battery capacity fade. As SVSF inhibits the chattering effect, the author attributes a smoothing layer Ψ width lower than the existence layer β and hence creates a chattering effect with mean and standard deviation calculated along with the battery aging that can be applied for monitoring the capacity degradation. In the

same work, pure SVSF and EKF models are employed to estimate the battery SOC in new and aged cells (80% SOH). The outcome was similar to the two methods for the new cell SOC estimation, RMSE around 1% for both, and the advantage of SVSF presenting 1.9% SOC RMSE while EKF had 2.8% for the aged cell.

3.3 Concluding Remarks

There is a vast number of estimation algorithms. Through Figure 3.1, the developer can have a lead on what path to take. ECM based method combined with an adaptive filter shows a good relationship between implementation complexity and error, having the potential to achieve low errors similar to the electrochemical models but with less complexity. Smooth variable structure filter depicts good results in estimating the battery SOC and robustness to modelling uncertainties. This robustness is attractive as in a real application, especially because of noise and perturbations present in the instrument measurement and external factors. Also, it permits less accurate pieces of equipment to be installed onboard a vehicle, consequently contributing to a more affordable final product. The extended Kalman filter is a more spread and well-known estimation method that offers an optimal estimation, and working together with other estimation models such as SOH resistance and SOH capacity could provide very good results. Hence, the application of the estimation algorithm is a developers' choice based on his affinity with the method and scenario to be implemented.

Chapter 4

Fast Charging Aging Test: Design of

Experiment

The strong impact charging has on battery aging could be better investigated by controlling the anode voltage and preventing it from reaching negative values; however, this strategy would require prepared cells with a third terminal placed in the electrolyte. Therefore, an empirical aging test was developed. This chapter explores a design of experiment contemplating four charging profiles assumed in the literature to have some beneficial effect on the battery's lifespan. These tests took place in the the Battery Laboratory facility in Centre for Mechatronics and Hybrid Technologies at McMaster Automotive Resource Centre.

4.1 Design of experiment

4.1.1   Lithium-ion Cell Specifications

The Li-ion battery tested is a cylindrical cell model INR21700-30T, Figure 4.1, manufactured by Samsung SDI Co., Ltd. Its specifications considered for test design is described in Table 4.1.

Figure 4.1: INR21700-30T Samsung cell.

Table 4.1: Cell main specifications [97].

Parameter	Specification
Discharge capacity at 1C [mAh]	3000
Nominal voltage [V]	3.6
Maximum voltage [V]	4.2
Discharge cut-off voltage [V]	2.5
Maximum current discharge [A]	35 A (at 25°C)
Standard charge	CCCV, 1.5 A, 4.2 V, 150 mA cut-off
Fast charge	CCCV, 4A, 4.2V, 100mA cut-off
Charge operating temperature [°C]	0 to 50
Discharge operating temperature [°C]	-20 to50

4.1.2   Experimental Setup

The Samsung 30T cells were tested in an eight cubic feet Envirotronics thermal chamber with a -63 to 177°C temperature range, Figure 4.2, capable of fitting the four Arbin 60A cell holders used in the test, Figure 4.3. A 60 amperes/5 volts Arbin Battery Tester channel, Figure 4.2, of voltage and current accuracy of 0.04% of full scale (+/-2mV and +/-24mA) provided with an auxiliary temperature

module of +/-1°C accuracy was employed to power the batteries and data acquisition.

Figure 4.2: Environmental Chamber (left) and battery tester (right) utilized in the test.
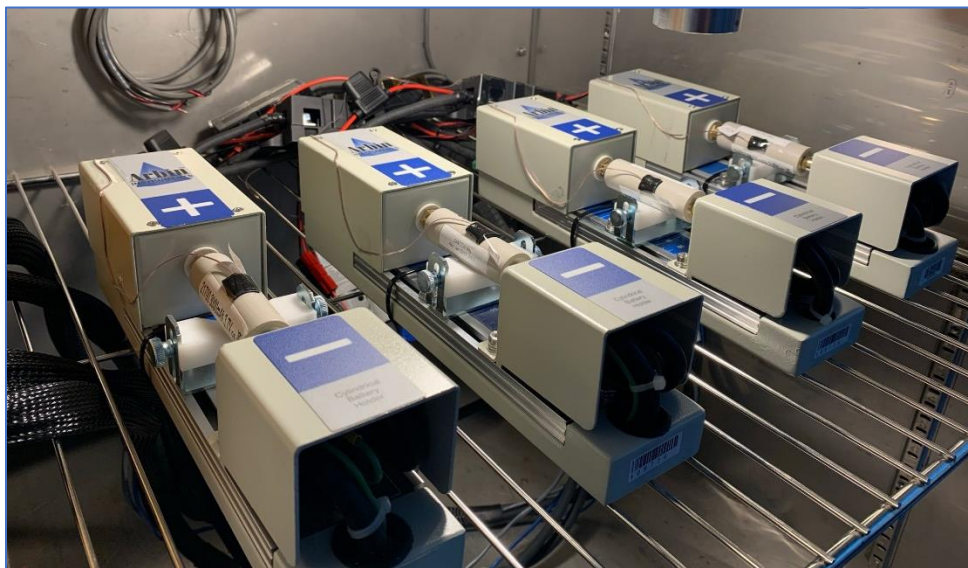
Figure 4.3: Cylindrical cells fixed on the cell holders inside the environmental chamber.

A computer equipped with the Arbin software MITS Pro was employed for the controlling and data analysis. The schematic of the test setup is presented in Figure 4.4. A CAN-bus communication between the battery tester thermal chamber is not depicted in the image once the temperature remained constant at 25°C the whole test; hence the communication between the equipment was eliminated.
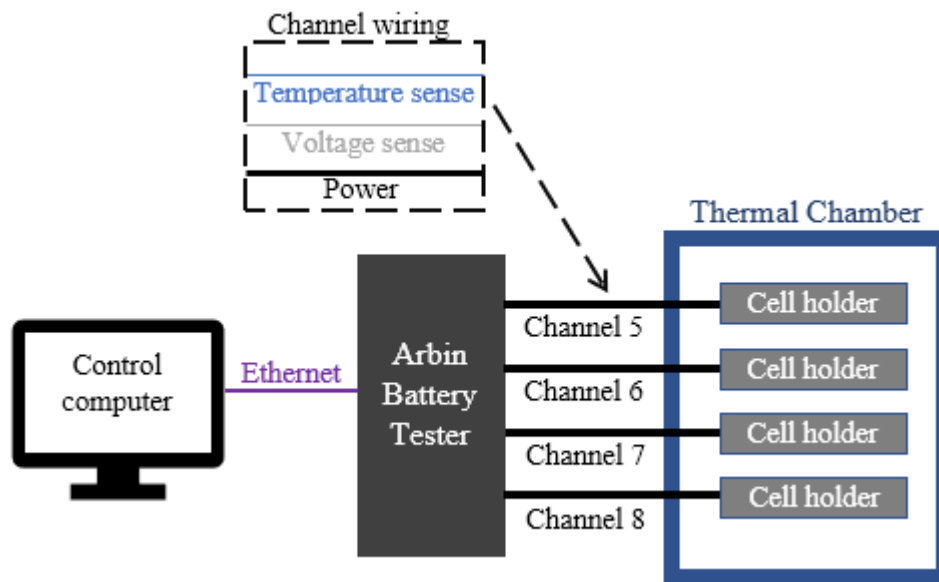
Figure 4.4: Battery test setup.

4.1.3   Test Limits definition

Test constraints are dictated by the cell and battery cycler specifications. The chamber does not impose any restrictions once the test is run at 25°C the whole time. Table 4.2 reveals the safe limits imposed by the Samsung cell and the Arbin battery cycler considered in the characterization tests and fast charging protocols design. It is noticeable the battery cycler is not the limiting variable in the test, hence the battery cell parameters are considered for safe control.

Table 4.2: Test safe limits.

Limited by	Parameter	Value
Cell	Maximum temperature on the cell surface [°C]	50
	Maximum voltage [V]	4.2
	Minimum voltage [V]	2.5
	Maximum current [A]	35
	Minimum current [A]	-35
Cycler	Maximum voltage [V]	5
	Maximum current [A]	60

4.1.4   Current Protocol Design

In the published literature, many authors present charging protocols claimed to impact positively in battery life. However, the variation of experiment design among the works and even different approaches in the same work inhibits a direct and fair comparison of charging protocols. For instance, some apply different mean currents leading to different charging times and compare the life cycle results; others test the cells submitting them to the same charging time but not the same mean current, which causes discrepancies in the depth-of-discharge. The designed protocols presented in this chapter had these issues considered for fair comparison at the end of life. Hence, all profiles were designed to have the same mean current and charging time.

The parameters considered for the design of the charging protocols are the limitations of the battery, the SOC range desired, equipment employed for the test

and the recent fast charging time of vehicles. Considerations made, the parameters shown in Table 4.3 were set for the profiles.

Table 4.3: Profile parameters.

SOC range [%]	10 to 80
Charging time [min]	15
Mean current [C-rate]	2.8

4.1.4.1   Constant Current (CC)

As mentioned in topic 2.2, the CCCV protocol is a benchmark for other designed charging algorithms in the literature. Therefore, it is the first of the four protocols created. The CV phase is only used in case the resistance increases and, consequently, the charging voltage V_{ch} surpasses the maximum voltage of the cell V_{max} before it reaches 80% SOC. The 2.8C CC charging follows the parameters in Table 4.3 and is illustrated in Figure 4.5.
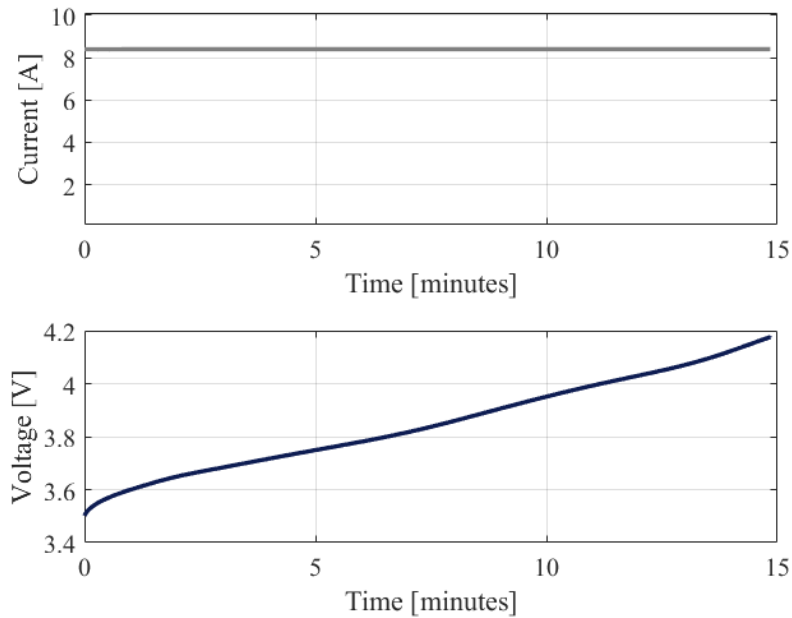
Figure 4.5: Designed Constant Current protocol.

4.1.4.2   Boost Charging (BC)

Boost charging comes as the second designed profile. As aforementioned, the strategy offers faster charging with no degradation to the battery. Also, it is appealing to customers as in a very short period, the battery can be charged from a low SOC to levels that would be enough to have a reasonable amount of the vehicle driving range. The profile was calculated to charge the first 33.3% SOC, starting from 10%, within five minutes, then a second phase charges up to 80%, totalizing the fifteen minutes fast charging. As a starting point, the boost phase is set to be a constant current phase and lasts five minutes. Consequently, the protocol configures a 4C CC followed by a 2.2C CC phase, Figure 4.6.
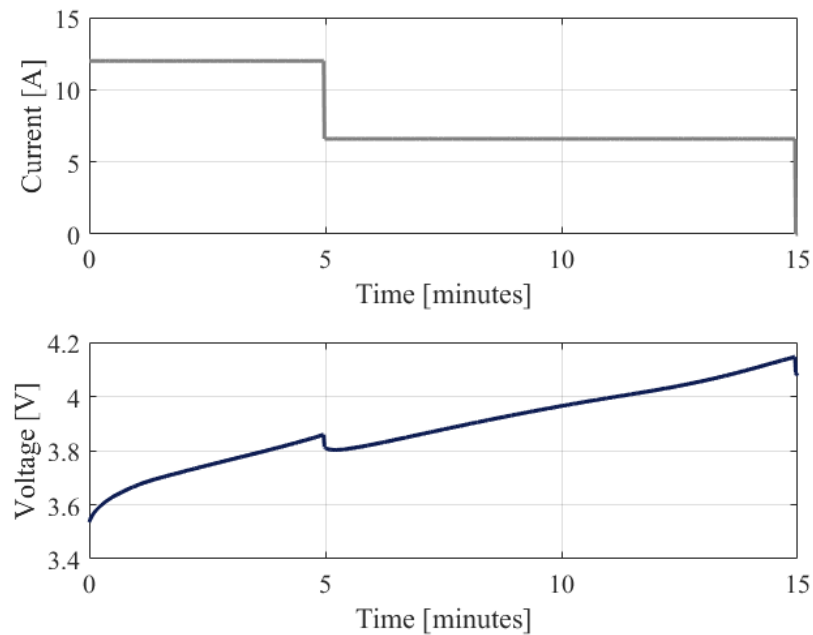
Figure 4.6: Designed boost charging protocol.

4.1.4.3   Boost Charging with Negative Pulse (BCNP)

Pulse charging has been investigated in the literature in many ways. PC with lower current protocols of different frequencies were compared, PC with negative pulse and current interrupt profiles were matched with same mean current, yet different frequency and duty cycle. Most of the works described in 2.5.1 do not study one variable only, maintaining other variables steady to conclude the influence this variable offers the battery. Therefore, the two last designed profiles were explicitly built to observe the influence of the negative pulses and rest periods in charging profiles. The third profile designed is the boost charging with negative pulse, Figure 4.7. The protocol features the parameters in Table 4.3, shares the same phase triggers exposed for BC, has 0.5Hz frequency and duty cycle of 95%.
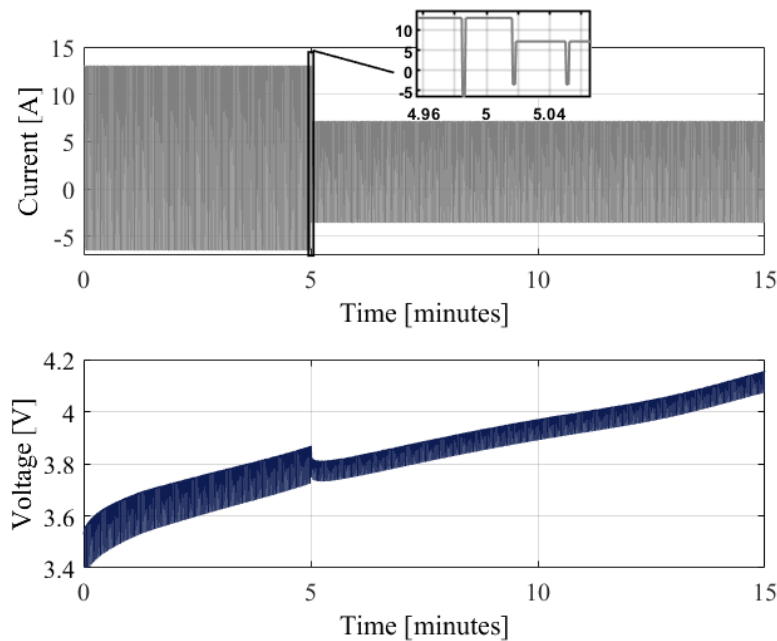
Figure 4.7: Designed boost charging with negative pulse protocol.

4.1.4.4   Boost Charging with Rest (BCR)

The last protocol is boost charging with rest, Figure 4.8. It shares all characteristics as BCNP except for the current amplitude of the positive pulses that is a little smaller in consequence of the rest instead of the negative pulses BCNP has. A summary of the profiles' parameters is portrayed in Table 4.4.
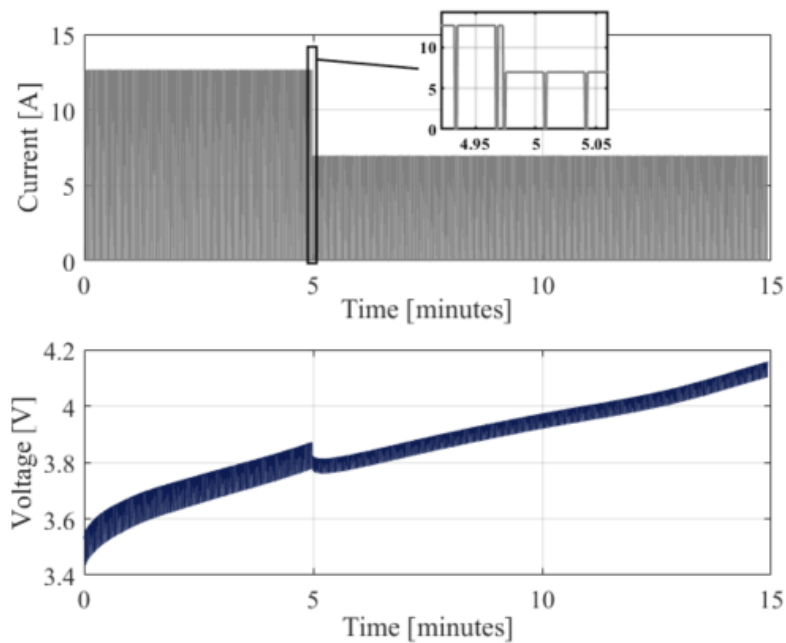
Figure 4.8: Designed boost charging with rest.

Table 4.4: Designed charging protocols summary.

Profile Step	CC	BC		BCNP		BCR	
	Step 1	Step 1	Step 2	Step 1	Step 2	Step 1	Step 2
	Constant Current	*Constant Current*	*Constant Current*	*PC with negative Pulse*	*PC with negative Pulse*	*PC with Rest*	*PC with Rest*
Transition Trigger	> 80% SOC or >4.2V	> 43.3% SOC	> 80% SOC or >4.2V	> 43.3% SOC	> 80% SOC or >4.2V	> 43.3% SOC	> 80% SOC or >4.2V
Charging current [C-rate]	2.80	4.00	2.20	4.32	2.38	4.21	2.32
Negative pulse current [C-rate]	-	-	-	2.16	1.19	-	-
Step length [min]	15	5	10	5	10	5	10
Charging Pulse width [s]	-	-	-	1.9	1.9	1.9	1.9
Negative Pulse width [s]	-	-	-	0.1	0.1	-	-
Rest time width [s]	-	-	-	-	-	0.1	0.1

4.1.5   Cell Characterization

In the experiment, cell characterization is performed every thirty fast charges to track the capacity retention and internal resistance of the batteries. The tests utilized for this aging test are explained as follows:

- **Open-Circuit-Voltage (OCV) Test:** Consists of discharging and charging the battery at a C/20 rate. It is employed every two schedules, or seventy-five cycles and is the first characterization test performed.

- **0.5C discharge:** It is a discharge at half a C-rate that is used in fast charges (FCs) and drive cycles (DCs) calculations. The schedule contains two 0.5C discharges at the beginning, and two additional ones after the first fifteen drive cycles of each schedule to update the battery capacity for the next fifteen FCs and DCs. The option of two discharges in a row is to provide a consistent value and not be influenced by the previous profiles the battery has been submitted to. So, the second 0.5C discharge is the one that feeds the inputs for the DCs and FCs triggers.

- **1C and 2C discharges:** These two tests keep tracking the battery's capability at higher depleting rates.

- **Hybrid pulse power characterization (HPPC):**   HPPC, described in [98], is employed every schedule to track the battery's internal

resistance over its SOC range throughout the aging test. Similarly, the

measured data in the test supports battery modelling.

- **Master Charge:** Before all characterization tests described above, a

    CCCV, 3 A, 4.2 V, 150 mA cut-off charging is performed to fully

    charge the cell.

- **0.33C 10% capacity charge:** This procedure is applied to prepare the

    battery for the first of the fast charges after either HPPC and 0.5C

    discharge procedures so that the SOC will be at 10%.

4.1.6 Cycle Discharging

Discharges post fast charging profiles are drive cycles calculated through a

backward-looking EV model to simulate the use of the cell in the Pacifica Plug-in

Hybrid (Chrysler) and be explored in the development of battery state estimation

models. A power simulation generated for a cell is scaled as demonstrated in

equation 4.1.

$$P_{cell}(t) = \frac{P_{d,in}(t) + P_{accessories}}{N_{cell,p} + N_{cell,s}} \qquad 4.1$$

Where $P_{d,in}(t)$ is the power requested by the drive at the instant t, $P_{accessories}$ is

the power consumed by the vehicle electrical accessories and is assumed to be

constant at 350 W, $N_{cell,p}$ and $N_{cell,s}$ are the number of cells in parallel and series

necessary to compose the 16.6KW Pacifica Plug-in Hybrid (Chrysler) battery pack.

The fifteen drive cycles deplete the battery from 80 to 10% SOC and are

assigned in the aging schedule in the following sequence: UDDS, HWFET, LA92,

US06, WLTP and Reordered_1 up to Reordered_9 and Reordered_US06. Reordered drive cycles are created from random small pieces chopped at every stop in the first four cited drive cycles listed, except for the Reordered_US06 that contains only random pieces of the US06 itself.

4.1.7 Test Procedure

At the test start, the chamber is set to 25°C, and a resting period of three hours is set to accommodate the cell's temperature. Additionally, the full schedule is manually selected to run, and the physical setup is verified through the temperature and voltage parameters reading in MITS Pro program.

The test is conducted with two alternating schedules that differ whether the OCV procedure is applied or not. Consequently, the lasting time of the schedules is 6.2 and 4.5 days with (full schedule) and without OCV, respectively. The test procedures durations are cell aging dependable and decrease as the cell ages.

Table 4.5 depicts the test steps ordered as they occur within the schedule.

Table 4.5: Aging test full schedule procedure.

Procedure	Duration Time [hours]
Master Charge	1.2
Open-circuit-voltage	41.3
0.5C discharge + master charge	3.2
0.5C discharge + master charge	3.2
1C discharge + master charge	2.2
2C discharge + master charge	1.7
Hybrid pulse power characterization	30
0.33C 10% capacity charge	0.3
Fast charging + drive cycles	29.6
Master charge + 0.5C discharge	3.2
Master charge + 0.5C discharge	3.2
0.33C 10% capacity charge	0.3
Fast charging + drive cycles	29.6
Master Charge	1.2

The end of the test is due when both the 0.5C discharging capacity reaches below eighty percent of the first capacity measurement and the cell internal resistance surpasses a rise of fifty percent of its original value. Figure 4.9 shows the sequence of actions taken along the battery aging test.
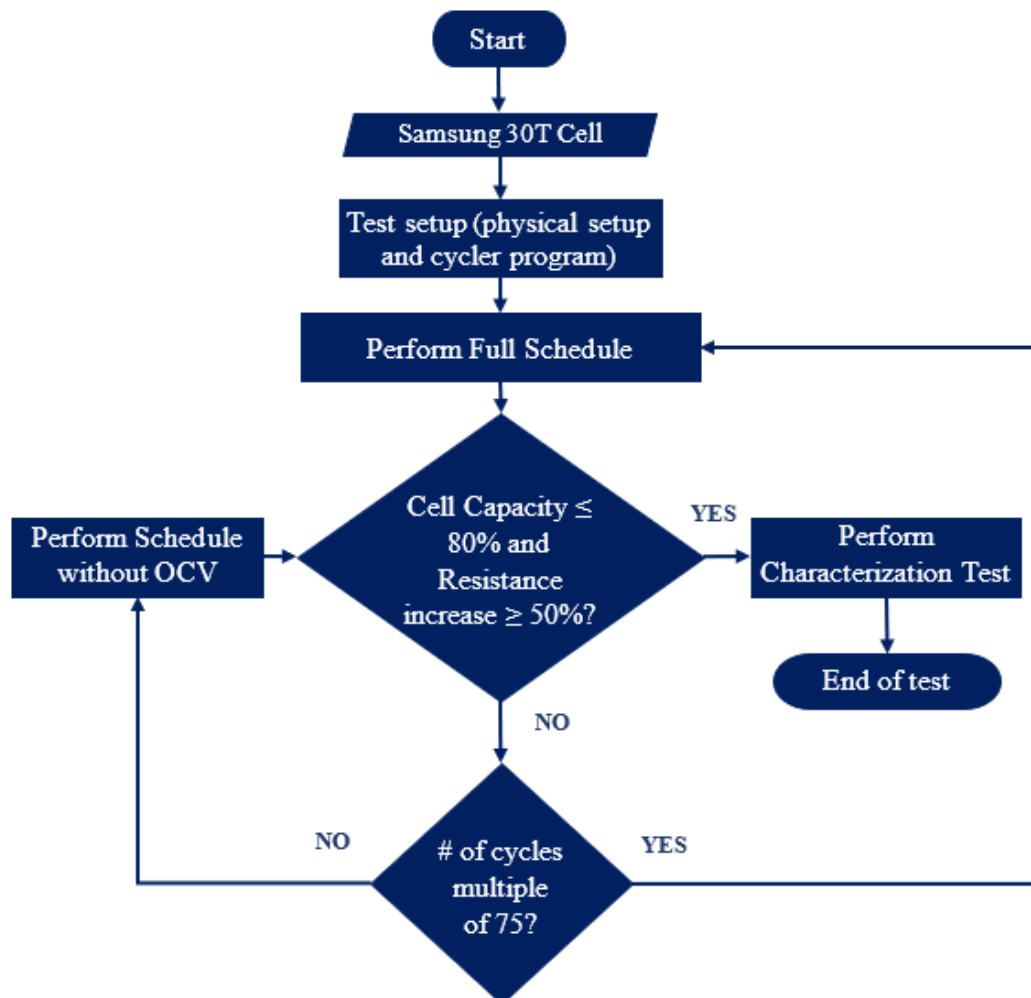
Figure 4.9: Aging test flowchart.

Chapter 5

Dual State Estimation Algorithm

State estimation methods are presented in Chapter 3. In this section, the dual state estimation algorithm (EKF/SVSF) created in MATLAB/Simulink has its development described from the choices concerning the type of battery modelling to the final tuning of the EKF/SVSF model.

5.1 Dual State Estimation Modelling

Chapter 3 presented various candidates for the state of charge and health estimation. The dual state estimation model is formed by an EKF to estimate the state of charge and an SVSF for capacity estimation. The combination of the two algorithms is illustrated in the following Figure 5.1. It requires voltage, current and temperature to process the calculations. Although it runs on symmetric parameters, the model is prepared to receive both charging and discharging ECM parameters.
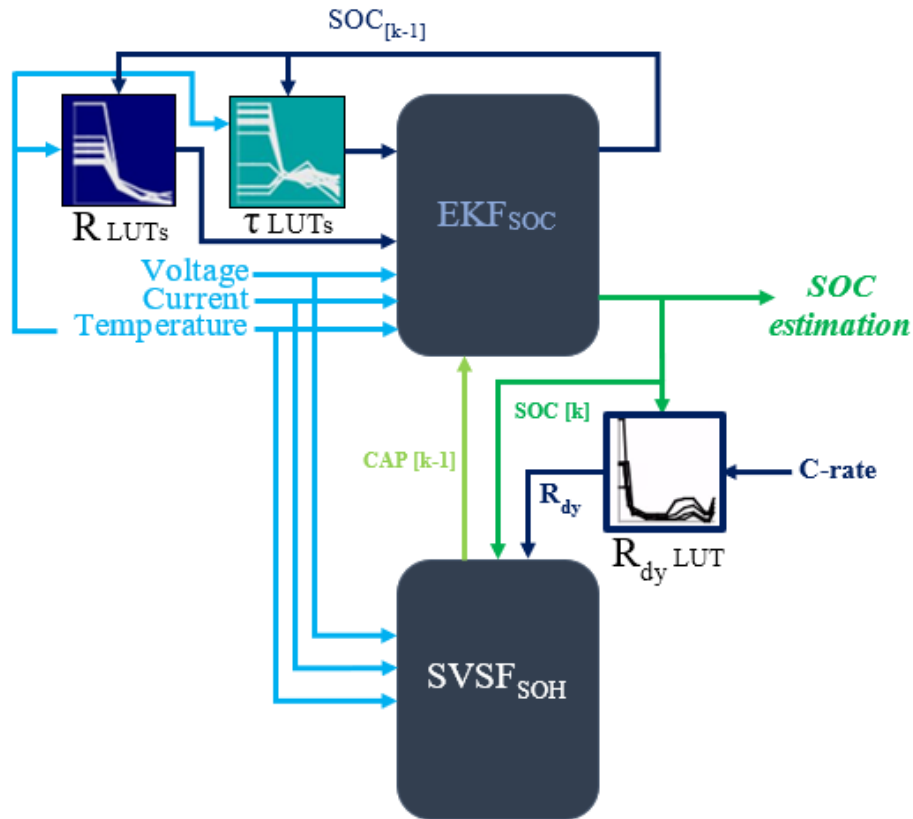
Figure 5.1: Dual state estimation algorithm.

For the initial SOC, the open circuit voltage based strategy presented in 3.1.2 is applied with the first voltage measurement considered as the OCV. The strategy eliminates the need for an initial SOC guess every time the algorithm starts. Additionally, this first measured voltage value is close to the actual OCV, even if there is a load from the low-voltage system, avoiding a large offset between the guess and actual SOC.

5.1.1   State of Charge Estimation Model

5.1.1.1 Battery Modelling

Battery modelling requires a series of characterization tests such as capacity discharges, open-circuit-voltage to obtain the SOC-OCV relationship, and hybrid pulse power characterization described in section 4.1.5. For its development, there are several approaches such as electrochemical models that describe the chemical reactions inside the battery, stochastic models that are supported on discrete-time Markov chains, analytical models that use empirical formulas to illustrate a battery characteristic, and the equivalent circuit models (ECM) that simulate the internal behaviour of the battery [99]. The latter is the method applied in this work's estimation model.

ECMs use compositions of resistances, capacitors and sometimes impedances to model the different behaviours happening inside the battery under charge/discharge currents. The approach has the advantage of delivering a reasonable performance for real-time applications. However, it lacks the ability to predict other battery states like aging, power and capacity losses.

The work in [63] compared the performance in the terminal voltage calculation of twelve types of ECM among combined, enhanced self-correcting of two and four-state low pass filters, RC models with and without hysteresis up to three branches. They show that the RC models present the lowest RMSE and that the use of hysteresis or the addition of RC branches can improve the accuracy of the voltage estimation. Nevertheless, RC with higher order than the second does

not decrease the error proportionally to increasing implementation complexity. [100] also demonstrated in his study that the second-order R-2RC model depicts a good trade-off between accuracy and implementation complexity.

Given the evidence shown by the previous works [63] and [100], and the circumstances of the proposed design of the experiment performed only at 25°C, a reasonable choice with a good trade-off between accuracy and model complexity is the 2nd order R-2RC equivalent circuit model, Figure 5.2.
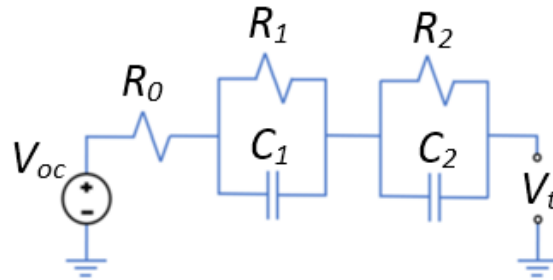
Figure 5.2: Second-order equivalent circuit model [63].

5.1.1.1.1   Second-order R-2RC model

Consider the Figure 5.2. R_0 represents the ohmic resistance of the battery concerning its internal components that is translated in the instantaneous drop in the terminal voltage of the battery at discharging. The branches containing the R's and C's describe the charge transfer resistance and the double layer capacitance of the cell, respectively, or in other words, the dynamics of the battery. V_{oc} stands for the open-circuit-voltage that is transformed from the state of charge through the SOC-OCV relationship curve, Figure 5.3. V_t is the output of the model that can be measured in the terminals of the cell.
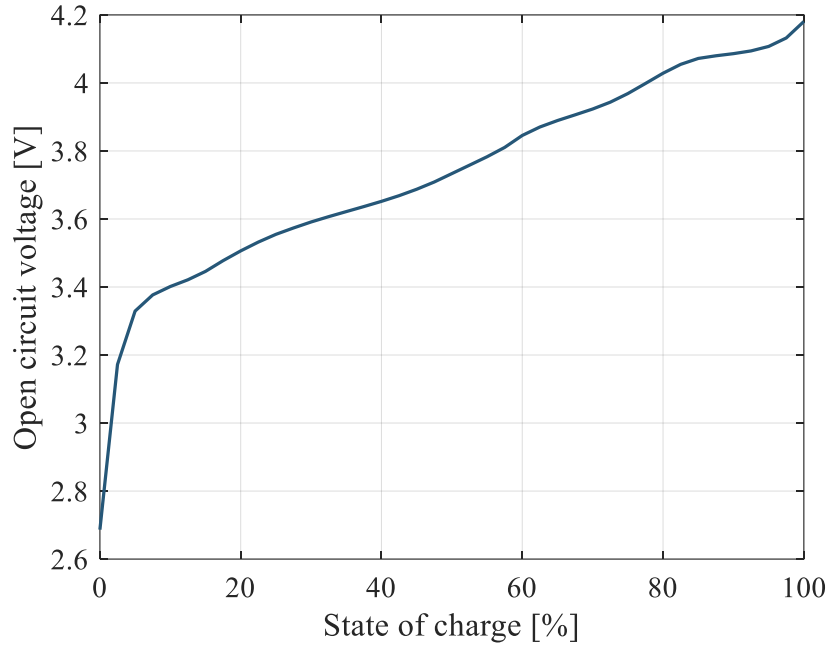
Figure 5.3: Samsung 30T SOC-OCV relationship curve calculated from the average C/20 charge/discharge curves (BCR protocol test).

The second-order R-2RC ECM is described in the discrete time domain in equations 5.1, 5.2 and 5.3.

$$V_{i,k} = 1 - \frac{\Delta t}{R_i C_i} V_{i,k-1} + \frac{\Delta t}{C_i} I_{k-1} \qquad 5.1$$

$$SOC_k = SOC_{k-1} - \frac{\eta \Delta t}{Q} I_{k-1} \qquad 5.2$$

$$Vt_k = OCV(z_k) - V_{1,k} - V_{2,k} - R_0 I_k \qquad 5.3$$

where $V_{i,k}$ denotes the states $V_{1,k}$ and $V_{2,k}$ that are the voltages of the RC elements, being i the number of the RC. R_i and C_i are the resistance and capacitance, Δt is the sampling period, and I_{k-1} stands for the current input. The state of charge SOC_k is computed with the previous SOC_{k-1}, the Columbic efficiency of the cell η, the battery capacity Q. The calculation of the output Vt_k is through the OCV achieved

as a function of the SOC calculated, the other states and the internal resistance multiplied by the current passing through the battery.

The designed model counts on symmetric parameters for charging and discharging. Consequently, for a 2nd-order R-2RC ECM, five parameters R_0, R_1, R_2, C_1, and C_2 are estimated for each SOC level in the HPPC curve, forming a lookup table (LUT) as a function of the SOC. The obtainment of these parameters is described in the following topic.

5.1.1.1.2   Parameter Estimation

The ECM parameter estimation task is performed using optimization methods/tools that input random values for the parameters to be estimated and compare the output with a measurement until either the minimum cost function is reached, the parameters change by less than the indicated tolerance between successive iterations, or the number of iterations set is achieved. This work employed an existing MATLAB/Simulink tool created by MathWorks employee Javier Gazzarri [101], capable of simulating first to fifth-order battery models. The tool receives raw time series current and voltage data collected during battery testing and outputs terminal voltage and SOC. For the estimation of the parameters, the HPPC curve served as the input data, and as a response, the estimation tool gave the curve illustrated in Figure 5.4.
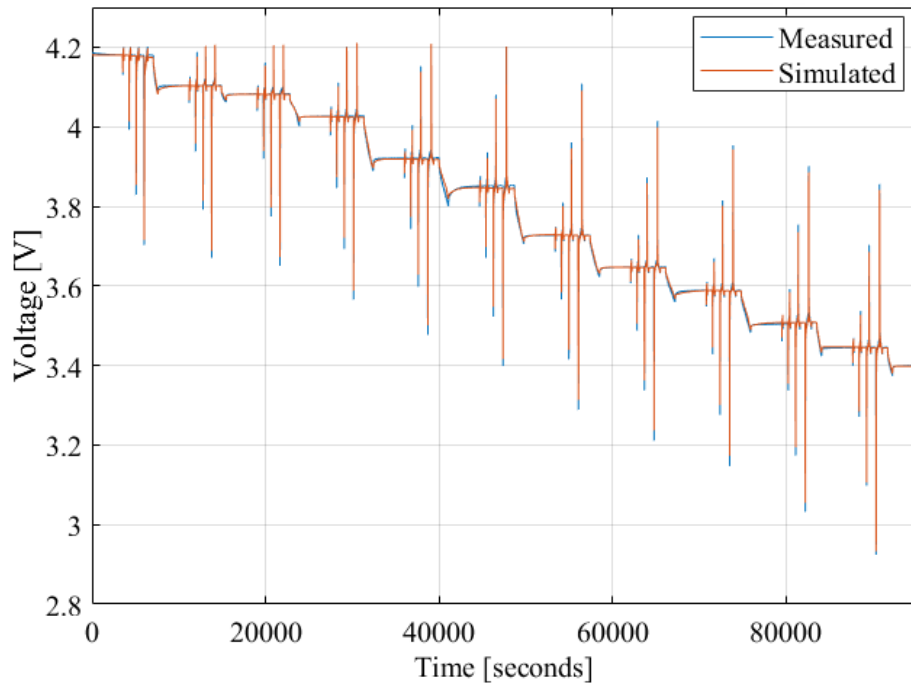
Figure 5.4: Hybrid pulse power characterization test input and response from estimation tool (BCR protocol test).

A set of optimized ECM parameters were generated for each step of the HPPC test, forming a row vector. This way, the voltage estimation is better provided over the SOC range. In order to have a model and results closer to the real application, parameters for the surrounding temperatures have to be estimated and included in the model, as the cell temperature is variable during the tests. Once the test did not count on an environment different from the 25°C, these surrounding temperature characterizations of the cell were attained from tests performed by Dr. Kollmeyer and Michael Skells at McMaster University that are available as open-source on Mendeley [102]. The HPPC tests performed at 10°C and 40°C were input into the parameter estimation tool, and their estimated parameters used to create a 2-D LUT with SOC and temperature as breakpoints.

Besides the data acquired in tests, the parameter estimation tool needs other inputs such as the initial guess for all parameters to be estimated, the battery capacity and others depending on the objective. As aforementioned, five parameters of the second-order R-2RC have to be estimated to satisfy equation 5.1. The MATLAB/Simulink tool requires the time constants τ_i ($\tau_i = R_i C_i$) instead of the capacitances C_i, so the estimated parameters given by the tool are R_0, R_1, R_2, τ_1, and τ_2, last point of Figure 5.5 repesenting the estimation after 41 iterations, and equation 5.1 is rewritten in equation 5.4 for the modelling.

$$V_{i,k} = 1 - \frac{\Delta t}{\tau_i} V_{i,k-1} + \frac{\Delta t R_i}{\tau_i} I_{k-1} \qquad\qquad 5.4$$
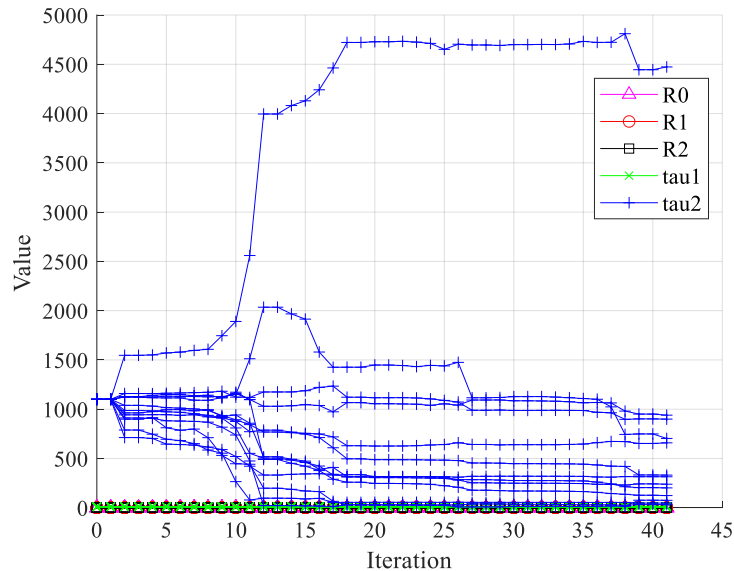
Figure 5.5: Estimated parameters over the iterations for the 25°C ($R_{1,2,3}$ depicted in Ohms and $\tau_{1,2}$ in seconds).

The test data provided for the battery modelling came from the boost charging with rest protocol aging test presented in 4.1.4.4, and the parameters estimated are found in Appendix A.

5.1.1.2   Extended Kalman Filter State of Charge Estimation Modelling (EKF$_{soc}$)

The state of charge estimation algorithm was modelled on the second-order R-2RC ECM; hence, three states are estimated. The state-space for the battery in the state estimate and measurement estimate is illustrated as follows:

$$\hat{x}_{k|k-1} = f(\hat{x}_{k-1|k-1}, u_{k-1}, w_{k-1}) = F\hat{x}_{k-1|k-1} + Gu_{k-1} + w_{k-1} \qquad 5.5$$

$$\hat{z}_{k|k-1} = h(\hat{x}_{k|k-1}, u_k, v_k) = H\hat{x}_{k|k-1} + Du_k + v_k \qquad 5.6$$

where,

$$
\begin{cases}
F = \begin{bmatrix} 1 & 0 & 0 \\ 0 & 1-\dfrac{\Delta t}{\tau_1} & 0 \\ 0 & 0 & 1-\dfrac{\Delta t}{\tau_2} \end{bmatrix} \\[2em]
\hat{x}_{k-1|k-1} = \begin{bmatrix} SOC_{k-1|k-1} \\ V_{1,k-1|k-1} \\ V_{2,k-1|k-1} \end{bmatrix} \\[2em]
G = \begin{bmatrix} -\dfrac{\eta \Delta t}{Q} \\ \dfrac{\Delta t R_1}{\tau_1} \\ \dfrac{\Delta t R_2}{\tau_2} \end{bmatrix} \\[2em]
H = \dfrac{\partial h}{\partial x}\bigg|_{\hat{x}_{k|k-1}, u_k} = [1 \; -1 \; -1] \\[1em]
D = R_0
\end{cases} \qquad 5.7
$$

u_k is the input and represents the current through the battery. Note that the state estimate $\hat{x}_{k|k-1}$ is modelled with the Coulomb Counting, so for the output $\hat{z}_{k|k-1}$ calculation, the SOC is transformed to OCV by the employment of the curve

shown in Figure 5.3 in the form of a LUT, and the calculated state estimate becomes:

$$\hat{x}_{k|k-1} = \begin{bmatrix} OCV_{k|k-1} \\ V_{1,k|k-1} \\ V_{2,k|k-1} \end{bmatrix} \qquad 5.8$$

The initialization of the algorithm is given in the following Table 5.1. Note that the SOC depends on the first voltage measurement, so a value is not attributed to it. The computation of the algorithm at each time step is illustrated in Table 3.3. Values attributed to the process noise covariance matrix Q are addressed in 6.2.1.

Table 5.1: EKF SOC estimation initialization.

Initial State	$\hat{x}_0 = [SOC\ 0\ 0]^T$
Initial Covariance	$P_0 = \begin{bmatrix} 8.0e-08 & 0 & 0 \\ 0 & 8.0e-08 & 0 \\ 0 & 0 & 8.0e-08 \end{bmatrix}$
Measurement Noise Covariance	$R = 4x10^{-6}$

5.1.2   State of Health Model

5.1.2.1 Capacity Estimation Modelling Based on Normalized Resistance Increase

The battery capacity state of health (SOHcap) was modelled using the vast data collected across the aging test. It is based on the resistance increase captured in the HPPC test. So, a so-called dynamic model and the modelling of the

relationship between the normalized resistance increase and capacity fading were designed as described in the following topics.

5.1.2.1.1   Dynamic Model

The dynamic model has the voltage drop as an output (V_{drop}). It utilizes the resistance calculated, the internal resistance plus charge-transfer resistance (R_{dy}), from the four pulses of the HPPC test performed on the fresh battery submitted to the aging test to create a 2D-LUT of C-rate and SOC breakpoints. The data interpolated in the LUT is then multiplied by the current in the battery to provide the voltage drop of a new cell at each time step, Figure 5.6, for the normalized resistance rise θ estimation by the SVSF algorithm.
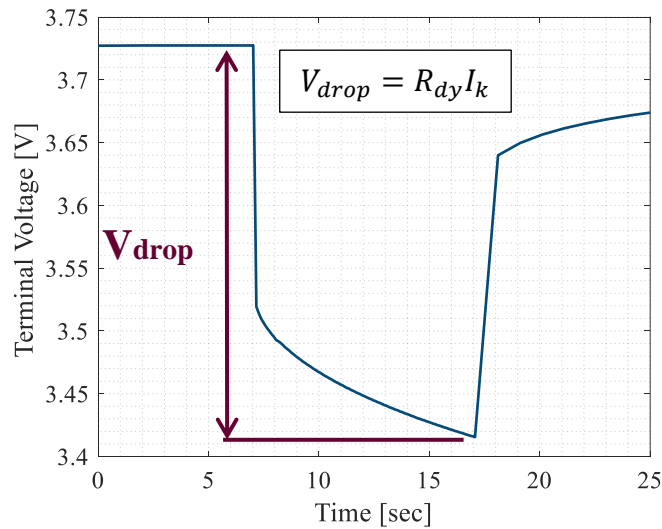
Figure 5.6: Ten seconds 8C discharge pulse at 50% SOC (BCR protocol test).

5.1.2.1.2   Normalized Resistance Increase - Capacity Fading Relationship (NRI-CF)

After the computation of the SVSF algorithm, Table 3.6, the updated estimate $\hat{\theta}_{k|k}$ is transformed into the capacity fading through the 1D-LUT created each time step through a process. The LUT created has the capacity fading as table data, and varying breakpoints computed from the interpolation of fitted curves calculated every 10% SOC step performed in the HPPC test. These normalized fitted curves were designed to ensure the breakpoints are consistently monotonically increasing to be implemented into LUTs, once the measurement of resistance can be influenced by external variables like the temperature and result in a lower value of subsequent data such as pointed out in Figure 5.7.
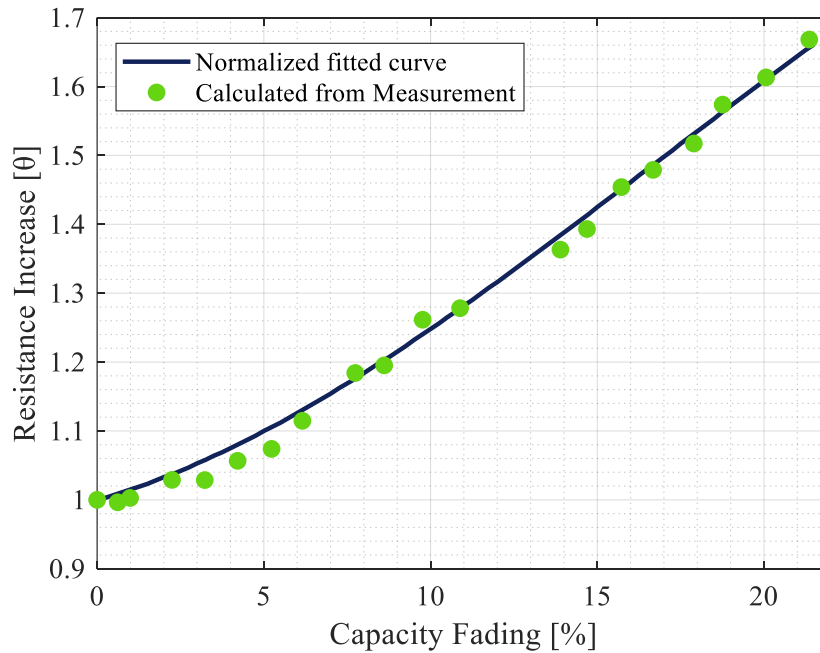
Figure 5.7: Normalized resistance increase–capacity fading relationship fitted curve at 50% SOC (BCR protocol test).

The process starts with selecting the upper and lower boundary curves from the direct LUTs dependent on the SOC presented by the battery. These curves, Figure 5.8, contain the normalized resistance increase calculated from the resistances retrieved from the HPPC test across the entire aging test.
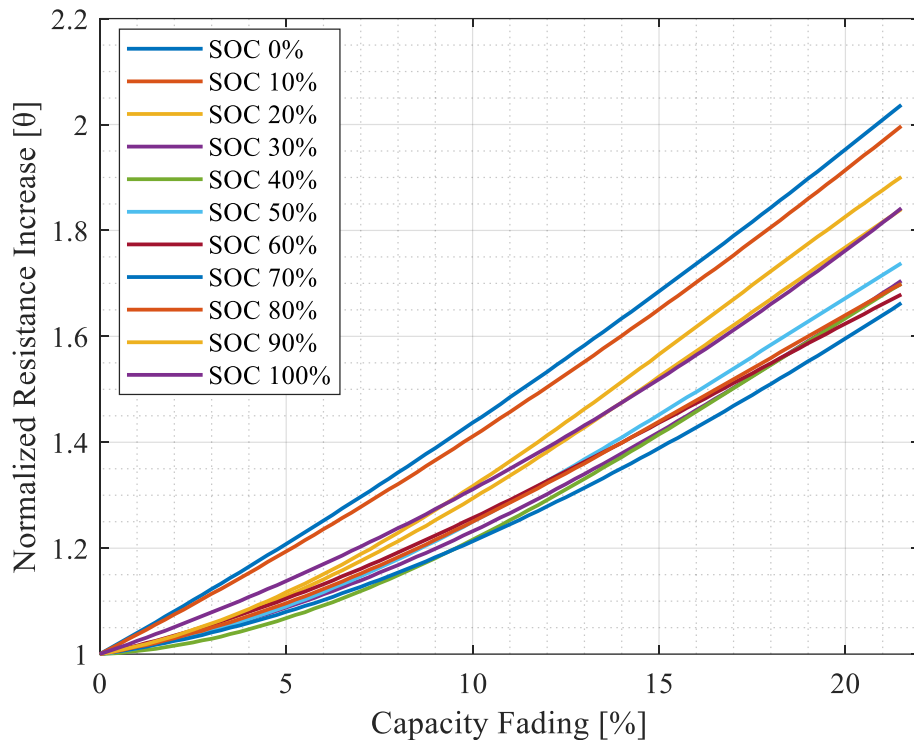
Figure 5.8: Normalized resistance increase–capacity fading relationship at different SOC levels (BCR protocol test).

Once both curves are selected, a new curve corresponding to the battery SOC is generated by interpolating the upper and lower curves, Figure 5.9, and used as breakpoints in a final LUT containing the capacity fading as table data. The capacity fading is then applied in the calculation of the battery capacity to feed the EKF model for the SOC estimation.
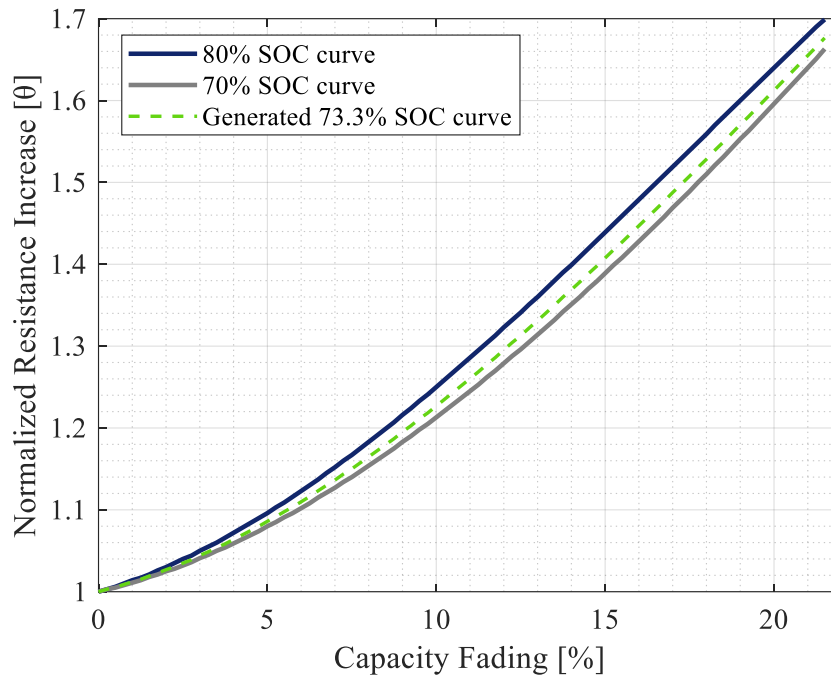
Figure 5.9: Illustration of an NRI-CF curve generated at 73.3% SOC (BCR protocol test).

5.1.2.2 Smooth Variable Structure Filter Parameter Estimation Modelling (SVSF$_{cap}$)

The SVSF model was built to support the EKF SOC estimation model with the estimated battery capacity. As there is not a direct measurement of the voltage drop, it considers the delta between the measured terminal voltage and the open circuit voltage estimated by EKF as the measurement. The initialization of the model is with the last SOH value recorded. Hence, for simplification purposes, the initialization in the simulations presented in Chapter 6 will be the true SOH of the cell.

The *a priori* calculations are presented as follows:

1. The state estimate $\hat{\theta}_{k|k-1}$ is considered as the estimated update from the previous time step.

$$\hat{\theta}_{k|k-1} = \hat{\theta}_{k-1|k-1} \qquad 5.9$$

2. Measurement estimate is calculated with the voltage drop from the dynamic model that assumes:

$$\hat{y}_{k|k-1} = H_k\hat{\theta}_{k|k-1} = V_{drop}\hat{\theta}_{k|k-1} = R_{dy}I_k\hat{\theta}_{k|k-1} \qquad 5.10$$

3. The measurement error is computed as illustrated in 5.11.

$$e_{y_{k|k-1}} = y_k - \hat{y}_{k|k-1} = z_k - OCV_{k|k} - \hat{y}_{k|k-1} \qquad 5.11$$

where z_k is the battery terminal voltage and $OCV_{k|k}$ the estimate update.

The a posteriori phase of SVSF is computed according to the following Table 5.2.

Table 5.2: SVSF capacity estimation *a posterori* phase algorithm.

SVSF gain	$K_{SVSF_k} = H^+ diag\left[\left(\left\|e_{y_{k\|k-1}}\right\| + \gamma\left\|e_{y_{k-1\|k-1}}\right\|\right)\right.$ $\left.\circ sat(\psi^{-1}e_{y_{k\|k-1}})\right]diag(e_{y_{k\|k-1}})^{-1}$
Estimate update	$\hat{\theta}_{k\|k} = \hat{\theta}_{k\|k} + K_{SVSF_k}e_{y_{k\|k-1}}$
Measurement estimate	$\hat{\theta}_{k\|k} = H_k\hat{\theta}_{k\|k-1}$
Measurement error	$e_{y_{k\|k}} = y_k - \hat{y}_{k\|k}$

Chapter 6

Aging Test Measurements and Dual State Estimation Modelling Validation

This section depicts the outcomes from both the extensive fast charging aging test performed in the Battery Laboratory facility in the Centre for Mechatronics and Hybrid Technologies at McMaster Automotive Resource Centre defined in Chapter 4 and the performance of the dual estimation model described in Chapter 5 for the battery state of charge and health estimation.

6.1 Fast Charging Aging Test Results

In section 4.1.7, the aging test procedure describes two battery parameters considered as the battery end of life (EOL), the capacity fading higher than 20% of the initial battery capacity, and the rise in internal resistance surpassing 50% of its original value. These data are acquired at every schedule's start (every 37 cycles) with a run of the characterization test. For the initial 1C discharge capacity, 3000mAh (min 2900mAh) [97], and the 0.5C discharge, the four cells presented the following numbers in Table 6.1.

Table 6.1: Four cells' capacities at the beginning of testing.

Discharge Test	Cell Capacity [Ah]			
	# 1 (CC)	*# 2 (BC)*	*# 3 (BCNP)*	*# 4 (BCR)*
0.5C	2.972	2.991	2.976	2.964
1C	2.949	2.969	2.951	2.949

This first 1C discharge was performed to verify if the samples were within specifications, whereas the 0.5C discharge was employed as a starting point for the capacity state of health (100% SOH). Regarding the second metric for comparison, the rise in internal resistance, data analyzed is collected from the HPPC test 1C pulse discharge at 50% battery SOC.

6.1.1   Capacity Retention

The capacity state of health after more than six months of testing is presented in Figure 6.1. It can be noticed that the four protocols had similar capacity fading up to a little over cycle 100 when they started to diverge, with both profiles featured with 1.9-second pulse depicting a higher capacity fading rate. Boost charging with rest (BCR) protocol had the fastest degradation of all, hitting the end of life around cycle 780. Boost charging with negative pulse (BCNP) reached 82.0% SOH capacity at cycle 970, the latest measurement, whereas, Constant current (CC) protocol presented the best capacity retention followed by the boost charging (BC) protocol with 87.7% and 87.0%, respectively.
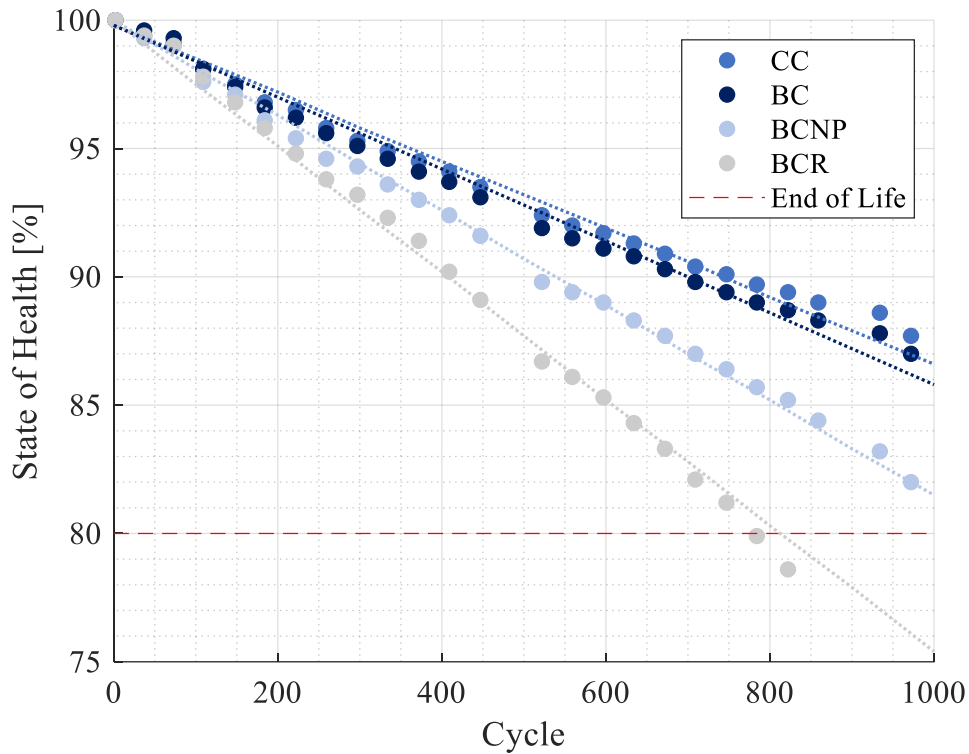
Figure 6.1: Capacity retention over the cycles.

Considering the maintenance of their capacity fading rate of around 0.39% every 37 cycles after cycle 500, the projected EOL of CC charging protocol will occur around cycle 1500 and BC a little after 1400. On the other hand, BCNP profile is due to reach 80% SOH around cycle 1050.

6.1.2   Internal Resistance Rise

Internal resistance (IR) rise, the second metric to decide the EOL, is illustrated in Figure 6.2. The BCR protocol displays a higher internal resistance over the cycles, followed by the BCNP, BC and CC protocols. Examining Figure 6.1, it can be concluded that there is a relationship between the two metrics

employed in verifying the battery EOF; nevertheless, it does not display the influence of the fast charging protocol in the resistance rise.
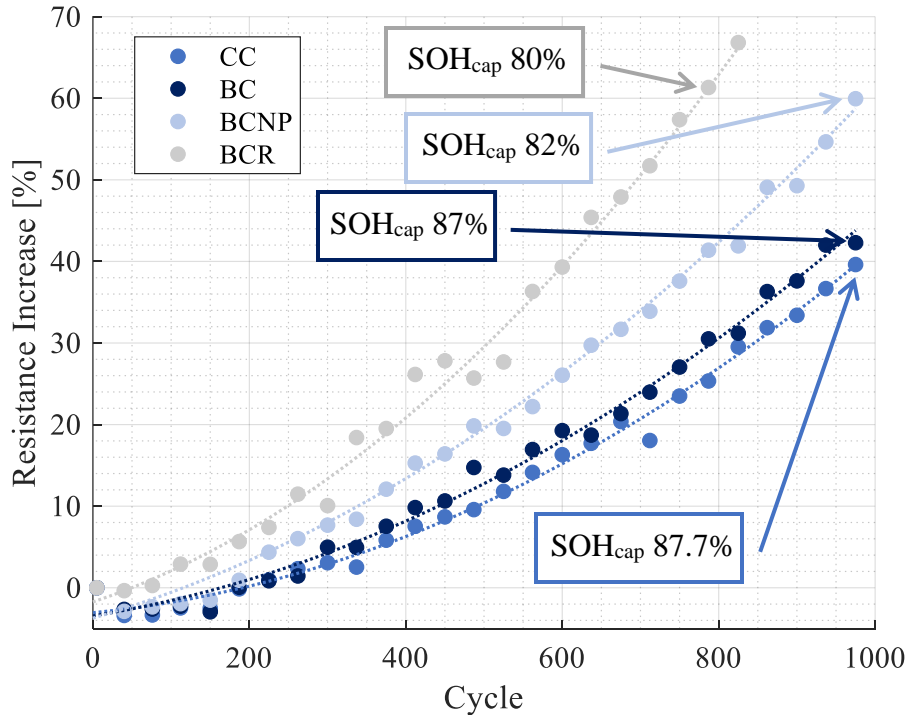
Figure 6.2: Discharge resistance increase at 50% SOC over the test cycles.

Figure 6.3 demonstrates the discharge resistance as a function of the capacity fading. Through the trendline up to 10% capacity fading, the image reveals the battery resistance increase to be similar for all four charging algorithms with a percentual increase of around 23% for BCNP, 24% for CC and BC, and 25% for the BCR after half of the batteries life. Therefore, up to half of the test, one can assume the battery does not increase its internal resistance as a function of the charging profile type. Nevertheless, past ten percent of the capacity fading, both protocols equipped with constant currents show a higher internal resistance increase than those with pulses. The increasing rate exhibited by CC and BC up to the latest

measurements indicates that both cells will reach 50% capacity rise before the cell age below 86% of capacity retention, while the BCNP and BCR protocols hit the 50% resistance raise mark at 84% and 82.5% SOH, respectively.
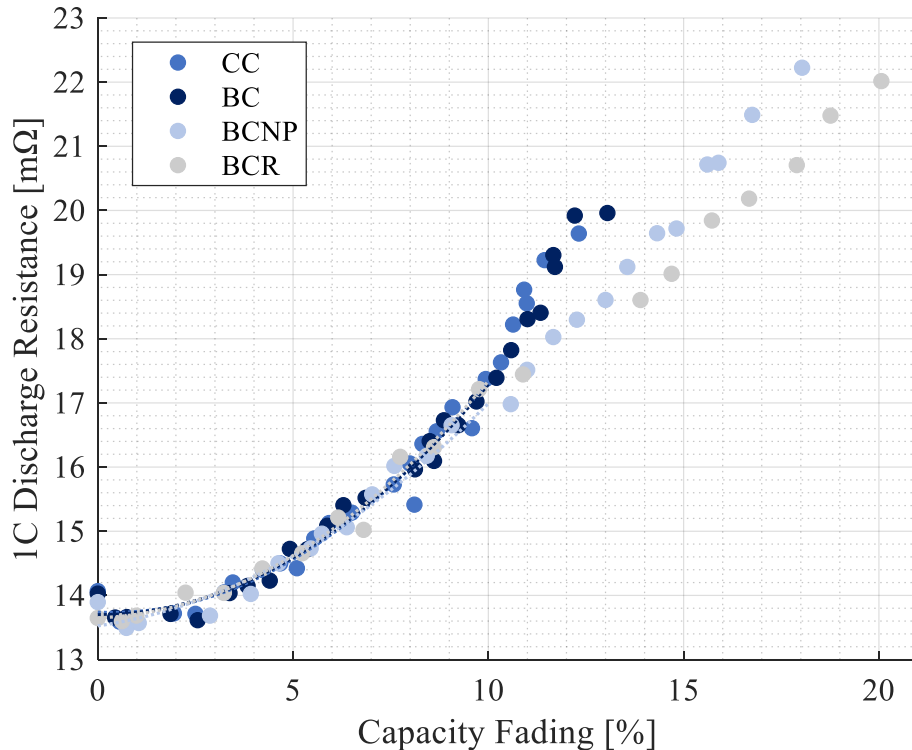
Figure 6.3: Discharge resistance increase in function of the capacity fading.

6.1.3   Fast Charge Temperature

Temperature is a key point in battery aging. A low temperature leads to lithium plating triggering loss of lithium inventory and active anode material. On the other hand, a high temperature could cause the solid electrolyte interphase (SEI) growth, SEI and electrolyte decomposition degradation mechanisms affecting the lithium inventory, or binder decomposition leading to loss of both anode and cathode active materials [103]. The concern in the designed aging test performed in

this work regarding the temperature is restricted to the rise that occurs during the fast charge that could favour the occurrence of the aforementioned degradations mechanisms at high temperature. Lithium plating could still be a problem, but the cause would be the current load on the battery and not the temperature.

The increase in the temperature during the fast charge is displayed in Figure 6.4. CC protocol depicts almost a linear rise in the temperature reaching about 5°C at the end of the 15 minutes charge, while BC, BCNP and BCR present a more steep increase until the boost phase terminates and the second phase of lower current mean starts. These three charging algorithms show comparable temperature profiles with the delta temperature hitting close to 5.5°C in BC and BCR cases and a little over 6°C for the BCNP.
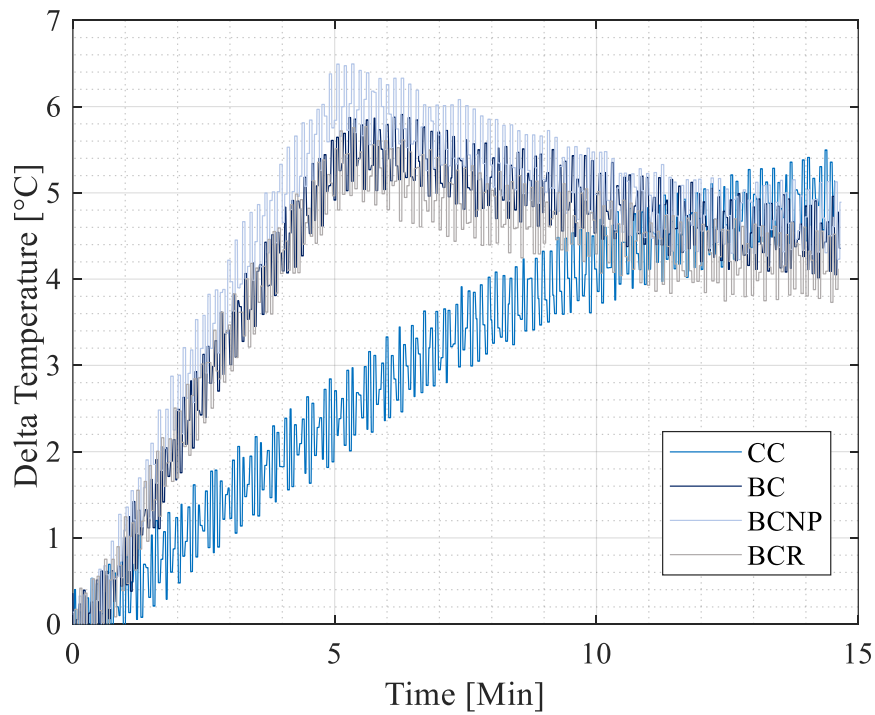
Figure 6.4: Temperature rise across fast charging (cycle 5).

Analyzing the similarity of the temperature measured in the three charging profiles featuring a boost charging phase and even a noticeable higher raise in BC and BCNP profiles compared to BCR, there is no correlation of the capacity fading shown in Figure 6.1 and delta temperature in Figure 6.4. That establishes that the temperature did not play a role in the faster aging presented in the BCR test.

The average temperature increase in the fast charge across the aging test up to almost 1000 cycles is presented in Figure 6.5. The image demonstrates that the average temperature rise in the fast charge remained unaltered over the test sustaining the statement that temperature rise as a consequence of the charging algorithm is not an influencing variable of the different aging rates presented by the four protocols.
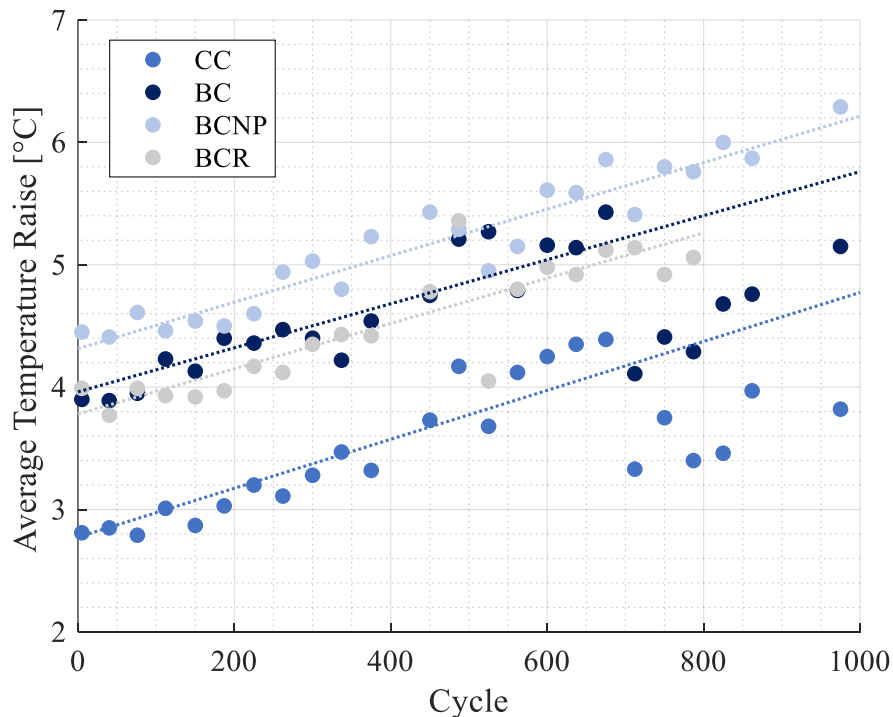
Figure 6.5: Average temperature rise in the fast charging across aging test.

6.1.4   Open Circuit Voltage Across the Battery Aging

Estimation models functioning with SOC-OCV curves are vastly used in the literature. The employment of this relationship can introduce error into the model when estimating the states of an aged battery. This is because the SOC-OCV relationship changes throughout the cell life [38], [104]. The change in the OCV curve is also different depending on the battery chemistry and shifts from a positive to a negative difference and vice versa over the entire SOC range, as demonstrated in [38]. So, tracking the behaviour of the SOC-OCV relationship over the battery life is important to minimize errors in modelling.

The OCV test is performed every 75 cycles in the aging test. Results show that the Samsung 30T cell submitted to the test also suffers a drift in the OCV curve as it ages, Figure 6.6. From 65% SOC down to about 7.5%, the curve drifts upwards, reaching a delta in the voltage of around 44mV at the battery's end of life. On the other hand, the curve presents a negative offset within about 75% and 95% SOC range. These values indicate that the SOC-OCV curve could introduce an error in the SOC estimation of around 4.5% when the OCV of an aged cell is at a value of 3.75V, for example. Figure 6.7 depicts the development of the OCV difference from the new and aged cell over its lifespan.
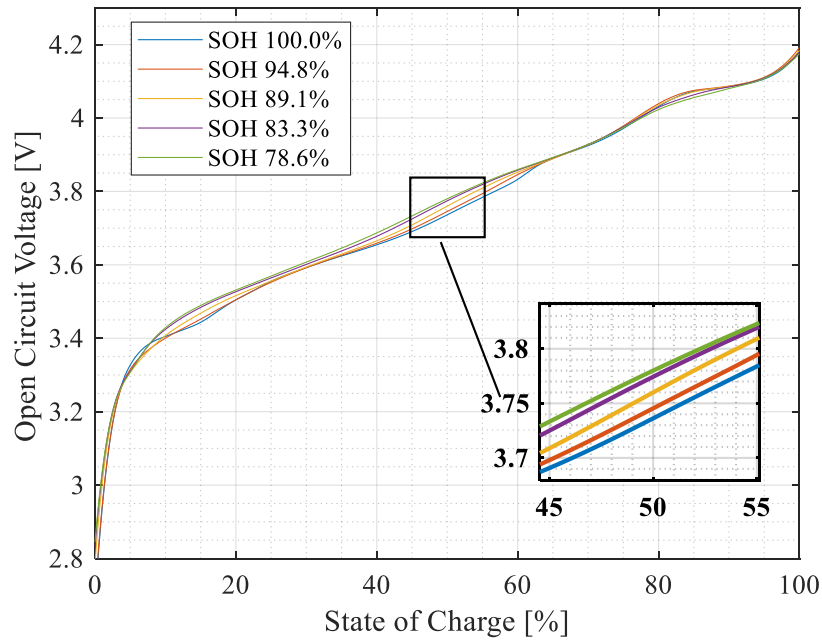
Figure 6.6: BCR protocol SOC-OCV relationship curves at different SOHs (zoom at 50% SOC).
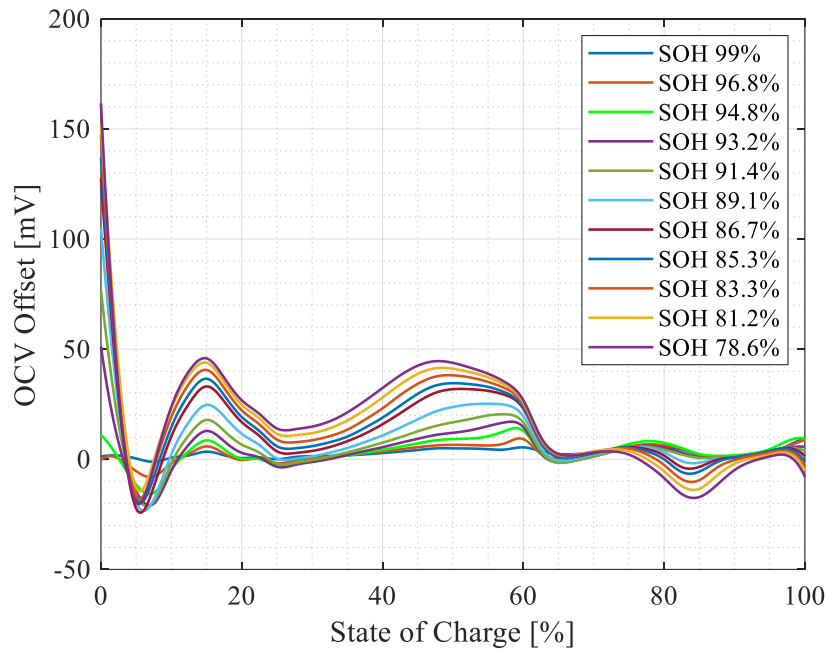
Figure 6.7: BCR protocol OCV difference evolution across the battery lifespan.

An analysis comparing the OCV curve drift across the four tested batteries' lifespans reveals that the charging protocol employed on fast charging directly affects the OCV curve drift behaviour. At a similar SOHcap, Figure 6.8, it can be observed that the charging protocols with pulse cause a higher OCV offset amplitude compared to the ones equipped with a constant current. The highest offset is close to zero SOC, where the CC and BC OCV curves drift towards 60mV, while with the pulse protocols, this number goes up to over 100mA.
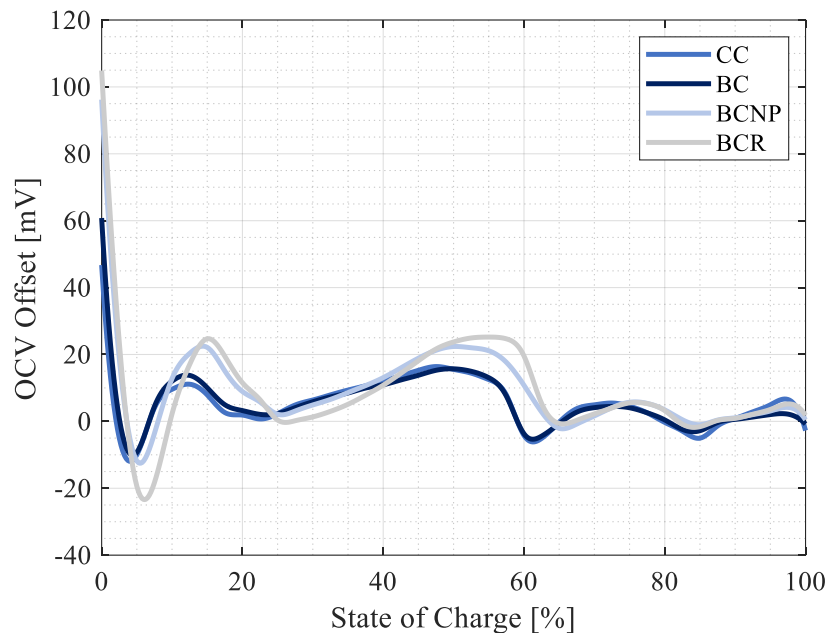
Figure 6.8: OCV difference between the new and aged cells (~ SOHcap 89%).

Another point to highlight is the similarity of the CC and BC curves, demonstrating that the higher current within the first five minutes of BC did not affect the OCV curve drift enough to present discrepancies as shown by BCNP and BCR protocols. When compared with similar discharge resistance increase, Figure 6.9, the CC and BC curves maintain the similarity shown in Figure 6.8, however,

with a more pronounced divergence within the range of 10% and 20% SOC. With respect to BCNP and BCR curves, the plot indicates a divergence between the curves.
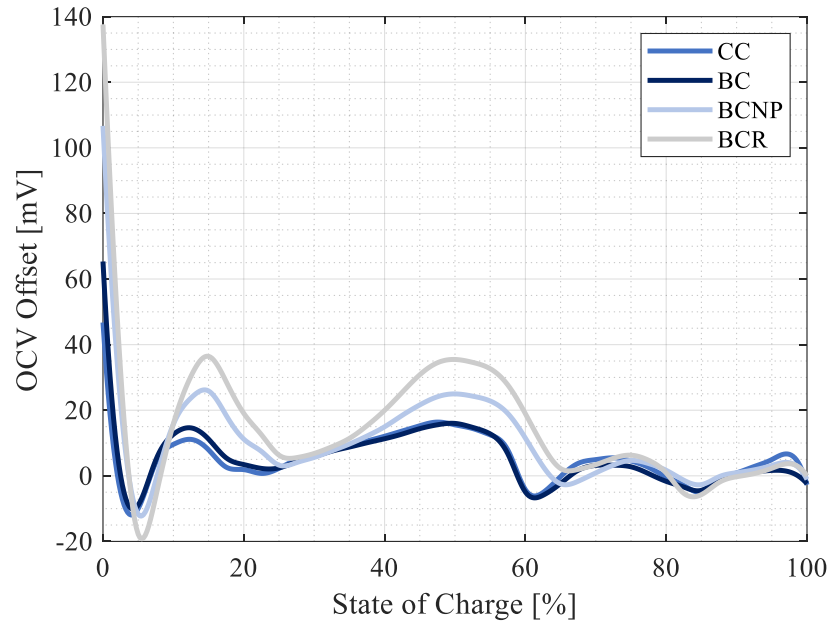
Figure 6.9: OCV difference between the new and aged cells (~ 32% IR rise).

6.2 Dual State Estimation Modelling Validation

All simulations and analyses presented in this topic were performed using the BCR protocol aging test data.

6.2.1   Model Tuning

The dual state estimation algorithm (EKF/SVSF) tuning was divided into two phases: A single EKF SOC estimation model tuned to attain good performance on robustness to sensor error and a posterior tuning of the SVSF SOHcap model coupled on the already tuned EKF.

6.2.1.1   Extended Kalman Filter State of Charge Model Tuning

As cited in topic 3.1.5, the model tuning is performed by trial and error. The process adopted in the EKF SOC estimation model followed the trial and error, running random drive cycles to find a good set of values, and a refinement of the tuning with five numbers within a range (from $2x10^{-12}$ to $1x10^{-11}$) established based on the trial and error tuning. The model counts on a second-order R-2RC equivalent circuit model; hence, the three process noise covariances "Q" together made 125 tuning combinations to be swept with the measurement noise covariance "R" fixed to $4x10^{-6}$ (0.04% of full scale (+/-2mV) of the battery tester).

The cost function utilized in the refinement sweep code was the average SOC RMSE of the following drive cycles run in a fresh battery: UDDS, HWFET, LA92, US06, and WLTP. The job was performed using two tactics to select the best tuning. The first employed the raw data of the drive cycles with no error input into the model. A second approach was taken in an attempt to improve the robustness of the model to sensor error by inputting a positive and negative current bias of 300mA (0.1C of the cell), making the cost function an average SOC RMSE of ten drive cycles simulated. The tuned parameter result of both approaches is given in Table 6.2.

Table 6.2: Final EKF SOC estimation model tuning values.

Approach	Q_{11}	Q_{22}	Q_{33}
No Error input	$2x10^{-12}$	$1x10^{-11}$	$1x10^{-11}$
+-300mA bias input	$1x10^{-11}$	$2x10^{-12}$	$2x10^{-12}$

6.2.1.2   Smooth Variable Structure Filter State of Health Model Tuning

SVSF relies on the smoothing boundary layer Ψ and convergence rate γ tuning parameters to direct the state estimate to the true value. For the capacity state of the health estimation model, the tuning values were obtained by the same methodology presented in the EKF model, except that the metric used was the average SOHcap RMSE achieved in the five drive cycles performed on the new cell. The best tuning for the range of values swept from 0.3 to 1 (steps of 0.1) for γ, and 1 to 10 (steps of 0.5) for Ψ were 1 and 6, respectively.

6.2.2   Model Robustness to Sensor Error

Measurements are susceptible to errors introduced as noise or bias [38]. Sensors used on an online application can introduce an error of up to 1% of the current in a battery pack [105] and up to 5mV bias and values surpassing 5mV in the noise [38]. The estimation algorithms should absorb these measurement errors to avoid drifts in the estimated states. For instance, a positive current bias of 3% of the cell C-rate, +90mA in the Samsung 30T cell case, would diverge the SOC calculated through Coulomb counting from the true SOC value by 7.5% at the end of the over 9000 seconds of the successive UDDS power profiles employed in the aging tests, Figure 6.10. So, eight test cases were designed to verify the robustness of the model estimation to sensor errors, as displayed in Figure 6.11. The magnitude of the sensor error for each measurement was set reasonably high to push the model, being the current error gain 3%, current bias 300mA (0.1C), temperature 5°C and voltage 5mV.
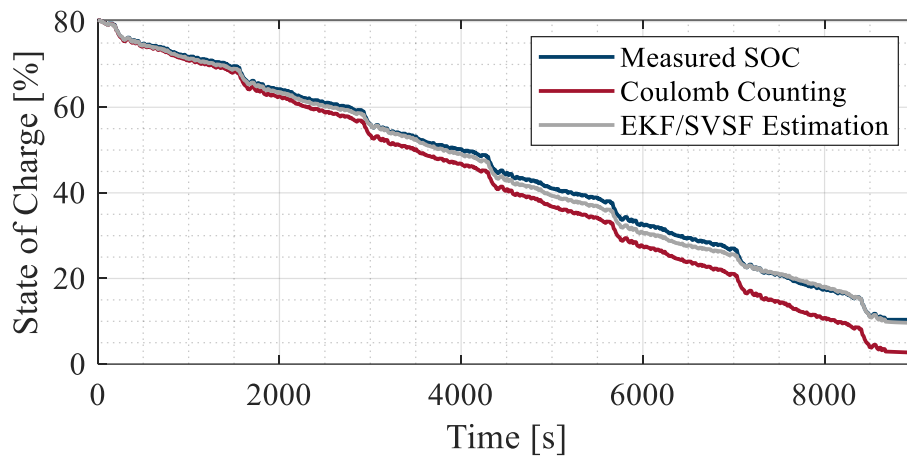
Figure 6.10: SOC estimated by Coulomb counting and the EKF/SVSF model ("+-300mA" tuning set) simulating a current sensor bias of +90mA at the UDDS drive cycle.
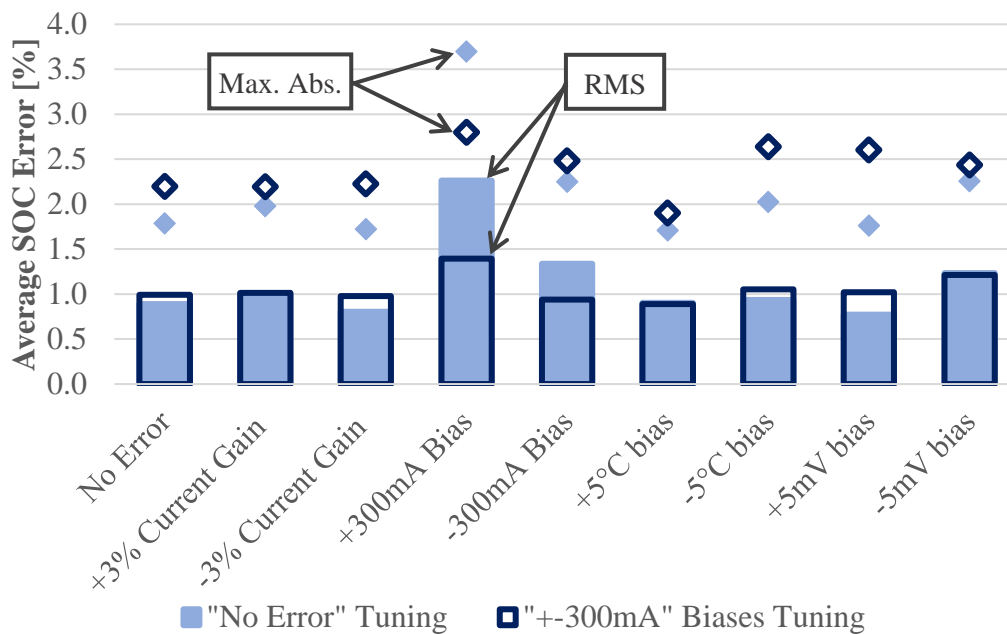
Figure 6.11: Model robustness to sensor error averaged over fifteen drive cycles.

The chart exhibits the averaged SOC RMSE and maximum absolute error over fifteen drive cycles of the eight cases plus the raw data (first bar) comparing the two tuning approaches described in 6.2.1.1. It can be noted that the "+-300mA"

101

biases tuning strategy could select a set of tuning parameter values that decreases the average SOC RMSE of both "+300mA" and "-300mA" bias cases compared to the "No Error" tuning without jeopardizing the other cases results.

Figure 6.12 illustrates the SOC estimation of both tunings for UDDS simulated with +300mA bias input, the highest RMSE (3.3%) and maximum absolute error (5.1%) found within all test cases. It is valid to mention that a bias of +300mA would lead to a 25% drift in the SOC by the end of the drive cycle, meaning that both tunings are doing a good job filtering the error input. The overall average SOC RMSE and absolute maximum error of all cases for the "No error" tuning were 1.1 and 2.1%, respectively. These numbers were 1.1 and 2.4% for the "+-300mA" tuning approach.
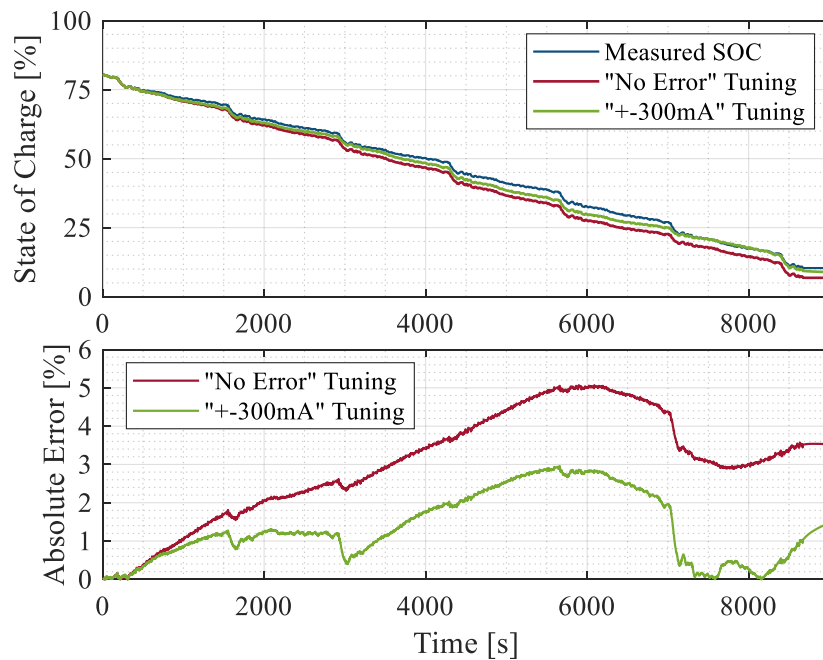
Figure 6.12: State of charge for both tunings approaches with an input bias in the current measurement of +300mA at UDDS (highest error of all scenarios).

All results displayed in the following topics are from the EKF/SVSF model trained with the "+-300mA" tuning approach.

6.2.3   Model Robustness to Initial SOC Offset

As addressed in topic 5.1, the model counts on a strategy that considers the first measured voltage value as the OCV transformed and considered the initial SOC. However, the approach is not immune to an offset of the initial SOC due to the relaxation of the battery. Therefore, initial SOC offsets were set up to 50% error to verify the model's behaviour to such a situation. A 2% SOC absolute error is used as the metric to determine the convergence of the estimation illustrated in Figure 6.13 and Table 6.3.
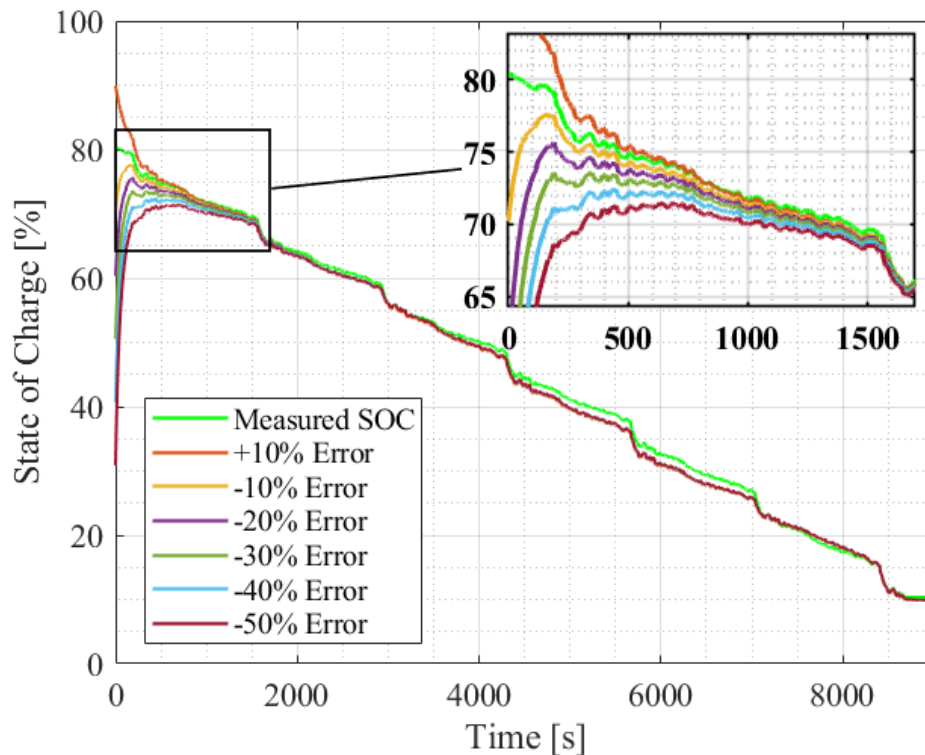
Figure 6.13: Model robustness to initial SOC error at UDDS for a new battery.

Table 6.3: Model performance to initial SOC error.

	Initial SOC Error					
	+10%	*-10%*	*-20%*	*-30%*	*-40%*	*-50%*
SOC RMSE [%]	1.2	1.1	1.6	2.3	3.0	3.4
SOC RMSE After Convergence [%]	1.0	0.9	0.9	0.9	1.0	1.0
Convergence Time [s]	240	159	272	455	679	874

6.2.4   Model State Estimation Performance Over Battery Lifespan

The core of the modelling presented in this work is to accurately estimate the battery state of charge of an aged battery with the auxiliary of a state of health model. The performance of a single EKF model, the EKF/SVSF model, and the EKF/SVSF model equipped with multiple OVC curves (OCVc) calculated from the average C/20 charge and discharge characterization test over the battery aging process are compared, Figure 6.14. Also, the real capacity is input into the EKF model and the EKF model equipped with the OCVc to simulate a "perfect" SOH model and be a benchmark for the SOH model performance.

The average error of simulations performed on fifteen drive cycles show certain robustness from the EKF model that keeps the SOC RMSE under 2% even with the battery at lower SOH, but still with a rise in the error as the battery ages. The model with true battery capacity simulating a "perfect" SOH model (EKF [Meas. CAP]) justifies that the use of a SOH capacity model can improve the EKF

performance, keeping the error close to 1% almost the entire battery lifespan. The EKF/SVSF model presented a similar performance to the EKF [Meas. CAP] over the battery lifespan, demonstrating it accomplished its purpose supporting the SOC estimation.
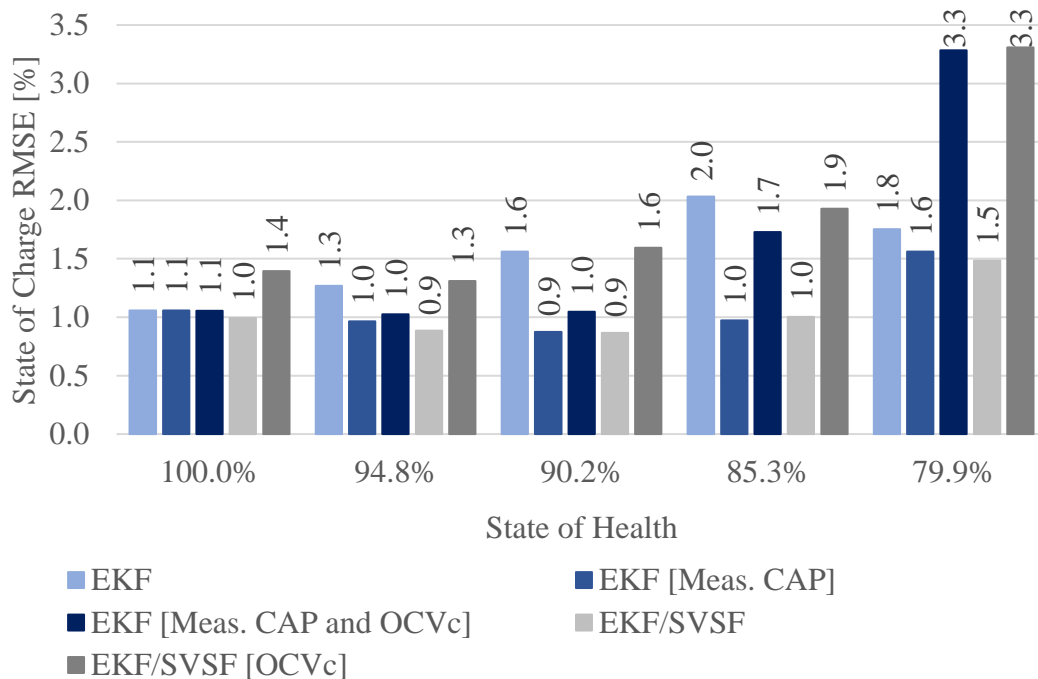
Figure 6.14: State of charge RMSE comparison of models at different states of health (average of fifteen drive cycles).

The employment of multiple OCV curves to the model was not effective in improving the SOC estimation. The fact happened even with the true capacity input into the model. As described in 6.1.4, the OCV curve is drifting upwards over most of its SOC range below 75% SOC. The unexpected performance may be explained by an overprediction of the EKF model, where the OCV estimation is lower than the true value, favouring the estimation from the model equipped with the OCV

curve from the new battery. The maintenance of the performance of both models using the multiple OCVc up to 90.2% SOH might be clarified by the fact that the OCV curve drifts up considerably at all the extension from 60% to 10% SOC beyond this point of the battery SOH. The results for maximum absolute error followed the same pattern displayed for the RMSE, Figure 6.15.
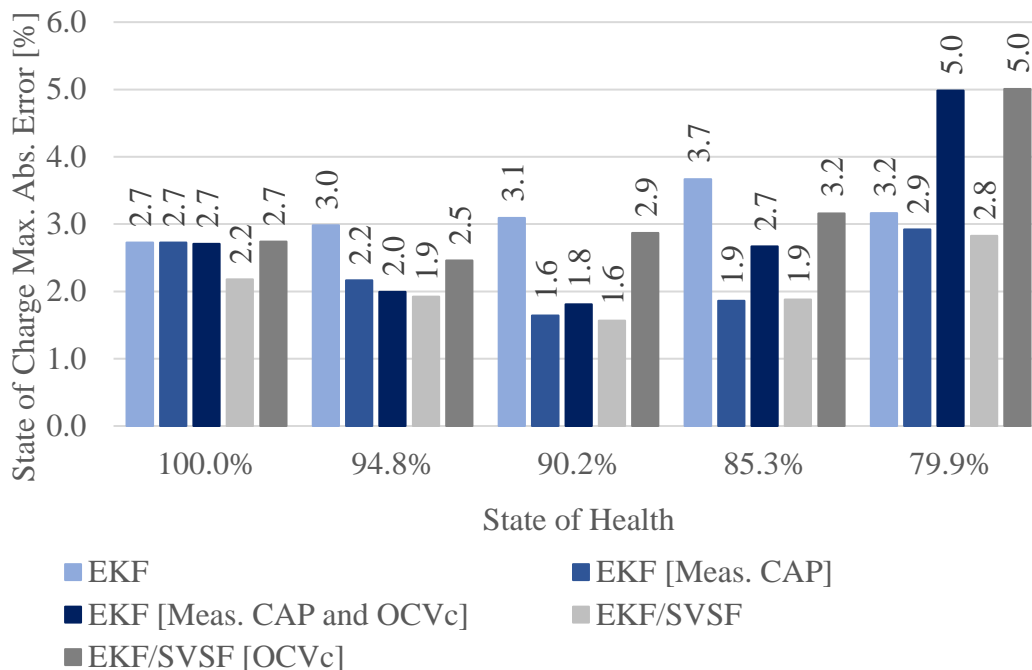
Figure 6.15: State of charge maximum absolute error comparison of models at different states of health (average of fifteen drive cycles).

The performance from the capacity estimation for the EKF/SVSF model is illustrated in Figure 6.16. The SVSFcap model, although it did not present a satisfactory performance in providing the SOH estimation close to the true value at earlier stages of the cell aging, still has an important role in the EKF/SVSF model supporting the EKF improving the SOC estimation. The poor performance of the

SVSFcap is mainly due to the attempted modelling approach. Two main error sources are identified to diminish the model's performance. The first is the measurement considered to be the delta between the voltage measured and updated estimate OCV, making the value susceptible to the SOC estimation error. A second error introduced into the model, the cause for the higher error for new battery SOH estimation, is the curve fitting to make the normalized resistance increase (see Figure 5.8), which converts the theta (normalized resistance increase) into capacity fading.
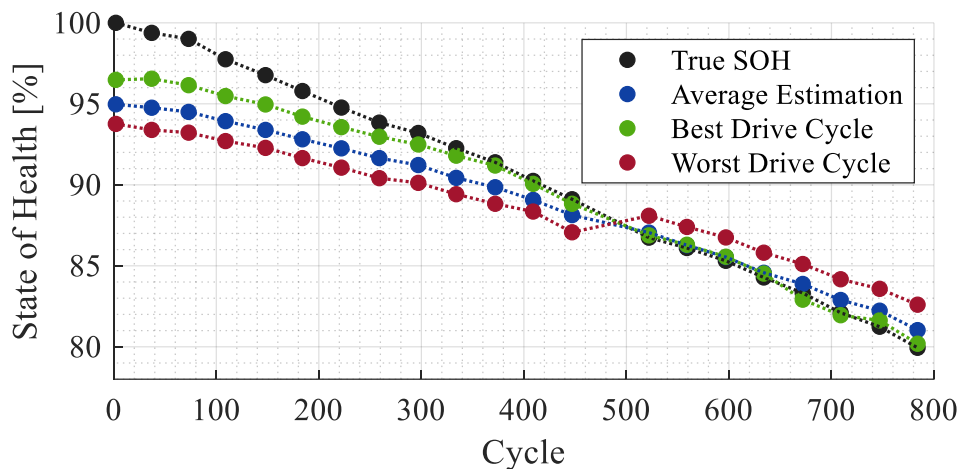
Figure 6.16: EKF/SVSF model state of health estimation over aging.

The overall SOHcap RMSE is 2.6% across the battery life. Figure 6.17 illustrates the capacity estimation of the best and worst cases for the new and aged battery.
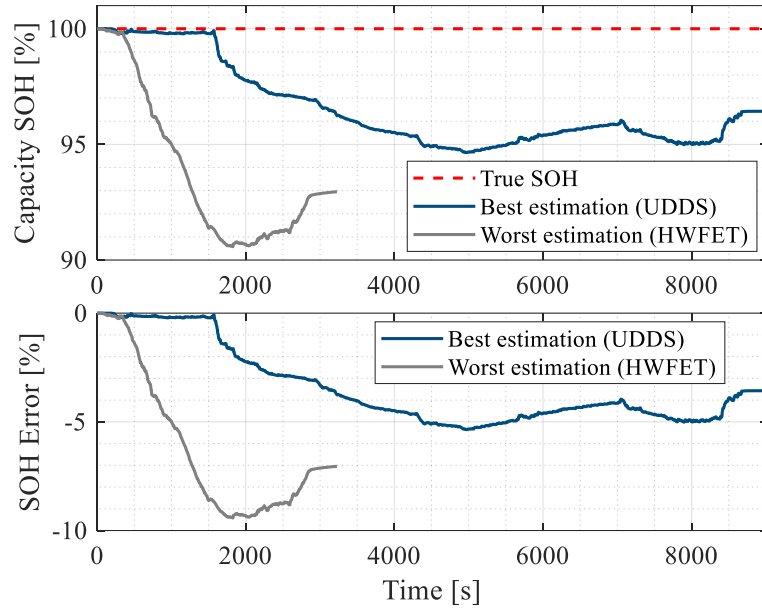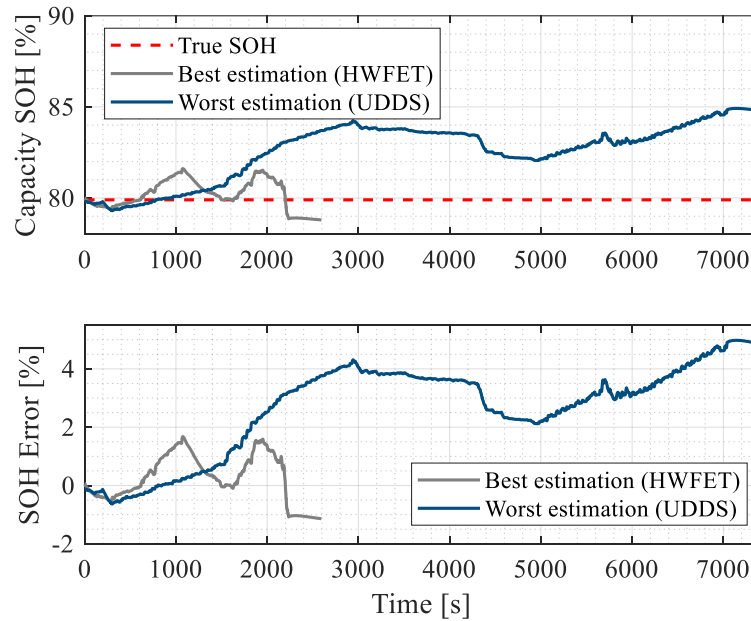
Figure 6.17: Capacity state of health estimation of new (a) and aged cell (b).

The states of estimation displayed previously were achieved with the initial

SOH set to be the true SOH for simplification. In order to simulate a more realistic

scenario, sets of fifteen subsequent drive cycles at different states of health were

employed. Figure 6.18 exhibits the mean SOH estimated for the set of fifteen drive cycles at different stages of aging. The plot depicts the influence of the initial SOH in the average estimated SOH, especially after cycle 500 when compared to the average shown in Figure 6.16. The lower values are explained by Figure 6.19 and Figure 6.20, which show a drop in the estimated SOH every charging period. Despite a reasonable overall average SOC RMSE, Table 6.4, a rise in the SOC estimation error can also be observed every time the battery is submitted to charging, revealing the necessity of a set of tuning parameters dedicated to the event.
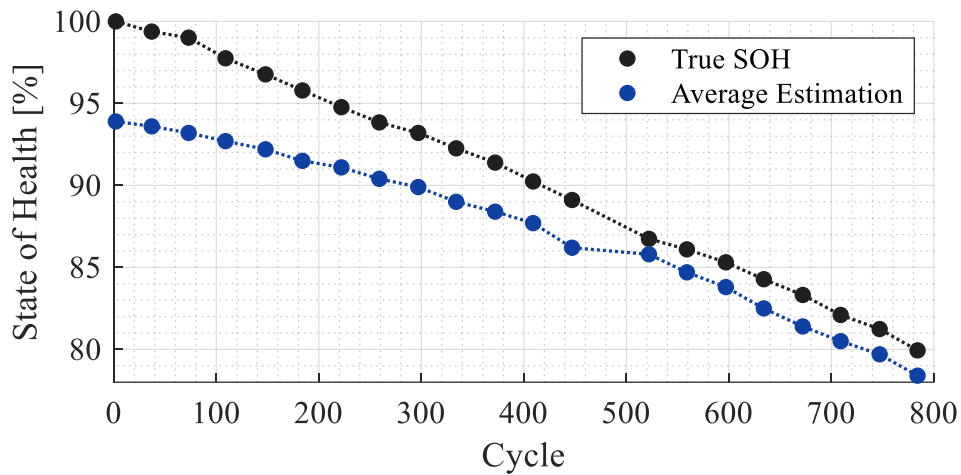
Figure 6.18: Mean SOH estimated for sets of fifteen subsequent drive cycles at different SOH stages.

Table 6.4: SOC and SOH average overall errors for the fifteen drive cycles simulated at once.

	Overall Average Error [%]		
	Mean	*RMS*	*Max. Abs.*
SOC	1.6	2.0	5.9
SOH	3.4	4.0	10.3
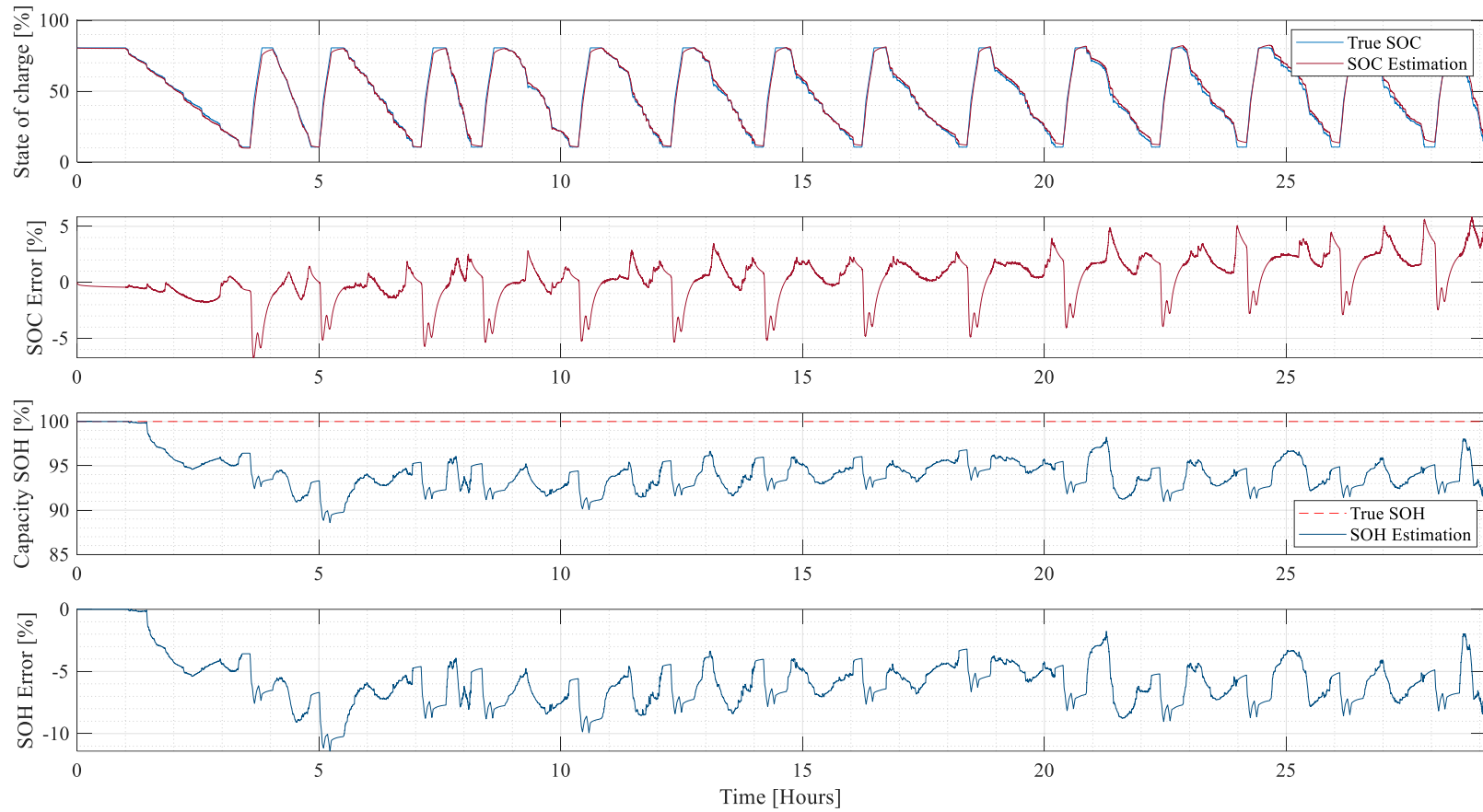
Figure 6.19: SOC and SOH estimation over fifteen drive cycles for a new cell.
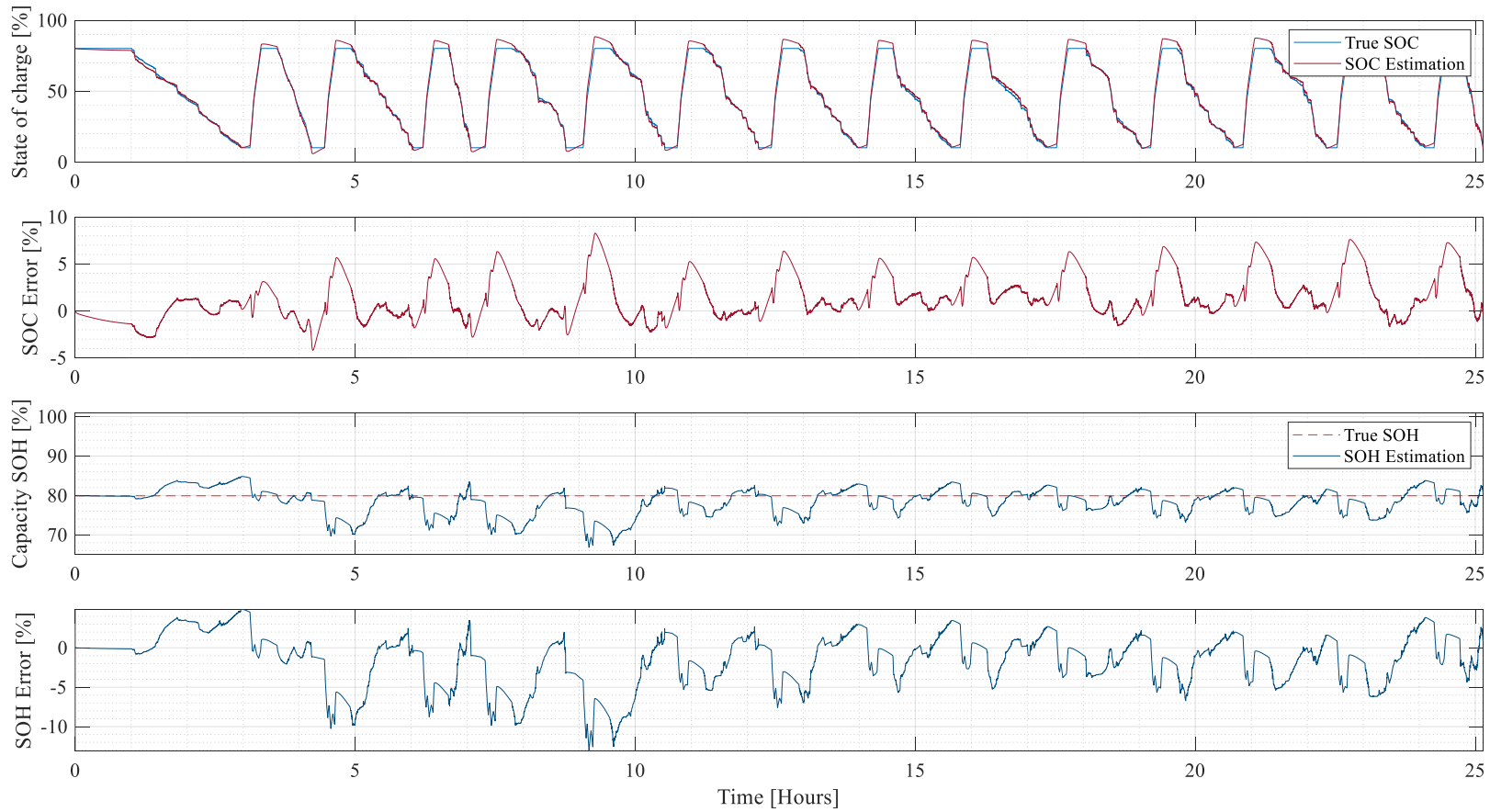
Figure 6.20: SOC and SOH estimation over fifteen drive cycles for an aged cell (80% SOH).

6.2.5   Model Robustness to Sensor Error on Aged Battery.

The robustnesses of the tuning approaches were compared in topic 6.2.2 for a new cell, where the decision of utilizing the "+-300mA" tuning to proceed with the model validation was taken. Figure 6.21 reveals the model still presenting good robustness to sensor error for a battery at its end of life. The overall SOC RMSE of the nine cases simulated had an increase from 1.1% presented in a new battery to 1.5% for an aged battery; however, no discrepancy occurred in any of the cases. The maximum absolute error was held within 3.5% on both SOHs.
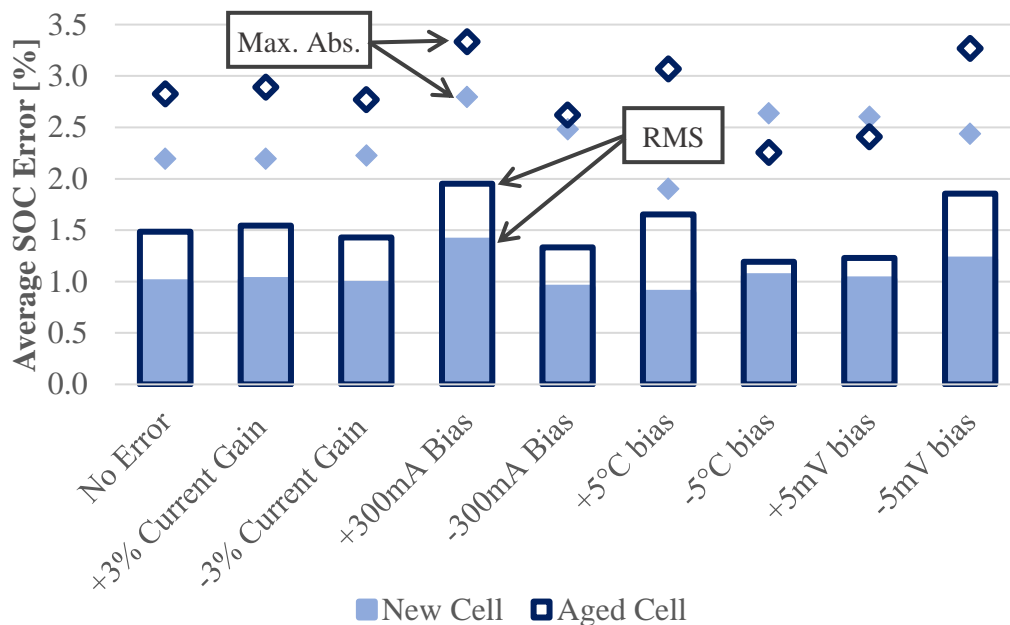
Figure 6.21: Model robustness to sensor error averaged over fifteen drive cycles for a new and aged battery (80% SOH).

Note: The charts presented in this chapter were created from the data displayed in Appendix B.

Chapter 7

Conclusion and Future Work

7.1 Summary and Conclusions

An extensive battery aging test performed in the battery laboratory facility in the Centre for Mechatronics and Hybrid Technologies at McMaster Automotive Resource Centre has been presented, along with a dual state estimation algorithm built to estimate the state of charge and capacity state of health. The test submitted four Samsung 30T cells of 3000mAh capacity to carefully designed fast charging protocols using constant currents or pulses ascribed to have benefits in either minimizing battery aging or maximizing the charging time with no further degradation to the battery. These charging profiles were employed to charge the battery from 10% to 80% SOC within fifteen minutes (2.8 charging C-rate), and fifteen drive cycles depleted the battery within the same SOC range.

The results gathered to date show a higher capacity fading on the cells tested with pulse current profiles. The cells tested with BCNP and BCR protocols hit the half-life mark with 400 and 525 cycles, respectively. The best capacity retention was observed on the constant current protocol, used as a benchmark in the study, that reached half of its life around cycle 750, followed closely by the boost charging

profile with 700 cycles at the same SOH. The charging algorithms designed with pulse charging were expected to have better or similar performance to CC protocol. That is because protocols equipped with pulses are described to ease the concentration polarization resistance or diffusion process[23], [24], enabling a higher power transfer rate and speeding up the battery charging. The result might be explained by the fact that pulse charging profiles could be detrimental to the battery due to higher strain throughout the cycles, causing cracks of electrode particles affecting material utilization [106]. The assumption for the results in the tests is that the benefits in preventing lithium plating did not occur because the cells did not reach their limits having the anode voltage going below 0V. The linear capacity fading over the entire lifespan of the cell tested with the BCR indicates the charging profile did not present the lithium plating as a consequence of the high current load or at least did not trigger the degradation mechanism up to the state of health it was tested. Studies attribute the primary degradation in linear capacity fading to be the solid electrolyte interphase (SEI) growth, and a sudden change in the slope featuring a nonlinear capacity loss would be led by a secondary degradation mechanism, the lithium plating [33], [107], [108].

The internal resistance raises the concern of the instant power capability of the cell. The internal resistance rise per cycle showed the same trend as depicted by capacity fading. The CC and BC protocols presented a lower internal resistance rise than the boost charging with negative pulse and boost charging with rest protocols. In topic 6.1.2, both cells tested with CC and BC charging protocols showed a

change in the increase of the internal resistance after 90% SOH, half of their capacity lifespan. Although CC and BC present a lower increase in the resistance raise per cycle, the projection of their trendlines in Figure 6.3 suggests that the internal resistance rise shall achieve the magnitude around 120%, against 74% of BCNP protocol when they reach the end of life. For the cell tested with the BCR protocol, the measured resistance rise was 61% at 80% SOH. Hence, studies in the product's power delivery capability designed with CC and BC fast charging past half their battery life should be verified more in-depth.

The aging tests showed the already known drift of the OCV curve over the battery lifespan. The OVC drift over the BCR protocol cell lifespan revealed the difference of the SOC-OCV curve for a new and aged cell could reach peaks of around 44mV across SOCs higher than 7.5%. The curves in Figure 6.7 also demonstrate the OCV difference is not exclusively positive or negative and switches signs over the SOC range. As examined in topic 6.1.4, the four protocols affect the OCV curve drift over the battery lifespan differently. The results showed that independent if the SOH or the resistances increase are equal, the curves are still depicting different amplitudes, with the cells tested with pulse protocols presenting higher values. This finding indicates that SOC estimation modelling should be individualized for each protocol if multiple SOC-OCV curves are to be implemented.

The data collected in the fast charging aging tests were utilized to validate the dual state estimation algorithm built to estimate the SOC and capacity SOH. An

EKF algorithm was employed to estimate the SOC, while an SVSF was applied in the capacity tracking. This EKF/SVSF model was then tuned to offer robustness to sensor error and initial SOC errors. Posteriorly, its performance in estimating the SOC across the battery cycle life was evaluated along with other approaches that would improve the model's error.

The EKF/SVSF model showed a good result to sensor error, presenting most of the cases with an average SOC RMSE close to 1% and not surpassing 1.5% in the worst-case simulated. The verification of robustness to initial SOC error showed the model could converge relatively quickly to the true value. The convergency of the estimation for a -50% in the initial SOC is almost fifteen minutes, which is a high period. However, the model does not use the initial SOC guess strategy but the initial value of the terminal voltage, which through a simulation of a 6C load demanded from the Samsung 30T cell at 50% SOC level, would have a value representing a SOC close to 5% error from the true initial SOC just after three seconds the load release. Therefore, it can be assured that the initial SOC offset will be close to the true value in normal use, less than 5% SOC, even if the battery has not reached full relaxation.

The different simulations of the model with aged battery data showed the approaches presented the average SOC RMSE of the fifteen drive cycles fairly well. The EKF model by itself maintained the SOC RMSE within 2% in the different stages of age demonstrated. The EKF with true capacity input simulating a "perfect" capacity SOH model (EKF [Meas. CAP]) demonstrated improvements in

the error, justifying the need of having a model to feed it with an estimated capacity. EKF SOC estimation, along with the SVSF SOHcap estimation, showed similar performance to the EKF [Meas. CAP].

The use of multiple OCV curves in the models to adequate the SOC-OCV relationship to the battery aging did not present improvements as expected. As discussed in 6.2.4, the reason for the unexpected outcome might be related to the model over prediction, which pushes the estimation of the OCV downwards, benefiting the lower curve measured for the new battery. Further investigation on the issue shall be performed.

7.2 Recommendation for Future Work

The work presented in this thesis reveals many exciting results from the fast aging tests that could contribute to the better performance of state estimation models. However, the experimental test in this work can not yet be considered statistically expressive due to the need to verify the repeatability of the charging profiles' results. Consequently, for future work, more cells shall be submitted to the same profiles.

The outcome in which the speed the cells aged is still unclear, although some leads on the causes were raised. Therefore, variation of the charging profiles with pulses, like different cycle frequencies of the pulse maintaining the duty cycle or employing the same tests in colder temperatures forcing a lithium plating, shall be performed for more details of the results found with the BCR and BCNP protocols. Another approach that might expose order conclusions is to use higher charging

rates to push the cells even further. In addition, based on the result of the boost charging protocol, the cell lifespan might benefit from the design of a multistage constant current protocol to ease the current load at the beginning and end of the fast charge. Alternatively, there might be room to push the charging time down with an additional intermediate current level step between the existing 4C and 2.2C steps.

The current model built for this thesis has some points that one could address to improve the errors found. For instance, it is currently working with symmetric resistance and capacitances modelled with discharging data, so a battery model with asymmetric resistances and capacitance shall bring more accuracy in the SOC estimation and also benefit the charging period that shows a poor SOC estimation. Aligned with asymmetric resistances and capacitances, the estimation would be improved by developing a set of tuning parameters for a charging mode. Of course, the tuning of the model in a more sophisticated way, such as using a genetic algorithm, might also offer enhancements. The SOHcap modelling methodology showed to be effective in supporting the SOC estimation; however, its accuracy is far from ideal at the early stages of the SOH. Besides the way the measurement was considered and the fact that the normalized resistance increase had the curves fitted, where errors were introduced, the approach with the capacity model does not consider the battery relaxation. In an eventual improvement of the model, battery relaxation should be considered. Finally, there is a need to investigate why the

models equipped with the multiple OCV curves failed in improving the SOC estimation on an aged battery.

Results from the literature, Table 3.1, showed an improvement in the SOC estimation when SVSF and VBL-SVSF were used instead of EKF. Therefore, it is also of interest to build a dual smooth variable structure filter to verify the algorithm's performance.

Appendix A

Table A. 1: Estimated equivalent circuit model parameters for different SOC levels at 10°C.

| | | State of Charge [%] | | | | | | | | | | | | |
		0	5	10	15	20	30	40	50	60	70	80	90	95	100
ECM Paremeter	R0 [Ω]	15.64	15.64	14.96	14.36	13.97	13.22	12.99	12.87	12.93	12.88	13.21	13.66	13.77	14.56
	R1 [Ω]	20.61	20.61	14.95	14.34	13.94	13.21	12.99	12.87	12.93	12.87	13.21	13.65	13.76	14.55
	R2 [Ω]	17.86	17.09	13.78	12.80	12.54	11.91	11.70	11.61	11.66	11.61	11.90	12.31	12.40	13.10
	Tau 1 [s]	12.82	12.82	9.98	9.99	9.99	10.01	10.01	10.01	10.01	10.01	10.01	10.01	10.01	10.01
	Tau 2 [s]	3493	3493	2836	2999	2995	2994	2995	3000	2997	2994	2996	2999	2990	3001

Table A. 2: Estimated equivalent circuit model parameters for different SOC levels at 25°C.

| | | State of Charge [%] | | | | | | | | | | | | |
		0	5	10	15	20	30	40	50	60	70	80	90	95	100
ECM Paremeter	R0 [Ω]	11.78	11.78	9.88	9.64	9.42	9.02	8.97	9.23	9.36	9.22	9.20	9.40	9.47	9.75
	R1 [Ω]	6.49	6.49	3.07	3.80	4.18	3.18	2.96	3.83	2.97	3.90	3.77	3.96	3.17	3.37
	R2 [Ω]	3.70	3.70	3.07	6.64	9.05	10.77	5.67	5.96	5.81	12.58	3.79	5.17	9.88	7.83
	Tau 1 [s]	6.49	6.49	9.81	11.62	15.56	9.25	8.80	13.00	12.33	13.02	11.70	13.12	8.91	10.71
	Tau 2 [s]	124	124	48	239	4473	76	331	899	659	315	202	703	940	32

Table A. 3: Estimated equivalent circuit model parameters for different SOC levels at 40°C.

		State of Charge [%]												
		0	5	10	15	20	30	40	50	60	70	80	90	95	100
ECM Paremeter	R0 [Ω]	9.72	7.49	8.03	8.68	8.12	8.28	7.97	7.75	8.08	8.20	8.25	8.22	8.07	8.40
	R1 [Ω]	5.46	4.99	3.01	3.12	2.33	3.85	3.36	2.92	2.51	3.12	4.34	3.06	2.51	2.48
	R2 [Ω]	4.58	3.24	4.04	5.40	9.71	9.98	5.04	2.93	5.79	4.71	10.30	5.18	8.55	8.91
	Tau 1 [s]	10.00	10.00	0.20	4.52	3.63	11.21	8.53	6.03	6.73	10.27	10.47	8.34	6.32	5.37
	Tau 2 [s]	400	400	30	43	190	305	182	460	151	87	174	403	336	59

Appendix B

Table B. 1: EKF SOC RMSE over battery lifespan.

SOHcap	UDDS	HWFET	LA92	US06	WLTP	Reo 1	Reo 2	Reo 3	Reo 4	Reo 5	Reo 6	Reo 7	Reo 8	Reo 9	Reo US06	Average
100.0%	0.68	1.29	0.67	2.34	0.88	0.93	0.95	0.77	0.77	0.82	0.85	1.15	0.72	1.16	1.88	1.06
99.4%	0.67	1.18	0.66	2.23	0.80	0.89	0.86	0.77	0.83	0.82	0.86	1.09	0.68	1.21	1.82	1.03
99.0%	0.70	1.14	0.67	2.17	0.79	0.80	0.82	0.79	0.87	0.82	0.85	1.10	0.71	1.23	1.70	1.01
97.8%	0.56	1.22	0.71	2.47	0.88	0.90	0.89	0.76	0.70	0.75	0.85	1.02	0.71	1.13	1.89	1.03
96.8%	0.55	1.35	0.74	2.66	0.93	1.04	1.04	0.78	0.70	0.71	0.92	1.09	0.68	1.20	2.00	1.09
95.8%	0.63	1.41	0.80	2.72	1.04	1.06	1.08	0.83	0.70	0.74	1.03	1.11	0.74	1.19	2.12	1.15
94.8%	0.76	1.54	0.91	3.02	1.18	1.21	1.20	0.91	0.80	0.74	1.09	1.11	0.85	1.25	2.46	1.27
93.8%	0.89	1.64	0.98	2.94	1.26	1.29	1.34	1.06	0.88	0.87	1.22	1.28	0.96	1.25	2.41	1.35
93.2%	0.96	1.56	1.01	3.06	1.30	1.29	1.33	1.09	0.84	0.83	1.23	1.10	0.96	1.17	2.24	1.33
92.3%	1.09	1.46	0.97	2.83	1.24	1.30	1.38	0.99	0.96	0.81	1.20	1.07	1.00	1.19	2.10	1.31
91.4%	1.24	1.64	1.07	2.88	1.49	1.39	1.45	1.15	1.04	0.90	1.27	1.20	1.06	1.23	2.29	1.42
90.2%	1.41	1.70	1.40	2.90	1.74	1.55	1.64	1.48	1.31	1.20	1.29	1.26	1.15	1.18	2.24	1.56
89.1%	1.71	1.78	1.43	3.07	1.90	1.50	1.65	1.60	1.45	1.37	1.31	1.37	1.27	1.20	2.46	1.67
86.7%	2.39	2.66	2.18	3.84	2.64	2.15	2.40	2.28	2.23	2.26	1.99	2.09	1.98	1.87	3.27	2.41
86.1%	2.39	2.16	1.94	3.30	2.30	1.92	2.16	1.98	1.98	1.91	1.68	1.68	1.60	1.54	2.57	2.07
85.3%	2.36	2.11	1.98	3.21	2.23	1.87	2.01	1.87	1.90	1.85	1.66	1.71	1.58	1.58	2.56	2.03
84.3%	2.40	1.86	1.83	2.88	1.97	1.65	1.83	1.77	1.75	1.74	1.47	1.49	1.45	1.41	2.11	1.84
83.3%	2.52	1.95	1.92	3.01	2.00	1.77	1.92	1.88	2.10	1.82	1.58	1.87	1.60	1.66	2.23	1.99
82.1%	2.68	1.93	2.00	2.87	2.11	1.62	1.88	1.98	1.66	1.61	1.59	1.58	1.54	1.61	1.94	1.91
81.2%	2.69	2.00	1.86	2.82	2.09	1.60	1.79	2.07	1.87	2.04	1.65	1.58	1.71	1.37	2.01	1.94
79.9%	2.69	1.82	1.70	2.47	1.83	1.56	1.67	1.94	1.65	1.85	1.39	1.31	1.51	1.18	1.71	1.75

Table B. 2: EKF SOC maximum absolute error over the battery lifespan.

SOHcap	UDDS	HWFET	LA92	US06	WLTP	Reo 1	Reo 2	Reo 3	Reo 4	Reo 5	Reo 6	Reo 7	Reo 8	Reo 9	Reo US06	Average
100.0%	1.26	3.05	2.20	3.58	3.21	2.93	2.90	1.78	2.08	2.38	2.92	3.41	2.48	3.20	3.50	2.72
99.4%	1.25	2.80	1.98	3.54	3.08	3.05	2.75	1.59	1.80	2.13	2.77	3.20	2.01	3.17	3.46	2.57
99.0%	1.31	2.64	1.88	3.54	3.02	2.70	2.70	1.74	1.75	1.89	2.69	3.01	1.62	2.83	3.34	2.44
97.8%	1.01	2.76	2.47	4.00	3.26	2.90	2.82	1.51	1.58	2.14	2.72	3.15	1.89	3.14	3.50	2.59
96.8%	1.20	2.91	2.59	4.57	3.34	2.99	3.18	2.05	2.06	2.26	2.99	3.46	1.66	3.31	3.51	2.81
95.8%	1.54	2.90	2.66	4.81	3.45	2.81	3.08	2.01	2.02	2.22	3.14	3.49	1.67	3.17	3.61	2.84
94.8%	1.86	3.11	2.86	5.27	3.48	2.90	3.05	1.87	1.95	2.31	3.10	3.53	1.92	3.34	4.17	2.98
93.8%	2.14	3.13	2.74	5.33	3.51	2.89	3.28	2.23	2.15	2.20	3.09	3.77	2.21	3.35	3.99	3.07
93.2%	2.21	2.95	2.70	5.36	3.43	2.88	3.08	2.11	1.75	2.16	3.08	3.28	1.97	2.96	3.71	2.91
92.3%	2.50	2.71	2.46	5.12	3.22	2.80	3.04	1.92	1.66	1.95	2.83	3.06	2.24	2.80	3.74	2.80
91.4%	2.72	2.90	2.49	5.24	3.39	2.98	3.13	2.19	1.69	2.11	2.84	3.34	2.24	2.91	4.07	2.95
90.2%	3.25	2.93	2.65	4.92	3.65	3.06	3.19	2.64	2.07	2.59	2.65	3.09	2.72	2.88	4.05	3.09
89.1%	3.68	3.04	2.71	5.20	4.45	3.59	3.48	2.95	2.74	2.62	2.99	2.79	2.68	3.08	4.50	3.37
86.7%	4.55	4.19	3.65	6.29	5.46	4.56	4.43	3.61	3.15	3.78	3.80	3.88	3.80	3.71	5.56	4.29
86.1%	4.38	3.57	3.34	5.56	4.94	4.20	4.13	3.22	2.87	3.29	3.22	3.31	3.08	3.08	4.58	3.78
85.3%	4.13	3.65	3.39	5.41	4.94	4.10	3.98	2.97	2.71	2.86	3.26	3.11	2.88	3.17	4.45	3.67
84.3%	3.99	3.31	3.13	4.79	4.46	3.58	3.55	2.80	2.61	2.53	2.79	2.62	2.60	2.78	3.73	3.29
83.3%	3.88	3.31	3.49	4.85	4.36	3.66	3.57	2.96	3.15	2.67	3.10	3.19	2.94	3.18	3.95	3.48
82.1%	4.03	3.17	3.85	4.56	4.43	3.44	3.44	3.07	2.54	2.45	3.03	2.89	2.73	3.24	3.24	3.34
81.2%	4.12	3.20	3.72	4.46	4.20	3.50	3.45	3.19	2.80	2.94	3.32	2.90	3.27	2.70	3.33	3.41
79.9%	4.07	2.91	3.15	3.99	3.72	3.60	3.35	3.10	2.53	2.74	2.96	2.70	2.90	2.48	3.26	3.16

Table B. 3: EKF [Meas. CAP] SOC RMSE over battery lifespan.

SOHcap	UDDS	HWFET	LA92	US06	WLTP	Reo 1	Reo 2	Reo 3	Reo 4	Reo 5	Reo 6	Reo 7	Reo 8	Reo 9	Reo US06	Average
100.0%	0.68	1.29	0.67	2.34	0.88	0.93	0.95	0.77	0.77	0.82	0.85	1.15	0.72	1.16	1.88	1.06
99.4%	0.70	1.11	0.67	2.13	0.78	0.85	0.84	0.78	0.85	0.84	0.86	1.09	0.68	1.20	1.73	1.01
99.0%	0.74	1.03	0.69	2.02	0.77	0.74	0.79	0.81	0.91	0.86	0.85	1.11	0.74	1.24	1.56	0.99
97.8%	0.63	0.98	0.70	2.12	0.78	0.76	0.80	0.80	0.77	0.83	0.85	1.00	0.77	1.12	1.55	0.96
96.8%	0.61	0.99	0.67	2.17	0.75	0.81	0.89	0.74	0.72	0.69	0.81	1.02	0.71	1.16	1.52	0.95
95.8%	0.63	0.93	0.66	2.06	0.78	0.78	0.86	0.73	0.68	0.63	0.82	0.99	0.77	1.10	1.48	0.93
94.8%	0.70	0.95	0.67	2.19	0.82	0.82	0.88	0.73	0.68	0.67	0.87	0.92	0.84	1.06	1.66	0.96
93.8%	0.77	0.92	0.67	1.95	0.83	0.87	0.92	0.76	0.72	0.67	0.88	0.91	0.80	0.99	1.48	0.94
93.2%	0.82	0.81	0.67	1.95	0.82	0.87	0.88	0.74	0.70	0.67	0.95	0.88	0.92	1.04	1.24	0.93
92.3%	0.88	0.70	0.66	1.55	0.76	0.86	0.83	0.73	0.73	0.75	0.99	0.81	1.04	1.05	1.01	0.89
91.4%	0.98	0.74	0.67	1.47	0.86	0.91	0.86	0.75	0.80	0.78	1.08	0.80	1.07	1.00	1.07	0.92
90.2%	1.05	0.69	0.79	1.26	0.97	0.85	0.83	0.82	0.85	0.72	0.97	0.71	0.94	0.82	0.87	0.88
89.1%	1.21	0.81	0.77	1.34	0.92	0.82	0.79	0.82	0.87	0.70	0.96	0.71	0.85	0.87	0.90	0.89
86.7%	1.71	0.97	1.19	1.57	1.38	1.00	1.10	1.18	1.33	1.27	1.02	0.94	1.04	0.94	1.17	1.19
86.1%	1.68	0.75	0.99	1.06	1.07	0.95	0.91	0.89	1.11	1.00	1.19	0.75	1.14	1.02	1.00	1.03
85.3%	1.63	0.80	0.95	0.93	0.88	0.94	0.81	0.72	0.97	0.92	1.20	0.71	1.09	1.02	1.01	0.97
84.3%	1.63	1.05	0.86	0.87	0.89	1.14	0.86	0.66	0.89	0.88	1.54	0.81	1.29	1.23	1.51	1.07
83.3%	1.70	1.16	0.83	0.95	0.93	1.05	0.85	0.65	0.96	0.86	1.45	0.72	1.18	1.16	1.57	1.07
82.1%	1.77	1.36	0.82	1.08	0.92	1.29	0.95	0.63	0.88	0.88	1.58	0.88	1.31	1.20	2.13	1.18
81.2%	1.74	1.52	0.90	1.28	1.01	1.44	1.11	0.61	0.87	0.95	1.51	0.94	1.28	1.59	2.20	1.26
79.9%	1.65	1.95	1.15	1.89	1.34	1.60	1.39	0.71	0.98	0.99	2.01	1.34	1.59	1.99	2.87	1.56

Table B. 4: EKF [Meas. CAP] SOC maximum absolute error over the battery lifespan.

SOHcap	UDDS	HWFET	LA92	US06	WLTP	Reo 1	Reo 2	Reo 3	Reo 4	Reo 5	Reo 6	Reo 7	Reo 8	Reo 9	Reo US06	Average
100.0%	1.26	3.05	2.20	3.58	3.21	2.93	2.90	1.78	2.08	2.38	2.92	3.41	2.48	3.20	3.50	2.72
99.4%	1.30	2.68	1.91	3.43	2.98	2.93	2.67	1.52	1.75	2.05	2.66	3.09	1.90	3.07	3.35	2.49
99.0%	1.37	2.45	1.77	3.36	2.86	2.51	2.57	1.63	1.72	1.76	2.51	2.82	1.50	2.65	3.15	2.31
97.8%	1.18	2.30	2.20	3.58	2.88	2.47	2.50	1.69	1.52	1.82	2.31	2.74	1.53	2.76	3.07	2.30
96.8%	1.08	2.28	2.17	3.90	2.77	2.40	2.69	1.69	1.78	1.76	2.39	2.87	1.22	2.78	2.89	2.31
95.8%	1.28	2.07	2.04	3.84	2.70	2.03	2.42	1.53	1.65	1.67	2.31	2.69	1.22	2.53	2.69	2.18
94.8%	1.53	2.10	2.07	4.06	2.53	1.95	2.21	1.32	1.48	1.64	2.07	2.64	1.28	2.53	3.03	2.16
93.8%	1.72	1.98	1.85	3.76	2.34	1.94	2.25	1.54	1.62	1.59	1.87	2.67	1.51	2.38	2.64	2.11
93.2%	1.74	1.68	1.76	3.67	2.14	1.84	1.94	1.39	1.29	1.30	1.74	2.10	1.40	1.95	2.28	1.88
92.3%	1.97	1.38	1.49	3.08	1.72	1.52	1.72	1.32	1.18	1.47	1.55	1.78	1.59	1.68	1.93	1.69
91.4%	2.08	1.46	1.39	2.94	1.70	1.58	1.67	1.24	1.25	1.40	1.76	1.97	1.67	1.79	2.05	1.73
90.2%	2.38	1.24	1.62	2.23	1.89	1.51	1.53	1.58	1.39	1.45	1.64	1.49	1.57	1.44	1.63	1.64
89.1%	2.65	1.35	1.47	2.60	2.23	1.69	1.75	1.58	1.69	1.29	1.62	1.41	1.50	1.66	1.75	1.75
86.7%	3.27	1.90	2.16	2.90	2.77	2.29	2.44	2.07	2.19	2.12	1.98	2.13	1.82	1.88	2.15	2.27
86.1%	3.06	1.46	1.69	2.09	2.11	1.63	1.89	1.84	2.10	1.72	1.97	1.66	1.94	1.97	2.25	1.96
85.3%	2.92	1.50	1.63	1.89	1.65	1.66	1.72	1.40	1.90	1.83	1.99	1.62	1.96	1.93	2.31	1.86
84.3%	2.89	1.83	1.84	1.79	1.67	1.82	1.88	1.62	2.37	2.24	2.29	1.95	2.28	2.17	2.88	2.10
83.3%	2.86	2.31	1.81	1.68	1.67	1.73	1.83	1.60	2.14	2.31	2.17	1.75	2.18	2.04	2.99	2.07
82.1%	2.84	2.71	1.82	2.08	1.65	1.94	1.96	1.65	2.82	2.64	2.31	2.04	2.38	2.11	3.38	2.29
81.2%	2.57	3.28	1.99	2.33	2.05	2.02	2.04	1.76	2.86	2.77	2.33	2.17	2.38	2.49	3.58	2.44
79.9%	2.40	4.23	2.32	3.60	3.11	2.57	2.39	1.88	3.24	3.08	2.85	2.36	2.57	3.18	4.04	2.92

Table B. 5: EKF [Meas. CAP and OCVc] SOC RMSE over battery lifespan.

SOHcap	UDDS	HWFET	LA92	US06	WLTP	Reo 1	Reo 2	Reo 3	Reo 4	Reo 5	Reo 6	Reo 7	Reo 8	Reo 9	Reo US06	Average
100.0%	0.69	1.28	0.67	2.33	0.87	0.92	0.95	0.76	0.76	0.81	0.85	1.15	0.72	1.17	1.87	1.05
99.4%	0.89	0.98	0.77	1.94	0.79	0.82	0.83	0.87	0.96	0.97	0.92	1.17	0.80	1.29	1.56	1.04
99.0%	1.05	0.84	0.89	1.73	0.85	0.75	0.86	0.97	1.11	1.10	1.00	1.29	1.00	1.41	1.30	1.08
97.8%	0.96	0.80	0.88	1.81	0.81	0.82	0.87	1.03	0.99	1.12	1.04	1.19	1.01	1.30	1.27	1.06
96.8%	0.93	0.80	0.84	1.82	0.81	0.85	0.95	0.87	0.89	0.93	0.93	1.21	0.95	1.35	1.23	1.02
95.8%	0.91	0.74	0.85	1.67	0.81	0.87	0.94	0.87	0.86	0.84	0.92	1.19	1.03	1.29	1.16	1.00
94.8%	0.94	0.76	0.82	1.75	0.83	0.90	0.96	0.84	0.82	0.97	1.02	1.12	1.09	1.23	1.28	1.02
93.8%	0.93	0.70	0.82	1.48	0.84	0.94	0.94	0.80	0.84	0.91	0.95	1.01	0.96	1.15	1.10	0.96
93.2%	0.95	0.68	0.83	1.43	0.82	0.97	0.95	0.78	0.91	0.97	1.09	1.18	1.15	1.30	0.93	1.00
92.3%	0.92	0.80	0.95	1.00	0.93	1.01	0.93	1.03	0.90	1.20	1.21	1.20	1.32	1.34	0.85	1.04
91.4%	0.95	0.80	0.95	0.91	0.87	1.08	1.03	1.00	1.02	1.26	1.34	1.16	1.36	1.33	0.84	1.06
90.2%	0.98	0.98	0.93	0.65	0.88	1.04	0.98	0.92	1.02	1.13	1.29	1.24	1.37	1.28	1.04	1.05
89.1%	0.84	1.19	1.13	0.81	0.96	1.25	1.17	1.07	1.15	1.14	1.38	1.31	1.37	1.49	1.14	1.16
86.7%	0.87	1.10	1.14	0.74	0.97	1.26	1.14	1.12	1.13	1.03	1.37	1.27	1.27	1.41	1.11	1.13
86.1%	0.91	1.71	1.47	1.09	1.35	1.54	1.42	1.46	1.48	1.53	1.86	1.76	1.88	1.88	1.85	1.54
85.3%	1.02	1.93	1.57	1.33	1.53	1.74	1.70	1.74	1.71	1.75	1.97	1.88	2.02	1.98	2.04	1.73
84.3%	1.18	2.46	1.94	1.87	1.92	2.15	2.05	2.07	2.15	2.17	2.48	2.35	2.50	2.43	2.80	2.17
83.3%	1.22	2.60	2.03	2.01	2.05	2.14	2.12	2.20	2.02	2.35	2.45	2.15	2.50	2.32	2.94	2.21
82.1%	1.34	2.93	2.24	2.49	2.15	2.55	2.41	2.37	2.83	2.94	2.72	2.77	2.92	2.66	3.63	2.60
81.2%	1.51	3.07	2.60	2.79	2.35	2.79	2.73	2.53	2.87	2.74	2.77	2.98	2.90	3.20	3.78	2.77
79.9%	1.73	3.61	3.01	3.42	2.85	3.10	3.11	2.97	3.46	3.32	3.46	3.62	3.46	3.69	4.48	3.28

Table B. 6: EKF [Meas. CAP and OCVc] SOC maximum absolute error over the battery lifespan.

SOHcap	UDDS	HWFET	LA92	US06	WLTP	Reo 1	Reo 2	Reo 3	Reo 4	Reo 5	Reo 6	Reo 7	Reo 8	Reo 9	Reo US06	Average
100.0%	1.27	3.04	2.18	3.57	3.18	2.92	2.88	1.76	2.05	2.36	2.89	3.40	2.47	3.19	3.48	2.71
99.4%	1.56	2.54	1.84	3.19	2.73	2.65	2.43	1.74	1.73	1.95	2.37	2.96	1.77	2.96	3.10	2.37
99.0%	1.78	2.22	1.73	3.04	2.48	2.06	2.20	1.96	2.07	2.04	2.07	2.62	1.78	2.49	2.71	2.22
97.8%	1.60	2.09	2.11	3.38	2.48	2.00	2.10	2.07	1.89	2.00	1.87	2.57	1.75	2.64	2.58	2.21
96.8%	1.52	2.07	2.09	3.65	2.34	1.91	2.25	1.66	1.70	1.68	1.90	2.74	1.55	2.72	2.38	2.15
95.8%	1.41	1.82	1.92	3.54	2.21	1.55	1.91	1.62	1.65	1.55	1.76	2.60	1.56	2.52	2.32	2.00
94.8%	1.54	1.80	1.90	3.72	2.00	1.67	1.66	1.53	1.60	1.70	1.57	2.53	1.61	2.52	2.53	1.99
93.8%	1.68	1.56	1.57	3.36	1.81	1.71	1.70	1.46	1.62	1.69	1.70	2.54	1.46	2.30	2.27	1.90
93.2%	1.71	1.22	1.52	3.22	1.62	1.59	1.54	1.44	1.82	1.81	1.70	1.95	1.75	1.91	1.86	1.78
92.3%	1.86	1.49	1.73	2.48	1.79	1.60	1.57	1.91	1.73	2.18	1.80	1.83	2.16	2.05	1.71	1.86
91.4%	1.83	1.50	1.71	2.25	1.64	1.69	1.80	1.84	1.91	2.23	1.97	1.75	2.21	2.03	1.68	1.87
90.2%	1.72	1.82	1.56	1.34	1.63	1.61	1.63	1.59	1.96	2.01	1.79	2.01	2.50	2.08	1.91	1.81
89.1%	1.44	2.12	1.91	1.87	1.86	1.96	1.95	1.90	2.16	1.99	2.05	2.11	2.32	2.40	2.09	2.01
86.7%	1.47	1.96	1.87	1.47	1.80	1.92	1.81	1.99	2.11	1.84	1.90	2.13	2.02	2.36	1.91	1.90
86.1%	1.53	2.72	2.25	2.02	2.38	2.41	2.26	2.38	2.49	2.40	2.56	2.76	2.92	3.02	2.96	2.47
85.3%	1.66	2.98	2.37	2.27	2.47	2.70	2.52	2.65	2.72	2.65	2.73	2.87	3.15	3.18	3.12	2.67
84.3%	1.78	3.85	2.83	2.97	2.93	3.38	2.85	3.08	3.17	3.06	3.53	3.48	3.80	3.81	4.09	3.24
83.3%	1.79	4.23	2.96	3.33	3.36	3.41	3.23	3.16	2.98	3.33	3.61	3.21	3.81	3.65	4.39	3.36
82.1%	1.87	4.67	3.34	4.00	3.62	4.22	3.70	3.41	3.94	4.07	4.06	3.99	4.52	4.03	5.01	3.90
81.2%	2.08	5.33	3.93	4.54	4.32	4.58	4.42	3.57	3.86	3.62	4.08	4.23	4.62	4.71	5.13	4.20
79.9%	2.37	6.17	4.77	5.71	5.29	5.08	5.05	4.10	4.50	4.47	5.04	4.90	5.51	5.42	6.37	4.98

Table B. 7: EKF/SVSF SOC RMSE over battery lifespan.

SOHcap	UDDS	HWFET	LA92	US06	WLTP	Reo 1	Reo 2	Reo 3	Reo 4	Reo 5	Reo 6	Reo 7	Reo 8	Reo 9	Reo US06	Average
100.0%	0.84	0.81	0.78	1.39	0.87	0.71	1.02	1.02	1.04	1.03	0.98	1.27	0.80	1.28	1.04	0.99
99.4%	0.84	0.81	0.85	1.28	0.91	0.79	0.94	1.08	1.20	1.11	1.08	1.24	0.86	1.36	0.96	1.02
99.0%	0.89	0.79	0.89	1.21	0.95	0.72	0.97	1.14	1.27	1.17	1.10	1.30	1.00	1.47	0.89	1.05
97.8%	0.73	0.76	0.79	1.37	0.83	0.75	0.91	1.07	1.06	1.07	1.06	1.12	0.97	1.27	0.94	0.98
96.8%	0.67	0.73	0.70	1.45	0.77	0.73	0.94	0.90	0.93	0.84	0.91	1.09	0.84	1.28	0.93	0.91
95.8%	0.65	0.68	0.67	1.38	0.75	0.71	0.88	0.85	0.85	0.71	0.86	1.05	0.88	1.20	0.96	0.87
94.8%	0.71	0.70	0.64	1.54	0.75	0.74	0.86	0.79	0.78	0.75	0.91	0.94	0.91	1.12	1.14	0.88
93.8%	0.77	0.67	0.64	1.40	0.75	0.79	0.87	0.78	0.79	0.71	0.87	0.88	0.81	1.03	1.00	0.85
93.2%	0.82	0.66	0.65	1.42	0.74	0.82	0.84	0.75	0.79	0.73	0.99	0.94	0.96	1.12	0.88	0.87
92.3%	0.88	0.70	0.68	1.10	0.71	0.85	0.78	0.79	0.78	0.84	1.04	0.87	1.11	1.16	0.79	0.87
91.4%	0.99	0.67	0.67	1.09	0.78	0.89	0.82	0.77	0.84	0.85	1.12	0.82	1.13	1.09	0.83	0.89
90.2%	1.06	0.67	0.79	1.06	0.87	0.84	0.79	0.79	0.85	0.73	1.02	0.75	1.00	0.92	0.84	0.87
89.1%	1.25	0.89	0.78	1.21	0.84	0.84	0.78	0.80	0.87	0.68	1.01	0.75	0.89	0.95	0.91	0.90
86.7%	1.82	0.91	1.29	1.59	1.41	1.05	1.18	1.21	1.34	1.33	1.07	0.98	1.09	0.97	1.17	1.23
86.1%	1.79	0.77	1.07	1.06	1.06	0.97	0.94	0.92	1.14	1.04	1.17	0.77	1.14	1.05	1.02	1.06
85.3%	1.74	0.84	1.05	0.96	0.89	0.95	0.83	0.74	1.00	0.96	1.17	0.73	1.10	1.05	1.03	1.00
84.3%	1.75	1.12	0.93	0.88	0.91	1.11	0.85	0.67	0.92	0.92	1.50	0.82	1.29	1.27	1.53	1.10
83.3%	1.84	1.19	0.91	0.94	0.95	1.01	0.83	0.66	1.01	0.92	1.37	0.74	1.18	1.18	1.52	1.08
82.1%	1.94	1.35	0.90	1.00	0.92	1.23	0.90	0.66	0.90	0.90	1.47	0.86	1.30	1.22	1.99	1.17
81.2%	1.92	1.47	0.91	1.10	0.99	1.36	1.01	0.66	0.89	1.02	1.39	0.89	1.26	1.60	2.03	1.23
79.9%	1.86	1.86	1.07	1.65	1.24	1.47	1.26	0.64	0.94	1.00	1.87	1.24	1.55	1.95	2.67	1.48

Table B. 8: EKF/SVSF SOC maximum absolute error over the battery lifespan.

SOHcap	UDDS	HWFET	LA92	US06	WLTP	Reo 1	Reo 2	Reo 3	Reo 4	Reo 5	Reo 6	Reo 7	Reo 8	Reo 9	Reo US06	Average
100.0%	1.63	1.60	1.63	2.69	2.88	2.45	2.58	2.07	1.84	1.95	2.52	2.26	1.78	2.14	2.67	2.18
99.4%	1.62	1.79	1.92	2.67	2.75	2.55	2.45	2.22	2.13	2.19	2.35	2.26	1.93	2.36	2.64	2.26
99.0%	1.69	1.72	1.98	2.60	2.67	2.20	2.38	2.33	2.35	2.31	2.27	2.42	2.16	2.62	2.33	2.27
97.8%	1.45	1.72	1.70	2.84	2.75	2.26	2.41	2.29	2.05	2.15	2.21	2.15	2.08	2.16	2.54	2.18
96.8%	1.30	1.51	1.62	2.78	2.67	2.25	2.56	1.87	1.80	1.79	2.25	1.96	1.75	2.16	2.37	2.04
95.8%	1.16	1.44	1.52	2.71	2.58	1.95	2.34	1.78	1.69	1.52	2.21	1.92	1.72	2.00	2.33	1.92
94.8%	1.41	1.50	1.66	2.79	2.45	1.93	2.14	1.60	1.50	1.61	2.03	1.99	1.62	1.96	2.64	1.92
93.8%	1.63	1.47	1.56	2.58	2.26	1.74	2.18	1.47	1.55	1.45	1.86	2.04	1.35	1.91	2.24	1.82
93.2%	1.65	1.36	1.49	2.70	2.09	1.63	1.87	1.36	1.62	1.51	1.73	1.76	1.57	1.84	1.96	1.74
92.3%	1.90	1.43	1.27	2.31	1.62	1.38	1.66	1.63	1.43	1.75	1.65	1.68	1.90	1.97	1.55	1.68
91.4%	2.04	1.23	1.20	2.30	1.67	1.34	1.58	1.44	1.53	1.63	1.76	1.59	1.80	1.80	1.70	1.64
90.2%	2.36	1.18	1.57	2.13	1.43	1.39	1.39	1.43	1.34	1.29	1.66	1.32	1.75	1.59	1.63	1.56
89.1%	2.73	1.75	1.53	2.52	1.81	1.49	1.52	1.52	1.54	1.24	1.63	1.33	1.50	1.68	1.73	1.70
86.7%	3.48	1.69	2.29	2.86	2.76	2.39	2.55	2.13	2.26	2.24	2.11	2.20	1.90	2.01	2.10	2.33
86.1%	3.26	1.48	1.80	2.18	2.05	1.72	1.93	1.89	2.17	1.75	1.95	1.63	1.92	1.98	2.24	2.00
85.3%	3.11	1.52	1.68	1.94	1.61	1.66	1.72	1.38	1.91	1.86	1.96	1.60	1.96	1.95	2.30	1.88
84.3%	3.03	1.95	1.86	1.78	1.68	1.82	1.88	1.61	2.40	2.29	2.28	1.93	2.27	2.19	2.88	2.12
83.3%	3.04	2.37	1.83	1.67	1.68	1.72	1.82	1.58	2.17	2.34	2.15	1.71	2.17	2.04	2.98	2.08
82.1%	3.03	2.66	1.83	2.07	1.65	1.85	1.95	1.64	2.85	2.69	2.28	2.02	2.36	2.11	3.37	2.29
81.2%	2.79	3.19	2.00	2.12	1.94	2.00	2.03	1.73	2.86	2.80	2.33	2.16	2.36	2.54	3.58	2.43
79.9%	2.65	4.05	2.27	3.14	2.83	2.29	2.20	1.85	3.27	3.11	2.71	2.35	2.55	3.17	3.95	2.83

Table B. 9: EKF/SVSF [OCVc] SOC RMSE over battery lifespan.

SOHcap	UDDS	HWFET	LA92	US06	WLTP	Reo 1	Reo 2	Reo 3	Reo 4	Reo 5	Reo 6	Reo 7	Reo 8	Reo 9	Reo US06	Average
100.0%	1.32	1.27	1.18	1.05	1.31	0.86	1.69	1.65	1.71	1.66	1.45	1.92	1.08	1.83	0.95	1.40
99.4%	1.31	1.37	1.27	1.01	1.45	1.06	1.59	1.72	1.91	1.75	1.60	1.92	1.22	1.97	1.00	1.48
99.0%	1.38	1.33	1.34	1.03	1.53	1.01	1.66	1.81	1.95	1.84	1.66	2.00	1.37	2.15	1.20	1.55
97.8%	1.23	1.40	1.21	1.01	1.33	1.13	1.51	1.70	1.77	1.74	1.68	1.78	1.38	1.93	1.04	1.46
96.8%	1.14	1.37	1.13	1.01	1.26	1.07	1.62	1.53	1.64	1.52	1.46	1.74	1.23	1.93	1.08	1.38
95.8%	1.08	1.31	1.13	0.99	1.25	1.05	1.46	1.50	1.62	1.33	1.40	1.74	1.30	1.87	1.00	1.34
94.8%	1.07	1.38	1.04	1.00	1.16	1.00	1.42	1.36	1.49	1.43	1.46	1.60	1.34	1.79	1.08	1.31
93.8%	1.05	1.32	1.05	0.96	1.26	1.11	1.46	1.33	1.61	1.40	1.32	1.50	1.15	1.74	1.18	1.30
93.2%	1.06	1.50	1.07	0.92	1.23	1.19	1.52	1.32	1.63	1.40	1.68	1.77	1.38	1.91	1.33	1.39
92.3%	1.01	1.82	1.23	0.98	1.56	1.38	1.55	1.71	1.59	1.71	1.81	1.83	1.68	2.19	1.50	1.57
91.4%	1.05	1.76	1.27	1.10	1.36	1.44	1.77	1.61	1.74	1.71	1.91	1.75	1.73	2.12	1.40	1.58
90.2%	1.12	1.86	1.12	0.94	1.40	1.31	1.56	1.48	1.77	1.72	1.87	2.03	1.81	2.13	1.82	1.60
89.1%	0.94	2.09	1.39	1.36	1.45	1.56	1.75	1.69	1.84	1.65	1.86	2.00	1.65	2.14	1.91	1.69
86.7%	0.96	1.46	1.10	0.92	1.07	1.31	1.28	1.31	1.35	1.07	1.47	1.47	1.17	1.70	1.40	1.27
86.1%	0.95	2.15	1.44	1.38	1.61	1.66	1.69	1.66	1.67	1.58	2.05	2.02	1.95	2.25	2.25	1.75
85.3%	1.00	2.37	1.51	1.61	1.80	1.85	1.98	1.94	1.88	1.81	2.18	2.13	2.09	2.38	2.42	1.93
84.3%	1.09	2.89	1.90	2.15	2.27	2.30	2.40	2.30	2.30	2.22	2.75	2.67	2.60	2.89	3.21	2.40
83.3%	1.08	2.96	1.92	2.18	2.34	2.19	2.39	2.39	2.07	2.34	2.59	2.36	2.55	2.68	3.24	2.35
82.1%	1.16	3.21	2.06	2.56	2.39	2.68	2.67	2.55	2.93	2.85	2.80	3.00	2.92	2.98	3.82	2.71
81.2%	1.26	3.27	2.42	2.74	2.50	2.86	2.86	2.54	2.85	2.66	2.84	3.15	2.84	3.50	3.92	2.81
79.9%	1.46	3.75	2.90	3.38	2.95	3.09	3.23	2.99	3.44	3.23	3.52	3.74	3.46	3.90	4.60	3.31

Table B. 10: EKF/SVSF [OCVc] maximum absolute error over the battery lifespan.

SOHcap	UDDS	HWFET	LA92	US06	WLTP	Reo 1	Reo 2	Reo 3	Reo 4	Reo 5	Reo 6	Reo 7	Reo 8	Reo 9	Reo US06	Average
100.0%	2.36	2.84	2.49	2.14	2.98	2.08	3.54	3.10	3.07	3.00	2.91	3.13	2.28	3.14	2.07	2.74
99.4%	2.33	3.01	2.63	2.00	3.21	2.51	3.24	3.21	3.43	3.15	3.19	3.11	2.39	3.45	2.20	2.87
99.0%	2.35	2.86	2.70	1.92	3.29	2.37	3.36	3.35	3.44	3.34	3.17	3.23	2.62	3.75	2.60	2.96
97.8%	2.13	3.01	2.48	2.04	2.86	2.42	3.01	3.21	3.19	3.12	3.15	2.95	2.63	3.37	2.18	2.78
96.8%	1.96	2.93	2.38	2.01	2.73	2.30	3.30	2.85	3.17	2.82	2.79	2.79	2.34	3.26	2.39	2.67
95.8%	1.85	2.77	2.38	1.88	2.75	2.12	2.92	2.86	3.10	2.53	2.69	2.83	2.39	3.16	2.05	2.55
94.8%	1.79	2.89	2.08	1.90	2.52	1.93	2.83	2.60	2.88	2.68	2.70	2.57	2.43	2.99	2.13	2.46
93.8%	1.70	2.73	2.13	1.74	2.75	2.19	2.93	2.53	3.16	2.63	2.52	2.44	2.20	2.94	2.31	2.46
93.2%	1.71	2.95	2.18	1.68	2.65	2.33	2.99	2.52	3.09	2.65	2.99	2.83	2.52	3.17	2.59	2.59
92.3%	1.76	3.34	2.38	1.98	3.19	2.69	2.99	3.09	3.03	3.09	3.13	2.91	3.12	3.69	2.81	2.88
91.4%	1.80	3.22	2.43	2.26	2.85	2.68	3.40	2.91	3.33	3.04	3.19	2.72	3.14	3.56	2.52	2.87
90.2%	1.74	3.30	2.04	1.99	2.88	2.31	2.89	2.59	3.33	3.06	2.97	3.34	3.50	3.88	3.24	2.87
89.1%	1.71	3.59	2.50	2.55	2.85	2.75	3.02	2.99	3.48	2.87	3.04	3.25	2.94	3.84	3.49	2.99
86.7%	2.19	2.68	1.89	1.81	2.11	2.21	2.21	2.42	2.65	1.97	2.27	2.53	1.99	3.18	2.64	2.32
86.1%	1.70	3.52	2.33	2.70	2.90	2.83	2.82	2.82	3.01	2.59	3.10	3.25	3.20	4.01	3.84	2.97
85.3%	1.68	3.75	2.41	2.95	2.99	3.13	3.06	3.12	3.25	2.82	3.29	3.37	3.34	4.26	3.97	3.16
84.3%	1.81	4.36	2.91	3.66	3.57	3.88	3.57	3.61	3.67	3.21	4.17	4.10	4.05	5.07	5.04	3.78
83.3%	1.81	4.58	2.95	3.56	3.78	3.75	3.48	3.70	3.37	3.22	4.00	3.77	3.99	4.72	5.16	3.72
82.1%	1.90	4.85	3.16	3.88	3.88	4.69	3.87	3.96	4.40	3.97	4.41	4.59	4.61	5.00	5.63	4.19
81.2%	2.00	5.49	3.62	4.20	4.44	4.75	4.24	3.85	4.05	3.52	4.41	4.72	4.54	5.68	5.66	4.34
79.9%	2.09	6.20	4.43	5.34	5.26	5.15	4.90	4.33	4.72	4.10	5.33	5.34	5.43	6.14	6.38	5.01

Table B. 11: EKF/SVSF capacity SOH RMSE over battery lifespan.

SOHcap	UDDS	HWFET	LA92	US06	WLTP	Reo 1	Reo 2	Reo 3	Reo 4	Reo 5	Reo 6	Reo 7	Reo 8	Reo 9	Reo US06	Average
100.0%	3.94	7.02	4.52	6.78	5.69	5.36	6.07	6.02	5.76	5.28	6.34	6.12	4.87	5.58	6.73	5.74
99.4%	3.28	6.79	4.28	6.59	5.39	5.24	5.45	5.52	5.42	4.78	5.94	5.75	4.82	5.47	6.58	5.42
99.0%	3.31	6.41	4.21	6.61	5.19	4.97	5.35	5.59	5.17	4.76	5.84	5.61	4.58	5.59	6.68	5.32
97.8%	2.63	5.89	3.51	5.84	4.53	4.29	4.43	4.47	4.47	4.01	4.99	4.73	4.02	4.73	5.96	4.57
96.8%	2.11	5.37	2.97	5.19	3.77	3.95	4.29	4.13	3.72	3.60	4.49	4.17	3.55	4.16	5.48	4.06
95.8%	1.84	4.67	2.64	4.79	3.46	3.23	3.49	3.66	3.52	2.97	3.98	3.90	3.23	3.67	4.67	3.58
94.8%	1.44	4.23	2.09	4.45	2.83	2.58	2.91	3.00	2.90	2.55	3.27	3.10	2.88	3.23	4.66	3.07
93.8%	1.12	3.67	1.76	3.77	2.57	2.43	2.58	2.51	2.67	2.34	2.75	2.88	2.41	2.79	4.25	2.70
93.2%	0.96	3.44	1.59	3.66	2.20	2.10	2.34	2.26	2.36	1.88	2.94	2.61	2.24	2.38	3.81	2.45
92.3%	0.77	3.23	1.38	3.42	2.21	2.00	2.02	2.27	1.99	1.93	2.41	2.29	2.40	2.61	3.24	2.28
91.4%	0.68	2.81	1.31	3.06	1.67	1.75	1.92	1.78	1.89	1.63	2.02	1.93	2.14	2.18	2.94	1.98
90.2%	0.68	2.19	0.79	1.56	1.40	1.29	1.21	1.26	1.63	1.56	1.87	2.03	2.07	2.08	2.30	1.59
89.1%	0.89	2.30	0.73	2.52	1.42	1.37	1.07	1.23	1.62	0.99	1.51	1.56	1.79	1.38	2.22	1.51
86.7%	1.65	0.81	1.25	1.18	0.89	0.87	0.70	0.75	1.21	1.03	0.97	0.56	1.46	0.83	1.13	1.02
86.1%	1.60	0.88	1.17	0.98	1.03	0.82	0.47	0.68	1.14	0.90	0.87	0.56	1.26	0.84	1.08	0.95
85.3%	1.76	0.84	1.30	0.92	1.50	0.88	0.48	0.65	1.17	0.91	1.02	0.61	1.22	0.99	1.16	1.03
84.3%	1.88	0.78	1.27	0.89	1.26	0.86	0.47	0.74	1.29	1.03	0.98	0.58	1.26	1.21	1.07	1.04
83.3%	2.15	0.71	1.46	1.28	1.86	0.90	0.89	1.14	1.50	1.21	1.16	0.84	1.30	1.57	1.01	1.27
82.1%	2.45	0.64	1.70	1.00	1.77	0.94	1.11	1.55	1.51	1.58	1.62	1.21	1.44	1.69	1.06	1.42
81.2%	2.71	1.20	1.79	1.22	1.82	0.96	1.30	2.01	1.69	1.71	1.56	1.29	1.67	1.71	1.10	1.58
79.9%	3.09	0.84	1.79	1.40	1.47	1.16	1.21	1.97	2.03	1.89	1.37	1.40	1.55	1.78	1.19	1.61

Table B. 12: EKF/SVSF mean capacity SOH estimation over battery lifespan.

SOHcap	UDDS	HWFET	LA92	US06	WLTP	Reo 1	Reo 2	Reo 3	Reo 4	Reo 5	Reo 6	Reo 7	Reo 8	Reo 9	Reo US06	Average
100.0%	96.48	93.76	96.02	93.89	95.25	95.83	94.89	94.38	94.45	94.89	94.70	94.37	96.23	95.28	94.14	94.97
99.4%	96.55	93.39	95.73	93.58	95.04	95.56	94.94	94.30	94.19	94.79	94.62	94.16	95.81	94.90	93.78	94.76
99.0%	96.15	93.39	95.46	93.22	94.88	95.52	94.70	93.89	94.06	94.44	94.36	93.94	95.71	94.37	93.37	94.50
97.8%	95.48	92.59	94.78	92.70	94.17	94.79	94.29	93.70	93.47	93.92	93.83	93.53	94.95	93.86	92.91	93.93
96.8%	94.96	92.06	94.27	92.29	93.82	93.98	93.33	93.05	93.26	93.33	93.28	93.05	94.44	93.37	92.28	93.39
95.8%	94.21	91.70	93.58	91.65	93.06	93.54	93.02	92.51	92.45	92.96	92.70	92.31	93.68	92.78	92.02	92.81
94.8%	93.56	91.08	93.02	90.97	92.57	93.05	92.46	92.15	92.05	92.36	92.29	92.03	92.90	92.13	91.06	92.25
93.8%	92.97	90.65	92.44	90.62	91.83	92.18	91.81	91.69	91.41	91.64	91.76	91.31	92.42	91.57	90.41	91.65
93.2%	92.49	90.21	91.95	90.08	91.51	91.78	91.35	91.28	91.05	91.48	90.98	90.91	91.87	91.24	90.12	91.22
92.3%	91.80	89.44	91.19	89.42	90.52	90.90	90.67	90.30	90.53	90.50	90.48	90.26	90.72	90.10	89.69	90.43
91.4%	91.19	88.94	90.39	88.83	90.15	90.24	89.85	89.93	89.77	89.96	89.94	89.73	90.09	89.61	89.14	89.85
90.2%	90.06	88.35	89.88	89.05	89.16	89.64	89.36	89.34	89.03	88.91	88.91	88.41	89.01	88.52	88.42	89.07
89.1%	89.60	87.08	88.83	87.07	88.09	88.31	88.28	88.26	88.12	88.41	88.17	87.79	88.38	88.10	87.47	88.13
86.7%	88.09	86.15	87.71	86.27	86.77	87.13	87.25	87.07	87.12	87.35	87.19	86.88	87.36	86.92	86.45	87.05
86.1%	87.40	85.41	86.96	85.71	85.75	86.40	86.30	86.41	86.45	86.44	86.37	86.13	86.35	86.18	85.75	86.27
85.3%	86.75	84.64	86.32	85.03	84.86	85.59	85.56	85.67	85.73	85.70	85.71	85.47	85.63	85.49	84.93	85.54
84.3%	85.81	83.69	85.25	84.11	84.03	84.55	84.52	84.72	84.86	84.74	84.62	84.35	84.54	84.58	84.15	84.57
83.3%	85.11	82.91	84.52	83.16	83.09	83.75	83.71	84.13	84.30	84.05	84.12	83.88	83.79	84.14	83.62	83.88
82.1%	84.17	81.95	83.52	82.52	82.18	82.31	82.58	83.25	83.06	83.25	83.30	82.91	82.90	82.94	82.52	82.89
81.2%	83.58	81.03	82.70	82.00	81.60	81.63	82.16	82.95	82.55	82.48	82.40	82.23	82.26	82.09	81.82	82.23
79.9%	82.60	80.19	81.16	80.53	80.41	80.68	80.85	81.66	81.50	81.39	80.91	81.04	80.85	80.96	80.74	81.03

Table B. 13: EKF/SVSF [OCVc] capacity RMSE over battery lifespan.

SOHcap	UDDS	HWFET	LA92	US06	WLTP	Reo 1	Reo 2	Reo 3	Reo 4	Reo 5	Reo 6	Reo 7	Reo 8	Reo 9	Reo US06	Average
100.0%	4.22	7.88	4.87	7.17	6.52	5.78	7.15	6.58	6.14	5.69	6.93	6.84	5.03	6.33	7.31	6.30
99.4%	3.52	7.53	4.59	7.00	6.18	5.76	6.42	6.04	5.78	5.13	6.57	6.44	4.95	6.26	7.18	5.96
99.0%	3.44	7.04	4.46	7.03	5.90	5.40	6.25	6.10	5.50	5.08	6.42	6.22	4.67	6.30	7.30	5.81
97.8%	2.77	6.59	3.70	6.23	5.05	4.68	5.10	4.78	4.77	4.26	5.59	5.24	4.12	5.35	6.51	4.98
96.8%	2.25	6.13	3.15	5.55	4.26	4.39	5.15	4.49	4.10	3.87	5.15	4.63	3.58	4.84	6.04	4.51
95.8%	1.96	5.38	2.81	5.17	3.97	3.64	4.22	4.01	3.92	3.20	4.72	4.37	3.27	4.35	5.16	4.01
94.8%	1.57	5.04	2.25	4.90	3.29	3.00	3.63	3.29	3.28	2.75	4.05	3.57	2.94	3.95	5.32	3.52
93.8%	1.26	4.48	1.96	4.21	3.16	2.95	3.52	2.90	3.20	2.58	3.56	3.35	2.39	3.61	4.91	3.20
93.2%	1.10	4.28	1.80	4.16	2.76	2.68	3.30	2.65	2.81	2.07	4.06	3.14	2.28	3.16	4.48	2.98
92.3%	0.86	4.14	1.63	3.93	2.87	2.72	2.99	2.71	2.48	2.10	3.56	2.84	2.47	3.68	3.92	2.86
91.4%	0.77	3.71	1.59	3.65	2.32	2.51	3.08	2.25	2.41	1.78	3.22	2.51	2.26	3.26	3.66	2.60
90.2%	0.80	3.08	1.05	2.21	2.22	1.94	2.40	1.88	2.38	1.90	3.03	2.70	1.97	3.24	3.07	2.26
89.1%	0.85	3.05	1.05	2.95	2.14	1.83	2.35	2.09	2.54	1.58	2.53	2.29	1.44	2.53	2.97	2.15
86.7%	1.36	1.60	1.09	1.56	1.10	1.13	1.17	1.27	1.96	1.26	1.47	1.07	0.95	1.79	1.84	1.38
86.1%	1.27	1.75	0.98	1.52	1.51	1.23	1.42	1.21	1.83	1.07	1.62	1.22	0.84	1.96	1.94	1.42
85.3%	1.36	1.65	1.04	1.42	1.77	1.39	1.53	1.25	1.85	1.14	1.61	1.21	0.80	2.08	1.88	1.47
84.3%	1.41	1.55	0.94	1.40	1.79	1.52	1.77	1.36	1.87	1.33	1.68	1.37	0.88	2.40	1.94	1.55
83.3%	1.62	1.34	1.04	1.21	1.86	0.96	1.31	1.59	1.97	1.46	1.45	1.35	0.86	2.32	1.77	1.47
82.1%	1.89	1.22	1.01	1.08	1.54	1.07	1.34	1.90	2.10	1.98	1.63	2.00	1.12	2.52	1.51	1.59
81.2%	2.09	1.21	1.07	1.20	1.46	1.07	1.19	1.89	1.99	1.88	1.66	1.62	1.21	2.54	1.52	1.57
79.9%	2.38	1.01	1.24	1.53	1.26	1.72	1.51	1.91	2.36	2.00	1.59	1.74	1.24	2.54	1.77	1.72

Table B. 14: EKF/SVSF SOC and SOH estimation results for fifteen subsequent drive cycles.

| SOHcap | Error [%] | | | | | | Mean SOH Estimated |
| | Mean Abs. | | RMS | | Max. Abs. | | |
	SOC	SOH	SOC	SOH	SOC	SOH	
100.0%	1.5	6.1	2.0	6.4	6.7	11.5	93.9
99.4%	1.4	5.8	1.9	6.2	6.8	11.5	93.6
99.0%	1.3	5.8	1.7	6.2	6.7	11.2	93.2
97.8%	1.6	5.1	2.0	5.4	6.3	10.7	92.7
96.8%	1.3	4.6	1.7	5.0	6.2	10.3	92.2
95.8%	1.2	4.3	1.6	4.6	5.8	9.5	91.5
94.8%	1.5	3.7	1.8	4.0	5.4	9.1	91.1
93.8%	1.2	3.5	1.5	3.8	4.8	8.6	90.4
93.2%	1.3	3.3	1.6	3.7	4.5	8.5	89.9
92.3%	1.4	3.3	1.6	3.7	4.2	9.1	89.0
91.4%	1.5	3.0	1.8	3.4	4.7	8.4	88.4
90.2%	1.1	2.6	1.4	3.0	3.4	7.2	87.7
89.1%	1.0	3.0	1.2	3.6	4.5	9.3	86.2
86.7%	1.7	1.6	2.0	2.1	4.6	7.2	85.8
86.1%	2.0	1.8	2.3	2.3	5.2	6.9	84.7
85.3%	1.7	2.0	2.0	2.7	5.1	9.0	83.8
84.3%	2.0	2.3	2.5	3.0	6.5	11.3	82.5
83.3%	1.9	2.6	2.4	3.7	7.9	14.8	81.4
82.1%	2.2	2.5	2.8	3.6	8.3	14.3	80.5
81.2%	2.1	2.5	2.8	3.6	8.4	14.4	79.7
79.9%	2.0	2.6	2.8	3.6	8.3	13.1	78.4

Table B. 15: "No Error" tuning robustness to sensor error for a new battery.

Case	ERROR [%]	UDDS	HWFET	LA92	US06	WLTP	Reo 1	Reo 2	Reo 3	Reo 4	Reo 5	Reo 6	Reo 7	Reo 8	Reo 9	Reo US06	Average
No error	RMSE	0.87	0.83	0.72	1.19	0.70	0.46	0.86	1.02	1.09	1.05	0.78	1.10	0.79	0.98	0.90	0.89
	Max Abs	1.68	1.59	1.58	2.40	1.43	1.19	1.76	1.90	1.76	1.99	1.55	2.15	1.62	1.89	2.28	1.79
+3% Current Gain	RMSE	1.00	1.01	0.88	1.11	0.80	0.58	0.94	1.15	1.24	1.22	0.92	1.26	1.00	1.13	0.84	1.01
	Max Abs	1.87	1.94	1.86	2.31	1.64	1.32	2.06	2.14	1.99	2.23	1.82	2.38	1.94	2.09	2.09	1.98
-3% Current Gain	RMSE	0.74	0.69	0.58	1.31	0.66	0.44	0.82	0.90	0.94	0.88	0.69	0.95	0.60	0.86	1.01	0.80
	Max Abs	1.48	1.23	1.29	2.57	1.78	1.50	1.91	1.65	1.79	1.72	1.50	1.92	1.30	1.68	2.47	1.72
+300mA Bias	RMSE	3.33	1.71	2.44	1.17	1.96	1.90	2.06	2.62	2.88	2.63	2.47	2.71	2.37	2.68	1.03	2.26
	Max Abs	5.07	2.91	3.89	2.17	3.17	3.22	3.72	4.14	4.24	4.17	3.95	4.58	3.87	4.45	1.88	3.70
-300mA Bias	RMSE	1.50	0.82	1.40	1.74	1.44	1.48	1.55	1.36	1.46	1.08	1.41	1.08	1.05	1.27	1.43	1.34
	Max Abs	2.08	1.64	2.04	2.93	2.51	2.69	2.75	1.90	2.21	2.08	2.38	1.61	2.15	1.97	2.78	2.25
+5°C bias	RMSE	0.92	0.89	0.79	0.90	0.72	0.52	0.86	1.05	1.12	1.12	0.86	1.17	0.90	1.02	0.72	0.90
	Max Abs	1.63	1.66	1.58	1.86	1.39	1.15	1.74	1.87	1.74	1.99	1.58	2.14	1.69	1.90	1.71	1.71
-5°C bias	RMSE	0.70	0.93	0.60	1.85	0.66	0.44	0.84	1.03	1.24	1.15	0.69	1.01	0.59	0.80	1.49	0.94
	Max Abs	1.34	1.45	1.22	3.30	1.90	1.50	2.12	2.22	3.05	2.86	1.69	1.92	1.24	1.57	3.00	2.03
+5mV bias	RMSE	0.47	0.77	0.50	1.60	0.66	0.53	0.80	0.78	0.85	0.77	0.59	0.78	0.50	0.69	1.27	0.77
	Max Abs	1.01	1.48	0.96	2.94	1.93	1.75	2.07	1.77	2.20	1.82	1.75	1.50	0.97	1.45	2.80	1.76
-5mV bias	RMSE	1.38	1.17	1.18	0.91	1.04	0.86	1.18	1.45	1.52	1.51	1.23	1.58	1.30	1.46	0.78	1.24
	Max Abs	2.36	2.20	2.21	1.92	1.92	1.65	2.39	2.57	2.43	2.62	2.20	2.82	2.26	2.54	1.76	2.26

Table B. 16:: "+-300mA" tuning robustness to sensor error for a new battery.

Case	ERROR [%]	UDDS	HWFET	LA92	US06	WLTP	Reo 1	Reo 2	Reo 3	Reo 4	Reo 5	Reo 6	Reo 7	Reo 8	Reo 9	Reo US06	Average
No error	*RMSE*	0.84	0.81	0.77	1.48	0.87	0.72	1.01	0.99	1.01	1.00	0.97	1.25	0.77	1.26	1.15	0.99
	Max Abs	1.62	1.59	1.66	2.80	2.88	2.52	2.65	2.00	1.87	1.89	2.63	2.20	1.70	2.13	2.83	2.20
+3% Current Gain	*RMSE*	0.89	0.84	0.82	1.42	0.87	0.71	1.02	1.03	1.07	1.06	0.98	1.30	0.84	1.30	1.08	1.01
	Max Abs	1.72	1.78	1.67	2.74	2.71	2.38	2.49	2.10	1.90	2.00	2.43	2.29	1.83	2.17	2.72	2.19
-3% Current Gain	*RMSE*	0.79	0.80	0.72	1.55	0.87	0.75	1.00	0.95	0.95	0.94	0.95	1.20	0.71	1.23	1.23	0.98
	Max Abs	1.53	1.49	1.67	2.90	3.06	2.69	2.80	1.88	1.89	1.76	2.77	2.16	1.57	2.24	2.95	2.22
+300mA Bias	*RMSE*	1.62	1.00	1.25	1.29	1.11	0.99	1.36	1.58	1.66	1.52	1.52	1.93	1.27	1.86	0.98	1.40
	Max Abs	2.95	2.31	2.56	2.59	2.49	2.28	2.96	3.08	2.94	2.85	3.11	3.40	2.63	3.23	2.57	2.80
-300mA Bias	*RMSE*	0.44	0.91	0.76	1.82	1.05	1.05	1.09	0.71	0.63	0.68	0.90	0.87	0.70	0.99	1.48	0.94
	Max Abs	1.10	1.77	2.08	3.14	3.39	3.11	3.16	1.87	1.96	2.15	3.16	2.60	1.98	2.62	3.15	2.48
+5°C bias	*RMSE*	0.85	0.70	0.73	1.03	0.77	0.59	0.90	0.97	1.01	0.99	0.94	1.17	0.79	1.14	0.77	0.89
	Max Abs	1.54	1.60	1.52	2.14	2.27	1.93	2.10	1.92	1.71	1.84	1.94	2.14	1.75	2.02	2.13	1.90
-5°C bias	*RMSE*	0.58	1.00	0.64	2.22	0.88	0.86	0.98	0.93	1.08	0.99	0.91	1.14	0.59	1.15	1.82	1.05
	Max Abs	1.09	1.74	1.77	3.52	3.41	3.01	3.18	2.49	3.09	2.92	3.02	2.48	1.62	2.63	3.61	2.64
+5mV bias	*RMSE*	0.56	1.04	0.74	1.93	0.99	0.96	1.05	0.86	0.86	0.87	0.92	1.09	0.73	1.13	1.57	1.02
	Max Abs	1.22	1.94	2.13	3.37	3.38	3.15	3.08	2.03	2.31	2.27	3.18	2.72	2.12	2.74	3.37	2.60
-5mV bias	*RMSE*	1.31	0.92	1.10	1.09	1.03	0.85	1.22	1.36	1.40	1.37	1.29	1.62	1.15	1.61	0.86	1.21
	Max Abs	2.34	2.20	2.20	2.27	2.37	1.91	2.65	2.69	2.48	2.57	2.58	2.91	2.35	2.77	2.29	2.44

Table B. 17: "+-300mA" tuning robustness to sensor error for an aged battery (80% SOH).

Case	ERROR [%]	UDDS	HWFET	LA92	US06	WLTP	Reo 1	Reo 2	Reo 3	Reo 4	Reo 5	Reo 6	Reo 7	Reo 8	Reo 9	Reo US06	Average
No error	*RMSE*	1.86	1.86	1.07	1.65	1.24	1.47	1.26	0.64	0.94	1.00	1.87	1.24	1.55	1.95	2.67	1.48
	Max Abs	2.65	4.05	2.27	3.14	2.83	2.29	2.20	1.85	3.27	3.11	2.71	2.35	2.55	3.17	3.95	2.83
+3% Current Gain	*RMSE*	1.82	1.97	1.11	1.73	1.32	1.56	1.35	0.67	0.94	0.99	1.95	1.32	1.61	2.06	2.77	1.54
	Max Abs	2.58	4.20	2.33	3.27	2.95	2.37	2.29	1.96	3.21	3.10	2.76	2.46	2.63	3.32	3.92	2.89
-3% Current Gain	*RMSE*	1.90	1.75	1.04	1.58	1.16	1.39	1.16	0.61	0.94	1.02	1.80	1.17	1.49	1.83	2.58	1.43
	Max Abs	2.73	3.90	2.19	3.00	2.71	2.20	2.12	1.74	3.32	3.12	2.72	2.25	2.49	3.01	4.02	2.77
+300mA Bias	*RMSE*	1.46	2.38	1.56	2.01	1.88	2.06	2.05	1.21	1.34	1.18	2.44	1.94	2.04	2.65	3.08	1.95
	Max Abs	2.72	4.73	2.87	3.77	3.36	3.06	3.05	2.18	3.14	3.06	3.42	3.02	3.19	4.04	4.34	3.33
-300mA Bias	*RMSE*	2.78	1.43	1.16	1.29	1.04	0.87	0.76	1.08	1.27	1.57	1.27	0.74	1.23	1.20	2.28	1.33
	Max Abs	4.32	3.35	2.29	2.50	2.12	1.57	1.34	2.05	3.39	3.16	2.79	2.11	2.22	2.02	4.05	2.62
+5°C bias	*RMSE*	1.78	2.08	1.17	1.95	1.40	1.64	1.45	0.72	1.09	1.10	2.06	1.42	1.70	2.16	3.07	1.65
	Max Abs	2.63	4.30	2.43	3.51	3.24	2.55	2.35	2.14	3.66	3.46	2.83	2.66	2.71	3.40	4.16	3.07
-5°C bias	*RMSE*	2.00	1.46	0.90	1.27	0.99	1.16	0.89	0.59	0.67	0.89	1.50	0.85	1.21	1.50	2.04	1.19
	Max Abs	3.04	3.68	1.75	2.60	2.41	1.94	1.79	1.35	1.83	1.87	2.12	1.55	2.08	2.54	3.26	2.25
+5mV bias	*RMSE*	2.25	1.47	0.93	1.29	0.91	1.04	0.80	0.67	0.91	1.13	1.39	0.81	1.21	1.45	2.18	1.23
	Max Abs	3.29	3.53	1.76	2.56	2.20	1.69	1.70	1.47	2.88	2.72	2.30	1.95	2.05	2.57	3.46	2.41
-5mV bias	*RMSE*	1.58	2.29	1.43	2.05	1.68	1.95	1.78	0.99	1.24	1.15	2.37	1.74	1.96	2.46	3.17	1.86
	Max Abs	2.42	4.56	2.77	3.65	3.44	2.88	2.71	2.25	3.65	3.51	3.18	2.75	3.07	3.76	4.39	3.27

Appendix C

This appendix contains screenshots of one of the fast charging aging test programs, boost charging protocol, created in the Arbin Instruments MITS Pro. It is intended to be a source for other researchers to build their test schedules or replicate this work.

	Step Label	Number Of Limits	Control Type	Control Value	Extra Control Value 1	Extra Control Value 2	Max Current(A)	Extended Definition	Extended Definition 1
1	Volt_Max	1	SetValue(s)	MV_UD1	=4.2				
	Add Limit		Goto Step	Variable1	Operator1	Value1	Variable2	Operator2	Value2
	Step Limits	1	Next Step						
2	Volt_Min	1	SetValue(s)	MV_UD2	=2.5				
	Add Limit		Goto Step	Variable1	Operator1	Value1	Variable2	Operator2	Value2
	Step Limits	1	Next Step						
3	Loop_Variable (set 1 to run C/20 dc)	1	SetValue(s)	MV_UD3	=1				
	Add Limit		Goto Step	Variable1	Operator1	Value1	Variable2	Operator2	Value2
	Step Limits	1	Next Step						
4	Cutoff_Current	1	SetValue(s)	MV_UD4	=0.15				
	Add Limit		Goto Step	Variable1	Operator1	Value1	Variable2	Operator2	Value2
	Step Limits	1	Next Step						
5	Temp_Low	1	SetValue(s)	MV_UD5	=23				
	Add Limit		Goto Step	Variable1	Operator1	Value1	Variable2	Operator2	Value2
	Step Limits	1	Next Step						
6	Temp_High	1	SetValue(s)	MV_UD6	=27				
	Add Limit		Goto Step	Variable1	Operator1	Value1	Variable2	Operator2	Value2
	Step Limits	1	Next Step						
7	Counters_reset	1	Set Variable(s)	Reset	Increment	Decrement			
	Add Limit		Goto Step	Variable1	Operator1	Value1	Variable2	Operator2	Value2
	Step Limits	1	Next Step	PV_CHAN_Step_Time	>=	00:00:00			
8	REST_overlap	1	SetValue(s)	MV_UD7	=37				
	Add Limit		Goto Step	Variable1	Operator1	Value1	Variable2	Operator2	Value2
	Step Limits	1	Next Step						
9	Master_Charge_Start	2	Rest						
	Add Limit		Goto Step	Variable1	Operator1	Value1	Variable2	Operator2	Value2
	Step Limits	1	Next Step	AV_T[1]	>=	MV_UD5	AV_T[1]	<=	MV_UD6
	Log Limits	2		DV_Time	>=	00:00:10			
10	Master_Charge_Rest	2	Rest						
	Add Limit		Goto Step	Variable1	Operator1	Value1	Variable2	Operator2	Value2
	Step Limits	1	Next Step	PV_CHAN_Step_Time	>=	00:15:00			
	Log Limits	2		DV_Time	>=	00:00:10			
11	Master_Charge_I	3	C-Rate	1			35		
	Add Limit		Goto Step	Variable1	Operator1	Value1	Variable2	Operator2	Value2
	Step Limits	1	Next Step	PV_CHAN_Voltage	>=	MV_UD1			
		2	Unsafe	AV_T[1]	>=	MV_UD7			
	Log Limits	3		DV_Time	>=	00:00:10			
12	Master_Charge_V	2	Voltage(V)	(V):MV_UD1		IR(ohm):0	35		
	Add Limit		Goto Step	Variable1	Operator1	Value1	Variable2	Operator2	Value2
	Step Limits	1	Next Step	PV_CHAN_Current	<=	MV_UD4			
	Log Limits	2		DV_Time	>=	00:00:10			
13	cycle_counter_4	1	Set Variable(s)	Reset	Increment	Decrement			
	Add Limit		Goto Step	Variable1	Operator1	Value1	Variable2	Operator2	Value2
	Step Limits	1	Next Step	PV_CHAN_Step_Time	>=	00:00:00			
14	TempSet_Wait	2	Rest						
	Add Limit		Goto Step	Variable1	Operator1	Value1	Variable2	Operator2	Value2
	Step Limits	1	Next Step	AV_T[1]	>=	MV_UD5	AV_T[1]	<=	MV_UD6
	Log Limits	2		DV_Time	>=	00:01:00			

#		Step Label	Number Of Limits	Control Type	Control Value	Extra Control Value 1	Extra Control Value 2	Max Current(A)	Extended Definition	Extended Definition 1
15		TempSet_Rest	2	Rest						
		Add Limit		Goto Step	Variable1	Operator1	Value1	Variable2	Operator2	Value2
		Step Limits		1 Next Step	PV_CHAN_Step_Time	>=	00:10:00			
		Log Limits		2	DV_Time	>=	00:01:00			
16		End_test_desision	2	Rest						
		Add Limit		Goto Step	Variable1	Operator1	Value1	Variable2	Operator2	Value2
		Step Limits		1 Test_End_Rest	TC_Counter3	>=	2			
				2 Next Step	TC_Counter3	<=	1			
17		Ah_Wh_Reset_Mastercharge	1	Set Variable(s)	Reset	Increment	Decrement			
		Add Limit		Goto Step	Variable1	Operator1	Value1	Variable2	Operator2	Value2
		Step Limits		1 Next Step	PV_CHAN_Step_Time	>=	00:00:00			
18		Characterization_Loop	5	Rest						
		Add Limit		Goto Step	Variable1	Operator1	Value1	Variable2	Operator2	Value2
		Step Limits		1 C/20_Dch_and_Ch_Start	MV_UD3	>=	1	MV_UD3	<	2
				2 Ah_Wh_rest_afterC/20	MV_UD3	>=	2	MV_UD3	<	3
				3 1C_Discharge_Start	MV_UD3	>=	3	MV_UD3	<	4
				4 2C_Discharge_Start	MV_UD3	>=	4	MV_UD3	<	5
				5 HPPC_Start	MV_UD3	>=	5	MV_UD3	<	6
19		C/20_Dch_and_Ch_Start	2	Rest						
		Add Limit		Goto Step	Variable1	Operator1	Value1	Variable2	Operator2	Value2
		Step Limits		1 Next Step	PV_CHAN_Step_Time	>=	00:50:00			
		Log Limits		2	DV_Time	>=	00:01:00			
20		C/20_Discharge	3	C-Rate	-0.05			0		
		Add Limit		Goto Step	Variable1	Operator1	Value1	Variable2	Operator2	Value2
		Step Limits		1 Next Step	PV_CHAN_Voltage	<=	MV_UD2			
				2 Unsafe	AV_T[1]	>=	MV_UD7			
		Log Limits		3	DV_Time	>=	00:01:00			
21		Capacity_Value	1	SetValue(s)	MV_UD7	=LS_CHAN_Discha				
		Add Limit		Goto Step	Variable1	Operator1	Value1	Variable2	Operator2	Value2
		Step Limits		1 Next Step						
22		C/20_Rest1	2	Rest						
		Add Limit		Goto Step	Variable1	Operator1	Value1	Variable2	Operator2	Value2
		Step Limits		1 Next Step	PV_CHAN_Step_Time	>=	01:00:00			
		Log Limits		2	DV_Time	>=	00:01:00			
23		C/20_Charge	4	C-Rate	0.05			0		
		Add Limit		Goto Step	Variable1	Operator1	Value1	Variable2	Operator2	Value2
		Step Limits		1 Next Step	PV_CHAN_Voltage	>=	MV_UD1			
				2 C/20_Rest2	F_A	>=	0			
				3 Unsafe	AV_T[1]	>=	MV_UD7			
		Log Limits		4	DV_Time	>=	00:01:00			
24		C/20_Charge_cv	3	Voltage(V)	(V):MV_UD1		IR(ohm):0	0		
		Add Limit		Goto Step	Variable1	Operator1	Value1	Variable2	Operator2	Value2
		Step Limits		1 Next Step	F_A	>=	0			
				2 Next Step	PV_CHAN_Step_Time	>=	00:30:00			
		Log Limits		3	DV_Time	>=	00:01:00			

#		Step Label	Number Of Limits	Control Type	Control Value	Extra Control Value 1	Extra Control Value 2	Max Current(A)	Extended Definition	Extended Definition 1
25		C/20_Rest2	2	Rest						
		Add Limit		Goto Step	Variable1	Operator1	Value1	Variable2	Operator2	Value2
		Step Limits		1 Next Step	PV_CHAN_Step_Time	>=	01:00:00			
		Log Limits		2	DV_Time	>=	00:01:00			
26		MV_UD3_set2	1	SetValue(s)	MV_UD3	=2				
		Add Limit		Goto Step	Variable1	Operator1	Value1	Variable2	Operator2	Value2
		Step Limits		1 Next Step						
27		Ah_Wh_rest_afterC/20	1	Set Variable(s)	Reset	Increment	Decrement			
		Add Limit		Goto Step	Variable1	Operator1	Value1	Variable2	Operator2	Value2
		Step Limits		1 Next Step	PV_CHAN_Step_Time	>=	00:00:00			
28		0.5C_Discharge_Start	3	C-Rate	-0.5			35		
		Add Limit		Goto Step	Variable1	Operator1	Value1	Variable2	Operator2	Value2
		Step Limits		1 Next Step	PV_CHAN_Voltage	<=	MV_UD2			
				2 Unsafe	AV_T[1]	>=	MV_UD7			
		Log Limits		3	DV_Time	>=	00:00:01			
29		Ah_Wh_rest_0.5C (used in HPPC)	1	Set Variable(s)	Reset	Increment	Decrement			
		Add Limit		Goto Step	Variable1	Operator1	Value1	Variable2	Operator2	Value2
		Step Limits		1 Next Step	PV_CHAN_Step_Time	>=	00:00:00			
30		MV_UD10_check1	2	Rest						
		Add Limit		Goto Step	Variable1	Operator1	Value1	Variable2	Operator2	Value2
		Step Limits		1 Next Step	MV_UD10	<=	0			
				2 MV_UD3_set_3	MV_UD10	>=	1			
31		MV_UD10_setto1_#1	1	SetValue(s)	MV_UD10	=1				
		Add Limit		Goto Step	Variable1	Operator1	Value1	Variable2	Operator2	Value2
		Step Limits		1 Master_Charge_Start						
32		MV_UD3_set_3	1	SetValue(s)	MV_UD3	=3				
		Add Limit		Goto Step	Variable1	Operator1	Value1	Variable2	Operator2	Value2
		Step Limits		1 Master_Charge_Start						
33		1C_Discharge_Start	3	C-Rate	-1			35		
		Add Limit		Goto Step	Variable1	Operator1	Value1	Variable2	Operator2	Value2
		Step Limits		1 Next Step	PV_CHAN_Voltage	<=	MV_UD2			
				2 Unsafe	AV_T[1]	>=	MV_UD7			
		Log Limits		3	DV_Time	>=	00:00:01			
34		MV_UD3_set_4	1	SetValue(s)	MV_UD3	=4				
		Add Limit		Goto Step	Variable1	Operator1	Value1	Variable2	Operator2	Value2
		Step Limits		1 Master_Charge_Start						
35		2C_Discharge_Start	3	C-Rate	-2			35		
		Add Limit		Goto Step	Variable1	Operator1	Value1	Variable2	Operator2	Value2
		Step Limits		1 Next Step	PV_CHAN_Voltage	<=	MV_UD2			
				2 Unsafe	AV_T[1]	>=	MV_UD7			
		Log Limits		3	DV_Time	>=	00:00:01			
36		MV_UD3_set_5	1	SetValue(s)	MV_UD3	=5				
		Add Limit		Goto Step	Variable1	Operator1	Value1	Variable2	Operator2	Value2
		Step Limits		1 Master_Charge_Start						

		Step Label	Number Of Limits	Control Type	Control Value	Extra Control Value 1	Extra Control Value 2	Max Current(A)	Extended Definition	Extended Definition 1
37		HPPC_Start	3	Rest						
		Add Limit		Goto Step	Variable1	Operator1	Value1	Variable2	Operator2	Value2
		Step Limits	1	Next Step	PV_CHAN_Step_Time	>=	01:00:00			
			2	Unsafe	AV_T[1]	>=	MV_UD7			
		Log Limits	3		DV_Time	>=	00:01:00			
38		P1_Ah_reset1	1	SetValue(s)	TC_Charge_Capacity1	=0				
		Add Limit		Goto Step	Variable1	Operator1	Value1	Variable2	Operator2	Value2
		Step Limits	1	Next Step						
39		P1_Ah_reset2	1	SetValue(s)	TC_Discharge_Capacity1	=0				
		Add Limit		Goto Step	Variable1	Operator1	Value1	Variable2	Operator2	Value2
		Step Limits	1	Next Step						
40		P1_dich	2	CCCV	CC(A):-LC_CHAN_Discharge_Capacity	CV(V):MV_UD2	IR(ohm):0	35		
		Add Limit		Goto Step	Variable1	Operator1	Value1	Variable2	Operator2	Value2
		Step Limits	1	Next Step	PV_CHAN_Step_Time	>=	00:00:10			
		Log Limits	2		DV_Time	>=	00:00:00.100			
41		P1_Rest1	2	Rest						
		Add Limit		Goto Step	Variable1	Operator1	Value1	Variable2	Operator2	Value2
		Step Limits	1	Next Step	PV_CHAN_Step_Time	>=	00:00:20			
		Log Limits	2		DV_Time	>=	00:00:01			
42		P1_return_Chrage	3	Current(A)	(A):0.333 * LC_CHAN_Discharge_Capac			35		
		Add Limit		Goto Step	Variable1	Operator1	Value1	Variable2	Operator2	Value2
		Step Limits	1	Next Step	F_A	>=	0			
			2	Next Step	PV_CHAN_Voltage	>	MV_UD1			
		Log Limits	3		DV_Time	>=	00:00:01			
43		P1_Rest2	2	Rest						
		Add Limit		Goto Step	Variable1	Operator1	Value1	Variable2	Operator2	Value2
		Step Limits	1	Next Step	PV_CHAN_Step_Time	>=	00:00:20			
		Log Limits	2		DV_Time	>=	00:00:01			
44		P2_Ah_reset1	1	SetValue(s)	TC_Charge_Capacity1	=0				
		Add Limit		Goto Step	Variable1	Operator1	Value1	Variable2	Operator2	Value2
		Step Limits	1	Next Step						
45		P2_Ah_reset2	1	SetValue(s)	TC_Discharge_Capacity1	=0				
		Add Limit		Goto Step	Variable1	Operator1	Value1	Variable2	Operator2	Value2
		Step Limits	1	Next Step						
46		P2_ch	2	CCCV	CC(A):0.5 * LC_CHAN_Discharge_Capa	CV(V):MV_UD1	IR(ohm):0	35		
		Add Limit		Goto Step	Variable1	Operator1	Value1	Variable2	Operator2	Value2
		Step Limits	1	Next Step	PV_CHAN_Step_Time	>=	00:00:10			
		Log Limits	2		DV_Time	>=	00:00:00.100			
47		P2_Rest1	2	Rest						
		Add Limit		Goto Step	Variable1	Operator1	Value1	Variable2	Operator2	Value2
		Step Limits	1	Next Step	PV_CHAN_Step_Time	>=	00:00:20			
		Log Limits	2		DV_Time	>=	00:00:01			
48		P2_return_Disch	3	Current(A)	(A):-0.333 * LC_CHAN_Discharge_Capa			35		
		Add Limit		Goto Step	Variable1	Operator1	Value1	Variable2	Operator2	Value2
		Step Limits	1	Next Step	F_A	<=	0			
			2	Next Step	PV_CHAN_Voltage	<	MV_UD2			
		Log Limits	3		DV_Time	>=	00:00:01			

		Step Label	Number Of Limits	Control Type	Control Value	Extra Control Value 1	Extra Control Value 2	Max Current(A)	Extended Definition	Extended Definition 1
49		P2_Rest2	2	Rest						
		Add Limit		Goto Step	Variable1	Operator1	Value1	Variable2	Operator2	Value2
		Step Limits	1	Next Step	PV_CHAN_Step_Time	>=	00:00:50			
		Log Limits	2		DV_Time	>=	00:00:10			
50		Long_Rest1	2	Rest						
		Add Limit		Goto Step	Variable1	Operator1	Value1	Variable2	Operator2	Value2
		Step Limits	1	Next Step	PV_CHAN_Step_Time	>=	00:09:00			
		Log Limits	2		DV_Time	>=	00:00:10			
51		Long_Rest2	2	Rest						
		Add Limit		Goto Step	Variable1	Operator1	Value1	Variable2	Operator2	Value2
		Step Limits	1	Next Step	PV_CHAN_Step_Time	>=	00:00:10			
		Log Limits	2		DV_Time	>=	00:00:01			
52		P3_Ah_reset1	1	SetValue(s)	TC_Charge_Capacity1	=0				
		Add Limit		Goto Step	Variable1	Operator1	Value1	Variable2	Operator2	Value2
		Step Limits	1	Next Step						
53		P3_Ah_reset2	1	SetValue(s)	TC_Discharge_Capacity1	=0				
		Add Limit		Goto Step	Variable1	Operator1	Value1	Variable2	Operator2	Value2
		Step Limits	1	Next Step						
54		P3_disch	2	CCCV	CC(A):-4 * LC_CHAN_Discharge_Capaci	CV(V):MV_UD2	IR(ohm):0	35		
		Add Limit		Goto Step	Variable1	Operator1	Value1	Variable2	Operator2	Value2
		Step Limits	1	Next Step	PV_CHAN_Step_Time	>=	00:00:10			
		Log Limits	2		DV_Time	>=	00:00:00.100			
55		P3_Rest1	2	Rest						
		Add Limit		Goto Step	Variable1	Operator1	Value1	Variable2	Operator2	Value2
		Step Limits	1	Next Step	PV_CHAN_Step_Time	>=	00:00:20			
		Log Limits	2		DV_Time	>=	00:00:01			
56		P3_return_ch	3	Current(A)	(A):0.333 * LC_CHAN_Discharge_Capac			35		
		Add Limit		Goto Step	Variable1	Operator1	Value1	Variable2	Operator2	Value2
		Step Limits	1	Next Step	F_A	>=	0			
			2	Next Step	PV_CHAN_Voltage	>	MV_UD1			
		Log Limits	3		DV_Time	>=	00:00:01			
57		P3_Rest2	2	Rest						
		Add Limit		Goto Step	Variable1	Operator1	Value1	Variable2	Operator2	Value2
		Step Limits	1	Next Step	PV_CHAN_Step_Time	>=	00:00:20			
		Log Limits	2		DV_Time	>=	00:00:01			
58		P4_Ah_reset1	1	SetValue(s)	TC_Charge_Capacity1	=0				
		Add Limit		Goto Step	Variable1	Operator1	Value1	Variable2	Operator2	Value2
		Step Limits	1	Next Step						
59		P4_Ah_reset2	1	SetValue(s)	TC_Discharge_Capacity1	=0				
		Add Limit		Goto Step	Variable1	Operator1	Value1	Variable2	Operator2	Value2
		Step Limits	1	Next Step						
60		P4_ch	2	CCCV	CC(A):2 * LC_CHAN_Discharge_Capacit	CV(V):MV_UD1	IR(ohm):0	35		
		Add Limit		Goto Step	Variable1	Operator1	Value1	Variable2	Operator2	Value2
		Step Limits	1	Next Step	PV_CHAN_Step_Time	>=	00:00:10			
		Log Limits	2		DV_Time	>=	00:00:00.100			

#	Step Label	Number Of Limits	Control Type	Control Value	Extra Control Value 1	Extra Control Value 2	Max Current(A)	Extended Definition	Extended Definition 1
61	P4_Rest1	2	Rest						
	Add Limit		Goto Step	Variable1	Operator1	Value1	Variable2	Operator2	Value2
	Step Limits	1	Next Step	PV_CHAN_Step_Time	>=	00:00:20			
	Log Limits	2		DV_Time	>=	00:00:01			
62	P4_return_disch	3	Current(A)	(A):-0.333 * LC_CHAN_Discharge_Capa			35		
	Add Limit		Goto Step	Variable1	Operator1	Value1	Variable2	Operator2	Value2
	Step Limits	1	Next Step	F_A	<=	0			
		2	Next Step	PV_CHAN_Voltage	<	MV_UD2			
	Log Limits	3		DV_Time	>=	00:00:01			
63	P4_Rest2	2	Rest						
	Add Limit		Goto Step	Variable1	Operator1	Value1	Variable2	Operator2	Value2
	Step Limits	1	Next Step	PV_CHAN_Step_Time	>=	00:00:50			
	Log Limits	2		DV_Time	>=	00:00:10			
64	Long_rest3	2	Rest						
	Add Limit		Goto Step	Variable1	Operator1	Value1	Variable2	Operator2	Value2
	Step Limits	1	Next Step	PV_CHAN_Step_Time	>=	00:09:00			
	Log Limits	2		DV_Time	>=	00:00:10			
65	Long_rest4	2	Rest						
	Add Limit		Goto Step	Variable1	Operator1	Value1	Variable2	Operator2	Value2
	Step Limits	1	Next Step	PV_CHAN_Step_Time	>=	00:00:10			
	Log Limits	2		DV_Time	>=	00:00:01			
66	P5_Ah_reset1	1	SetValue(s)	TC_Charge_Capacity1	=0				
	Add Limit		Goto Step	Variable1	Operator1	Value1	Variable2	Operator2	Value2
	Step Limits	1	Next Step						
67	P5_Ah_reset2	1	SetValue(s)	TC_Discharge_Capacity1	=0				
	Add Limit		Goto Step	Variable1	Operator1	Value1	Variable2	Operator2	Value2
	Step Limits	1	Next Step						
68	P5_Dich	2	CCCV	CC(A):-8 * LC_CHAN_Discharge_Capaci	CV(V):MV_UD2	IR(ohm):0	35		
	Add Limit		Goto Step	Variable1	Operator1	Value1	Variable2	Operator2	Value2
	Step Limits	1	Next Step	PV_CHAN_Step_Time	>=	00:00:10			
	Log Limits	2		DV_Time	>=	00:00:00.100			
69	P5_Rest1	2	Rest						
	Add Limit		Goto Step	Variable1	Operator1	Value1	Variable2	Operator2	Value2
	Step Limits	1	Next Step	PV_CHAN_Step_Time	>=	00:00:20			
	Log Limits	2		DV_Time	>=	00:00:01			
70	P5_return_ch	3	Current(A)	(A):0.333 * LC_CHAN_Discharge_Capac			35		
	Add Limit		Goto Step	Variable1	Operator1	Value1	Variable2	Operator2	Value2
	Step Limits	1	Next Step	F_A	>=	0			
		2	Next Step	PV_CHAN_Voltage	>	MV_UD1			
	Log Limits	3		DV_Time	>=	00:00:01			
71	P5_Rest2	2	Rest						
	Add Limit		Goto Step	Variable1	Operator1	Value1	Variable2	Operator2	Value2
	Step Limits	1	Next Step	PV_CHAN_Step_Time	>=	00:00:20			
	Log Limits	2		DV_Time	>=	00:00:01			
72	P6_Ah_reset1	1	SetValue(s)	TC_Charge_Capacity1	=0				
	Add Limit		Goto Step	Variable1	Operator1	Value1	Variable2	Operator2	Value2
	Step Limits	1	Next Step						

#	Step Label	Number Of Limits	Control Type	Control Value	Extra Control Value 1	Extra Control Value 2	Max Current(A)	Extended Definition	Extended Definition 1
73	P6_Ah_reset2	1	SetValue(s)	TC_Discharge_Capacity1	=0				
	Add Limit		Goto Step	Variable1	Operator1	Value1	Variable2	Operator2	Value2
	Step Limits	1	Next Step						
74	P6_Ch	2	CCCV	CC(A):6 * LC_CHAN_Discharge_Capacit	CV(V):MV_UD1	IR(ohm):0	35		
	Add Limit		Goto Step	Variable1	Operator1	Value1	Variable2	Operator2	Value2
	Step Limits	1	Next Step	PV_CHAN_Step_Time	>=	00:00:10			
	Log Limits	2		DV_Time	>=	00:00:00.100			
75	P6_Rest1	2	Rest						
	Add Limit		Goto Step	Variable1	Operator1	Value1	Variable2	Operator2	Value2
	Step Limits	1	Next Step	PV_CHAN_Step_Time	>=	00:00:20			
	Log Limits	2		DV_Time	>=	00:00:01			
76	P6_return_Disch	3	Current(A)	(A):-0.333 * LC_CHAN_Discharge_Capa			35		
	Add Limit		Goto Step	Variable1	Operator1	Value1	Variable2	Operator2	Value2
	Step Limits	1	Next Step	F_A	<=	0			
		2	Next Step	PV_CHAN_Voltage	<	MV_UD2			
	Log Limits	3		DV_Time	>=	00:00:01			
77	P6_Rest2	2	Rest						
	Add Limit		Goto Step	Variable1	Operator1	Value1	Variable2	Operator2	Value2
	Step Limits	1	Next Step	PV_CHAN_Step_Time	>=	00:00:50			
	Log Limits	2		DV_Time	>=	00:00:10			
78	Long_rest5	2	Rest						
	Add Limit		Goto Step	Variable1	Operator1	Value1	Variable2	Operator2	Value2
	Step Limits	1	Next Step	PV_CHAN_Step_Time	>=	00:09:00			
	Log Limits	2		DV_Time	>=	00:00:10			
79	Long_rest6	2	Rest						
	Add Limit		Goto Step	Variable1	Operator1	Value1	Variable2	Operator2	Value2
	Step Limits	1	Next Step	PV_CHAN_Step_Time	>=	00:00:10			
	Log Limits	2		DV_Time	>=	00:00:01			
80	P7_Ah_reset1	1	SetValue(s)	TC_Charge_Capacity1	=0				
	Add Limit		Goto Step	Variable1	Operator1	Value1	Variable2	Operator2	Value2
	Step Limits	1	Next Step						
81	P7_Ah_reset2	1	SetValue(s)	TC_Discharge_Capacity1	=0				
	Add Limit		Goto Step	Variable1	Operator1	Value1	Variable2	Operator2	Value2
	Step Limits	1	Next Step						
82	P7_Disch	2	CCCV	CC(A):-11.5 * LC_CHAN_Discharge_Ca	CV(V):MV_UD2	IR(ohm):0	35		
	Add Limit		Goto Step	Variable1	Operator1	Value1	Variable2	Operator2	Value2
	Step Limits	1	Next Step	PV_CHAN_Step_Time	>=	00:00:10			
	Log Limits	2		DV_Time	>=	00:00:00.100			
83	P7_Rest1	2	Rest						
	Add Limit		Goto Step	Variable1	Operator1	Value1	Variable2	Operator2	Value2
	Step Limits	1	Next Step	PV_CHAN_Step_Time	>=	00:00:20			
	Log Limits	2		DV_Time	>=	00:00:01			
84	P7_return_Ch	3	Current(A)	(A):0.333 * LC_CHAN_Discharge_Capac			35		
	Add Limit		Goto Step	Variable1	Operator1	Value1	Variable2	Operator2	Value2
	Step Limits	1	Next Step	F_A	>=	0			
		2	Next Step	PV_CHAN_Voltage	>	MV_UD1			
	Log Limits	3		DV_Time	>=	00:00:01			

		Step Label	Number Of Limits	Control Type	Control Value	Extra Control Value 1	Extra Control Value 2	Max Current(A)	Extended Definition	Extended Definition 1
85		P7_Rest2	2	Rest						
		Add Limit		Goto Step	Variable1	Operator1	Value1	Variable2	Operator2	Value2
		Step Limits	1	Next Step	PV_CHAN_Step_Time	>=	00:00:20			
		Log Limits	2		DV_Time	>=	00:00:01			
86		P8_Ah_reset1	1	SetValue(s)	TC_Charge_Capacity1	=0				
		Add Limit		Goto Step	Variable1	Operator1	Value1	Variable2	Operator2	Value2
		Step Limits	1	Next Step						
87		P8_Ah_reset2	1	SetValue(s)	TC_Discharge_Capacity1	=0				
		Add Limit		Goto Step	Variable1	Operator1	Value1	Variable2	Operator2	Value2
		Step Limits	1	Next Step						
88		P8_Ch	2	CCCV	CC(A):10 * LC_CHAN_Discharge_Capac	CV(V):MV_UD1	IR(ohm):0	35		
		Add Limit		Goto Step	Variable1	Operator1	Value1	Variable2	Operator2	Value2
		Step Limits	1	Next Step	PV_CHAN_Step_Time	>=	00:00:10			
		Log Limits	2		DV_Time	>=	00:00:00.100			
89		P8_Rest1	2	Rest						
		Add Limit		Goto Step	Variable1	Operator1	Value1	Variable2	Operator2	Value2
		Step Limits	1	Next Step	PV_CHAN_Step_Time	>=	00:00:20			
		Log Limits	2		DV_Time	>=	00:00:01			
90		P8_return_Disch	3	Current(A)	(A):-0.333 * LC_CHAN_Discharge_Capa			35		
		Add Limit		Goto Step	Variable1	Operator1	Value1	Variable2	Operator2	Value2
		Step Limits	1	Next Step	F_A	<=	0			
			2	Next Step	PV_CHAN_Voltage	<	MV_UD2			
		Log Limits	3		DV_Time	>=	00:00:01			
91		P8_Rest2	2	Rest						
		Add Limit		Goto Step	Variable1	Operator1	Value1	Variable2	Operator2	Value2
		Step Limits	1	Next Step	PV_CHAN_Step_Time	>=	00:00:20			
		Log Limits	2		DV_Time	>=	00:00:01			
92		Long_rest7	2	Rest						
		Add Limit		Goto Step	Variable1	Operator1	Value1	Variable2	Operator2	Value2
		Step Limits	1	Next Step	PV_CHAN_Step_Time	>=	00:00:50			
		Log Limits	2		DV_Time	>=	00:00:10			
93		Long_rest8	2	Rest						
		Add Limit		Goto Step	Variable1	Operator1	Value1	Variable2	Operator2	Value2
		Step Limits	1	Next Step	PV_CHAN_Step_Time	>=	00:09:00			
		Log Limits	2		DV_Time	>=	00:00:10			
94		HPPC_Loop_Check	3	Set Variable(s)	Reset	Increment	Decrement			
		Add Limit		Goto Step	Variable1	Operator1	Value1	Variable2	Operator2	Value2
		Step Limits	1	HPPC_5%Step	TC_Counter2	<=	3	TC_Counter2	>	10
			2	HPPC_10%Step	TC_Counter2	>	3	TC_Counter2	<=	10
			3	Pre_Aging_Counter3_Rese	TC_Counter2	>	15			
95		HPPC_5%Step	3	Current(A)	(A):-0.333 * LC_CHAN_Discharge_Capa			35		
		Add Limit		Goto Step	Variable1	Operator1	Value1	Variable2	Operator2	Value2
		Step Limits	1	HPPC_Start	TC_Discharge_Capacity2	>=	0.05 * LC_CHAN_Discharge_C	TC_Counter2	<=	13
			2	Pre_Aging_Counter3_Rese	PV_CHAN_Voltage	<	MV_UD2			
		Log Limits	3		DV_Time	>=	00:00:10			

		Step Label	Number Of Limits	Control Type	Control Value	Extra Control Value 1	Extra Control Value 2	Max Current(A)	Extended Definition	Extended Definition 1
96		HPPC_10%Step	3	Current(A)	(A):-0.333 * LC_CHAN_Discharge_Capa			35		
		Add Limit		Goto Step	Variable1	Operator1	Value1	Variable2	Operator2	Value2
		Step Limits	1	HPPC_Start	TC_Discharge_Capacity2	>=	0.1 * LC_CHAN_Discharge_Ca			
			2	Pre_Aging_Counter3_Rese	PV_CHAN_Voltage	<	MV_UD2			
		Log Limits	3		DV_Time	>=	00:00:10			
97		Pre_Aging_Counter3_Reset	1	Set Variable(s)	Reset	Increment	Decrement			
		Add Limit		Goto Step	Variable1	Operator1	Value1	Variable2	Operator2	Value2
		Step Limits	1	Next Step	PV_CHAN_Step_Time	>=	00:00:00			
98		Aging_Test_Start	1	Set Variable(s)	Reset	Increment	Decrement			
		Add Limit		Goto Step	Variable1	Operator1	Value1	Variable2	Operator2	Value2
		Step Limits	1	Next Step	PV_CHAN_Step_Time	>=	00:00:00			
99		MV_UD3_set_6	1	SetValue(s)	MV_UD3	=6				
		Add Limit		Goto Step	Variable1	Operator1	Value1	Variable2	Operator2	Value2
		Step Limits	1	Next Step						
100		pre_ten%charge	2	C-Rate	0.333			0		
		Add Limit		Goto Step	Variable1	Operator1	Value1	Variable2	Operator2	Value2
		Step Limits	1	Next Step	F_A	>=	0.1 * LC_CHAN_Discharge_Ca			
		Log Limits	2		DV_Time	>=	00:00:01			
101		Fast_Charge_Start	2	Rest						
		Add Limit		Goto Step	Variable1	Operator1	Value1	Variable2	Operator2	Value2
		Step Limits	1	Next Step	AV_T[1]	>=	MV_UD5	AV_T[1]	<=	MV_UD6
		Log Limits	2		DV_Time	>=	00:00:01			
102		Fast_Charge_Rest	2	Rest						
		Add Limit		Goto Step	Variable1	Operator1	Value1	Variable2	Operator2	Value2
		Step Limits	1	Next Step	PV_CHAN_Step_Time	>=	00:10:00			
		Log Limits	2		DV_Time	>=	00:00:01			
103		Ah_Rest_Ch_CAP	1	SetValue(s)	TC_Charge_Capacity1	=0				
		Add Limit		Goto Step	Variable1	Operator1	Value1	Variable2	Operator2	Value2
		Step Limits	1	Next Step						
104		Ah_Rest_Dch_CAP	1	SetValue(s)	TC_Discharge_Capacity1	=0				
		Add Limit		Goto Step	Variable1	Operator1	Value1	Variable2	Operator2	Value2
		Step Limits	1	Next Step						
105		Fast_Charge_BC	4	C-Rate	4			0		
		Add Limit		Goto Step	Variable1	Operator1	Value1	Variable2	Operator2	Value2
		Step Limits	1	Next Step	F_A	>=	0.333 * LC_CHAN_Discharge_			
			2	Fast_Charge_CV	PV_CHAN_Voltage	>=	MV_UD1			
			3	Unsafe	AV_T[1]	>=	MV_UD7			
		Log Limits	4		DV_Time	>=	00:00:01			
106		Fast_Charge_CC	4	C-Rate	2.2			35		
		Add Limit		Goto Step	Variable1	Operator1	Value1	Variable2	Operator2	Value2
		Step Limits	1	Fast_charge_Counter	F_A	>=	0.7 * LC_CHAN_Discharge_Ca			
			2	Next Step	PV_CHAN_Voltage	>=	MV_UD1			
			3	Unsafe	AV_T[1]	>=	MV_UD7			
		Log Limits	4		DV_Time	>=	00:00:01			

		Step Label	Number Of Limits	Control Type	Control Value	Extra Control Value 1	Extra Control Value 2	Max Current(A)	Extended Definition	Extended Definition 1
107		Fast_Charge_CV	3	Voltage(V)	(V):MV_UD1		IR(ohm):0	35		
		Add Limit		Goto Step	Variable1	Operator1	Value1	Variable2	Operator2	Value2
		Step Limits	1	Next Step	F_A	>=	0.7 * LC_CHAN_Discharge_Ca			
			2	Next Step	PV_CHAN_Current	<=	MV_UD4			
		Log Limits	3		DV_Time	>=	00:00:01			
108		Fast_charge_Counter	1	Set Variable(s)	Reset	Increment	Decrement			
		Add Limit		Goto Step	Variable1	Operator1	Value1	Variable2	Operator2	Value2
		Step Limits	1	Next Step	PV_CHAN_Step_Time	>=	00:00:00			
109		Pre_DC_Rest_Temp	2	Rest						
		Add Limit		Goto Step	Variable1	Operator1	Value1	Variable2	Operator2	Value2
		Step Limits	1	Next Step	AV_T[1]	>=	MV_UD5	AV_T[1]	<=	MV_UD6
		Log Limits	2		DV_Time	>=	00:00:01			
110		Pre_DC_Rest_Time	2	Rest						
		Add Limit		Goto Step	Variable1	Operator1	Value1	Variable2	Operator2	Value2
		Step Limits	1	Next Step	PV_CHAN_Step_Time	>=	00:10:00			
		Log Limits	2		DV_Time	>=	00:00:01			
111		Aging_Loop	15	Rest						
		Add Limit		Goto Step	Variable1	Operator1	Value1	Variable2	Operator2	Value2
			1	UDDS_Start	MV_UD3	>=	6	MV_UD3	<	7
			2	HWFET_Start	MV_UD3	>=	7	MV_UD3	<	8
			3	LA92_Start	MV_UD3	>=	8	MV_UD3	<	9
			4	US06_Start	MV_UD3	>=	9	MV_UD3	<	10
			5	WLTP_Start	MV_UD3	>=	10	MV_UD3	<	11
			6	Reo_1_Start	MV_UD3	>=	11	MV_UD3	<	12
			7	Reo_2_Start	MV_UD3	>=	12	MV_UD3	<	13
		Step Limits	8	Reo_3_Start	MV_UD3	>=	13	MV_UD3	<	14
			9	Reo_4_Start	MV_UD3	>=	14	MV_UD3	<	15
			10	Reo_5_Start	MV_UD3	>=	15	MV_UD3	<	16
			11	Reo_6_Start	MV_UD3	>=	16	MV_UD3	<	17
			12	Reo_7_Start	MV_UD3	>=	17	MV_UD3	<	18
			13	Reo_8_Start	MV_UD3	>=	18	MV_UD3	<	19
			14	Reo_9_Start	MV_UD3	>=	19	MV_UD3	<	20
			15	ReoUS06_Start	MV_UD3	>=	20	MV_UD3	<	21
112		UDDS_Start	2	Rest						
		Add Limit		Goto Step	Variable1	Operator1	Value1	Variable2	Operator2	Value2
		Step Limits	1	Next Step	PV_CHAN_Step_Time	>=	01:00:00			
		Log Limits	2		DV_Time	>=	00:00:01			
113		UDDS_Start_p	4	Power Simulation	UDDS_simu_30T.txt			0	non-repeat,no extra 2 poi	
		Add Limit		Goto Step	Variable1	Operator1	Value1	Variable2	Operator2	Value2
			1	MV_UD3_set_7	F_Battery_Ah	>=	0.7 * LC_CHAN_Discharge_Ca			
		Step Limits	2	Next Step	PV_CHAN_Step_Time	>=	00:22:49			
			3	Unsafe	AV_T[1]	>=	MV_UD7			
		Log Limits	4		DV_Time	>=	00:00:01			
114		UDDS_Repeat	1	Rest						
		Add Limit		Goto Step	Variable1	Operator1	Value1	Variable2	Operator2	Value2
		Step Limits	1	UDDS_Start_p	PV_CHAN_Step_Time	>=	00:00:00			

		Step Label	Number Of Limits	Control Type	Control Value	Extra Control Value 1	Extra Control Value 2	Max Current(A)	Extended Definition	Extended Definition 1
115		MV_UD3_set_7	1	SetValue(s)	MV_UD3	=7				
		Add Limit		Goto Step	Variable1	Operator1	Value1	Variable2	Operator2	Value2
		Step Limits	1	Fast_Charge_Start						
116		HWFET_Start	4	Power Simulation	HWFET_simu_30T.txt			0	non-repeat,no extra 2 poi	
		Add Limit		Goto Step	Variable1	Operator1	Value1	Variable2	Operator2	Value2
			1	MV_UD3_set_8	F_Battery_Ah	>=	0.7 * LC_CHAN_Discharge_Ca			
		Step Limits	2	Next Step	PV_CHAN_Step_Time	>=	00:12:45			
			3	Unsafe	AV_T[1]	>=	MV_UD7			
		Log Limits	4		DV_Time	>=	00:00:01			
117		HWFET_Repeat	1	Rest						
		Add Limit		Goto Step	Variable1	Operator1	Value1	Variable2	Operator2	Value2
		Step Limits	1	HWFET_Start	PV_CHAN_Step_Time	>=	00:00:00			
118		MV_UD3_set_8	1	SetValue(s)	MV_UD3	=8				
		Add Limit		Goto Step	Variable1	Operator1	Value1	Variable2	Operator2	Value2
		Step Limits	1	Fast_Charge_Start						
119		LA92_Start	4	Power Simulation	LA92_simu_30T.txt			0	non-repeat,no extra 2 poi	
		Add Limit		Goto Step	Variable1	Operator1	Value1	Variable2	Operator2	Value2
			1	MV_UD3_set_9	F_Battery_Ah	>	0.7 * LC_CHAN_Discharge_Ca			
		Step Limits	2	Next Step	PV_CHAN_Step_Time	>=	00:23:55			
			3	Unsafe	AV_T[1]	>=	MV_UD7			
		Log Limits	4		DV_Time	>=	00:00:01			
120		LA92_Repeat	1	Rest						
		Add Limit		Goto Step	Variable1	Operator1	Value1	Variable2	Operator2	Value2
		Step Limits	1	LA92_Start	PV_CHAN_Step_Time	>=	00:00:00			
121		MV_UD3_set_9	1	SetValue(s)	MV_UD3	=9				
		Add Limit		Goto Step	Variable1	Operator1	Value1	Variable2	Operator2	Value2
		Step Limits	1	Fast_Charge_Start						
122		US06_Start	4	Power Simulation	US06_simu_30T.txt			0	non-repeat,no extra 2 poi	
		Add Limit		Goto Step	Variable1	Operator1	Value1	Variable2	Operator2	Value2
			1	MV_UD3_set_10	F_Battery_Ah	>	0.7 * LC_CHAN_Discharge_Ca			
		Step Limits	2	Next Step	PV_CHAN_Step_Time	>=	00:10:00			
			3	Unsafe	AV_T[1]	>=	MV_UD7			
		Log Limits	4		DV_Time	>=	00:00:01			
123		US06_Repeat	1	Rest						
		Add Limit		Goto Step	Variable1	Operator1	Value1	Variable2	Operator2	Value2
		Step Limits	1	US06_Start	PV_CHAN_Step_Time	>=	00:00:00			
124		MV_UD3_set_10	1	SetValue(s)	MV_UD3	=10				
		Add Limit		Goto Step	Variable1	Operator1	Value1	Variable2	Operator2	Value2
		Step Limits	1	Fast_Charge_Start						
125		WLTP_Start	4	Power Simulation	WLTP_simu_30T.txt			0	non-repeat,no extra 2 poi	
		Add Limit		Goto Step	Variable1	Operator1	Value1	Variable2	Operator2	Value2
			1	MV_UD3_set_11	F_Battery_Ah	>=	0.7 * LC_CHAN_Discharge_Ca			
		Step Limits	2	Next Step	PV_CHAN_Step_Time	>=	00:30:00			
			3	Unsafe	AV_T[1]	>=	MV_UD7			
		Log Limits	4		DV_Time	>=	00:00:01			
126		WLTP_Repeat	1	Rest						
		Add Limit		Goto Step	Variable1	Operator1	Value1	Variable2	Operator2	Value2
		Step Limits	1	WLTP_Start	PV_CHAN_Step_Time	>=	00:00:00			

#	Step Label	Number Of Limits	Control Type	Control Value	Extra Control Value 1	Extra Control Value 2	Max Current(A)	Extended Definition	Extended Definition 1
127	MV_UD3_set_11	1	SetValue(s)	MV_UD3	=11				
	Add Limit		Goto Step	Variable1	Operator1	Value1	Variable2	Operator2	Value2
	Step Limits		1 Fast_Charge_Start						
128	Reo_1_Start	4	Power Simulation	REO1_simu_30T.txt			0	non-repeat,no extra 2 poi	
	Add Limit		Goto Step	Variable1	Operator1	Value1	Variable2	Operator2	Value2
	Step Limits		1 MV_UD3_set_12	F_Battery_Ah	>	0.7 * LC_CHAN_Discharge_Ca			
			2 Next Step	PV_CHAN_Step_Time	>=	01:32:28			
			3 Unsafe	AV_T[1]	>=	MV_UD7			
	Log Limits		4	DV_Time	>=	00:00:01			
129	Reo_1_Repeat	1	Rest						
	Add Limit		Goto Step	Variable1	Operator1	Value1	Variable2	Operator2	Value2
	Step Limits		1 Reo_1_Start	PV_CHAN_Step_Time	>=	00:00:00			
130	MV_UD3_set_12	1	SetValue(s)	MV_UD3	=12				
	Add Limit		Goto Step	Variable1	Operator1	Value1	Variable2	Operator2	Value2
	Step Limits		1 Fast_Charge_Start						
131	Reo_2_Start	4	Power Simulation	REO2_simu_30T.txt			0	non-repeat,no extra 2 poi	
	Add Limit		Goto Step	Variable1	Operator1	Value1	Variable2	Operator2	Value2
	Step Limits		1 MV_UD3_set_13	F_Battery_Ah	>	0.7 * LC_CHAN_Discharge_Ca			
			2 Next Step	PV_CHAN_Step_Time	>=	01:33:30			
			3 Unsafe	AV_T[1]	>=	MV_UD7			
	Log Limits		4	DV_Time	>=	00:00:01			
132	Reo_2_Repeat	1	Rest						
	Add Limit		Goto Step	Variable1	Operator1	Value1	Variable2	Operator2	Value2
	Step Limits		1 Reo_2_Start	PV_CHAN_Step_Time	>=	00:00:00			
133	MV_UD3_set_13	1	SetValue(s)	MV_UD3	=13				
	Add Limit		Goto Step	Variable1	Operator1	Value1	Variable2	Operator2	Value2
	Step Limits		1 Fast_Charge_Start						
134	Reo_3_Start	4	Power Simulation	REO3_simu_30T.txt			0	non-repeat,no extra 2 poi	
	Add Limit		Goto Step	Variable1	Operator1	Value1	Variable2	Operator2	Value2
	Step Limits		1 MV_UD3_set_14	F_Battery_Ah	>	0.7 * LC_CHAN_Discharge_Ca			
			2 Next Step	PV_CHAN_Step_Time	>=	01:44:19			
			3 Unsafe	AV_T[1]	>=	MV_UD7			
	Log Limits		4	DV_Time	>=	00:00:01			
135	Reo_3_Repeat	1	Rest						
	Add Limit		Goto Step	Variable1	Operator1	Value1	Variable2	Operator2	Value2
	Step Limits		1 Reo_3_Start	PV_CHAN_Step_Time	>=	00:00:00			
136	MV_UD3_set_14	1	SetValue(s)	MV_UD3	=14				
	Add Limit		Goto Step	Variable1	Operator1	Value1	Variable2	Operator2	Value2
	Step Limits		1 Fast_Charge_Start						
137	Reo_4_Start	4	Power Simulation	REO4_simu_30T.txt			0	non-repeat,no extra 2 poi	
	Add Limit		Goto Step	Variable1	Operator1	Value1	Variable2	Operator2	Value2
	Step Limits		1 MV_UD3_set_15	F_Battery_Ah	>	0.7 * LC_CHAN_Discharge_Ca			
			2 Next Step	PV_CHAN_Step_Time	>=	01:49:49			
			3 Unsafe	AV_T[1]	>=	MV_UD7			
	Log Limits		4	DV_Time	>=	00:00:01			
138	Reo_4_Repeat	1	Rest						
	Add Limit		Goto Step	Variable1	Operator1	Value1	Variable2	Operator2	Value2
	Step Limits		1 Reo_4_Start	PV_CHAN_Step_Time	>=	00:00:00			

#	Step Label	Number Of Limits	Control Type	Control Value	Extra Control Value 1	Extra Control Value 2	Max Current(A)	Extended Definition	Extended Definition 1
139	MV_UD3_set_15	1	SetValue(s)	MV_UD3	=15				
	Add Limit		Goto Step	Variable1	Operator1	Value1	Variable2	Operator2	Value2
	Step Limits		1 Fast_Charge_Start						
140	Reo_5_Start	4	Power Simulation	REO5_simu_30T.txt			0	non-repeat,no extra 2 poi	
	Add Limit		Goto Step	Variable1	Operator1	Value1	Variable2	Operator2	Value2
	Step Limits		1 MV_UD3_set_16	F_Battery_Ah	>	0.7 * LC_CHAN_Discharge_Ca			
			2 Next Step	PV_CHAN_Step_Time	>=	01:41:25			
			3 Unsafe	AV_T[1]	>=	MV_UD7			
	Log Limits		4	DV_Time	>=	00:00:01			
141	Reo_5_Repeat	1	Rest						
	Add Limit		Goto Step	Variable1	Operator1	Value1	Variable2	Operator2	Value2
	Step Limits		1 Reo_5_Start	PV_CHAN_Step_Time	>=	00:00:00			
142	MV_UD3_set_16	1	SetValue(s)	MV_UD3	=16				
	Add Limit		Goto Step	Variable1	Operator1	Value1	Variable2	Operator2	Value2
	Step Limits		1 Fast_Charge_Start						
143	Reo_6_Start	4	Power Simulation	REO6_simu_30T.txt			0	non-repeat,no extra 2 poi	
	Add Limit		Goto Step	Variable1	Operator1	Value1	Variable2	Operator2	Value2
	Step Limits		1 MV_UD3_set_17	F_Battery_Ah	>	0.7 * LC_CHAN_Discharge_Ca			
			2 Next Step	PV_CHAN_Step_Time	>=	01:34:49			
			3 Unsafe	AV_T[1]	>=	MV_UD7			
	Log Limits		4	DV_Time	>=	00:00:01			
144	Reo_6_Repeat	1	Rest						
	Add Limit		Goto Step	Variable1	Operator1	Value1	Variable2	Operator2	Value2
	Step Limits		1 Reo_6_Start	PV_CHAN_Step_Time	>=	00:00:00			
145	MV_UD3_set_17	1	SetValue(s)	MV_UD3	=17				
	Add Limit		Goto Step	Variable1	Operator1	Value1	Variable2	Operator2	Value2
	Step Limits		1 Fast_Charge_Start						
146	Reo_7_Start	4	Power Simulation	REO7_simu_30T.txt			0	non-repeat,no extra 2 poi	
	Add Limit		Goto Step	Variable1	Operator1	Value1	Variable2	Operator2	Value2
	Step Limits		1 MV_UD3_set_18	F_Battery_Ah	>	0.7 * LC_CHAN_Discharge_Ca			
			2 Next Step	PV_CHAN_Step_Time	>=	01:29:57			
			3 Unsafe	AV_T[1]	>=	MV_UD7			
	Log Limits		4	DV_Time	>=	00:00:01			
147	Reo_7_Repeat	1	Rest						
	Add Limit		Goto Step	Variable1	Operator1	Value1	Variable2	Operator2	Value2
	Step Limits		1 Reo_7_Start	PV_CHAN_Step_Time	>=	00:00:00			
148	MV_UD3_set_18	1	SetValue(s)	MV_UD3	=18				
	Add Limit		Goto Step	Variable1	Operator1	Value1	Variable2	Operator2	Value2
	Step Limits		1 Fast_Charge_Start						
149	Reo_8_Start	4	Power Simulation	REO8_simu_30T.txt			0	non-repeat,no extra 2 poi	
	Add Limit		Goto Step	Variable1	Operator1	Value1	Variable2	Operator2	Value2
	Step Limits		1 MV_UD3_set_19	F_Battery_Ah	>	0.7 * LC_CHAN_Discharge_Ca			
			2 Next Step	PV_CHAN_Step_Time	>=	01:37:02			
			3 Unsafe	AV_T[1]	>=	MV_UD7			
	Log Limits		4	DV_Time	>=	00:00:01			
150	Reo_8_Repeat	1	Rest						
	Add Limit		Goto Step	Variable1	Operator1	Value1	Variable2	Operator2	Value2
	Step Limits		1 Reo_8_Start	PV_CHAN_Step_Time	>=	00:00:00			

#	Step Label	Number Of Limits	Control Type	Control Value	Extra Control Value 1	Extra Control Value 2	Max Current(A)	Extended Definition	Extended Definition 1
150	Reo_8_Repeat	1	Rest						
	Add Limit		Goto Step	Variable1	Operator1	Value1	Variable2	Operator2	Value2
	Step Limits	1	Reo_8_Start	PV_CHAN_Step_Time	>=	00:00:00			
151	MV_UD3_set_19	1	SetValue(s)	MV_UD3	=19				
	Add Limit		Goto Step	Variable1	Operator1	Value1	Variable2	Operator2	Value2
	Step Limits	1	Fast_Charge_Start						
152	Reo_9_Start	4	Power Simulation	REO9_simu_30T.txt			0	non-repeat,no extra 2 poi	
	Add Limit		Goto Step	Variable1	Operator1	Value1	Variable2	Operator2	Value2
	Step Limits	1	MV_UD3_set_20	F_Battery_Ah	>	0.7 * LC_CHAN_Discharge_Ca			
		2	Next Step	PV_CHAN_Step_Time	>=	01:40:27			
		3	Unsafe	AV_T[1]	>=	MV_UD7			
	Log Limits	4		DV_Time	>=	00:00:01			
153	Reo_9_Repeat	1	Rest						
	Add Limit		Goto Step	Variable1	Operator1	Value1	Variable2	Operator2	Value2
	Step Limits	1	Reo_9_Start	PV_CHAN_Step_Time	>=	00:00:00			
154	MV_UD3_set_20	1	SetValue(s)	MV_UD3	=20				
	Add Limit		Goto Step	Variable1	Operator1	Value1	Variable2	Operator2	Value2
	Step Limits	1	Fast_Charge_Start						
155	ReoUS06_Start	4	Power Simulation	REO_US06_simu_30T.txt			0	non-repeat,no extra 2 poi	
	Add Limit		Goto Step	Variable1	Operator1	Value1	Variable2	Operator2	Value2
	Step Limits	1	decision-loop_or_end test	F_Battery_Ah	>=	0.7 * LC_CHAN_Discharge_Ca			
		2	Next Step	PV_CHAN_Step_Time	>=	00:37:21			
		3	Unsafe	AV_T[1]	>=	MV_UD7			
	Log Limits	4		DV_Time	>=	00:00:01			
156	ReoUS06_Repeat	1	Rest						
	Add Limit		Goto Step	Variable1	Operator1	Value1	Variable2	Operator2	Value2
	Step Limits	1	ReoUS06_Start	PV_CHAN_Step_Time	>=	00:00:00			
157	decision-loop_or_end test	2	Rest						
	Add Limit		Goto Step	Variable1	Operator1	Value1	Variable2	Operator2	Value2
	Step Limits	1	Next Step	TC_Counter3	=	1			
		2	Master_Charge_Start	TC_Counter3	>=	2			

#	Step Label	Number Of Limits	Control Type	Control Value	Extra Control Value 1	Extra Control Value 2	Max Current(A)	Extended Definition	Extended Definition 1
158	Temp_rest_mid_master	2	Rest						
	Add Limit		Goto Step	Variable1	Operator1	Value1	Variable2	Operator2	Value2
	Step Limits	1	Next Step	AV_T[1]	>=	MV_UD5	AV_T[1]	<=	MV_UD6
	Log Limits	2		DV_Time	>=	00:00:01			
159	Time_rest_mid_master	2	Rest						
	Add Limit		Goto Step	Variable1	Operator1	Value1	Variable2	Operator2	Value2
	Step Limits	1	Next Step	PV_CHAN_Step_Time	>=	00:10:00			
	Log Limits	2		DV_Time	>=	00:00:01			
160	Mid_Mastercharge_I	3	C-Rate	1			0		
	Add Limit		Goto Step	Variable1	Operator1	Value1	Variable2	Operator2	Value2
	Step Limits	1	Next Step	PV_CHAN_Voltage	>=	MV_UD1			
		2	Unsafe	AV_T[1]	>=	MV_UD7			
	Log Limits	3		DV_Time	>=	00:00:01			
161	Mid_Mastercharge_V	2	Voltage(V)	(V):MV_UD1		IR(ohm):0	35		
	Add Limit		Goto Step	Variable1	Operator1	Value1	Variable2	Operator2	Value2
	Step Limits	1	Next Step	PV_CHAN_Current	<=	MV_UD4			
	Log Limits	2		DV_Time	>=	00:00:01			
162	cyle_counter_4_2	1	Set Variable(s)	Reset	Increment	Decrement			
	Add Limit		Goto Step	Variable1	Operator1	Value1	Variable2	Operator2	Value2
	Step Limits	1	Next Step	PV_CHAN_Step_Time	>=	00:00:00			
163	rest_temp_m2	2	Rest						
	Add Limit		Goto Step	Variable1	Operator1	Value1	Variable2	Operator2	Value2
	Step Limits	1	Next Step	AV_T[1]	>=	MV_UD5	AV_T[1]	<=	MV_UD6
	Log Limits	2		DV_Time	>=	00:00:01			
164	rest_time_m2	2	Rest						
	Add Limit		Goto Step	Variable1	Operator1	Value1	Variable2	Operator2	Value2
	Step Limits	1	Next Step	PV_CHAN_Step_Time	>=	00:10:00			
	Log Limits	2		DV_Time	>=	00:00:01			
165	Ah_reset_sec_cap	1	Set Variable(s)	Reset	Increment	Decrement			
	Add Limit		Goto Step	Variable1	Operator1	Value1	Variable2	Operator2	Value2
	Step Limits	1	Next Step	PV_CHAN_Step_Time	>=	00:00:00			
166	Half_C_dchg	2	C-Rate	-0.5			0		
	Add Limit		Goto Step	Variable1	Operator1	Value1	Variable2	Operator2	Value2
	Step Limits	1	Next Step	PV_CHAN_Voltage	<=	MV_UD2			
	Log Limits	2		DV_Time	>=	00:00:01			
167	cycle_index_increment	1	Set Variable(s)	Reset	Increment	Decrement			
	Add Limit		Goto Step	Variable1	Operator1	Value1	Variable2	Operator2	Value2
	Step Limits	1	Next Step	PV_CHAN_Step_Time	>=	00:00:00			
168	MV_UD10_check2	2	Rest						
	Add Limit		Goto Step	Variable1	Operator1	Value1	Variable2	Operator2	Value2
	Step Limits	1	Next Step	MV_UD10	<=	1			
		2	Aging_Test_Start	MV_UD10	>=	2			
169	MV_UD10_setto2	1	SetValue(s)	MV_UD10	=2				
	Add Limit		Goto Step	Variable1	Operator1	Value1	Variable2	Operator2	Value2
	Step Limits	1	Temp_rest_mid_master						
170	Test_End_Rest	2	Rest						
	Add Limit		Goto Step	Variable1	Operator1	Value1	Variable2	Operator2	Value2
	Step Limits	1	End Test	PV_CHAN_Step_Time	>=	00:45:00			
	Log Limits	2		DV_Time	>=	00:01:00			

References

[1]   C. Park *et al.*, "Variables study for the fast charging lithium ion batteries," *J. Power Sources*, vol. 165, pp. 892–896, 2007, doi: 10.1016/j.jpowsour.2006.12.057.

[2]   A. Barré, B. Deguilhem, S. Grolleau, M. Gérard, F. Suard, and D. Riu, "A review on lithium-ion battery ageing mechanisms and estimations for automotive applications," *J. Power Sources*, vol. 241, pp. 680–689, 2013, doi: 10.1016/j.jpowsour.2013.05.040.

[3]   A. Emadi, *Advanced Electric Drive Vehicles*. New York: CRC Press, 2014.

[4]   X. G. Yang and C. Y. Wang, "Understanding the trilemma of fast charging, energy density and cycle life of lithium-ion batteries," *J. Power Sources*, vol. 402, no. September, pp. 489–498, 2018, doi: 10.1016/j.jpowsour.2018.09.069.

[5]   A. Tomaszewska *et al.*, "Lithium-ion battery fast charging: A review," *eTransportation*, vol. 1, p. 100011, 2019, doi: 10.1016/j.etran.2019.100011.

[6]   D. Anseán *et al.*, "Fast charging technique for high power LiFePO4 batteries: A mechanistic analysis of aging," *J. Power Sources*, vol. 321, pp. 201–209, 2016, doi: 10.1016/j.jpowsour.2016.04.140.

[7]   A. Meintz *et al.*, "Enabling fast charging – Vehicle considerations," *J. Power Sources*, vol. 367, pp. 216–227, 2017, doi: 10.1016/j.jpowsour.2017.07.093.

[8]   "DC Fast Charging Explained - EV Safe Charge." [Online]. Available: https://evsafecharge.com/dc-fast-charging-explained/. [Accessed: 27-Jan-2021].

[9]   R. Ahmed, M. El Sayed, I. Arasaratnam, J. Tjong, and S. Habibi, "Reduced-Order Electrochemical Model Parameters Identification and State of

Estimation for Healthy and Aged Li-Ion Batteries—Part II: Aged Battery Model and State of Charge Estimation," *IEEE J. Emerg. Sel. Top. Power Electron.*, vol. 2, no. 3, pp. 678–690, 2014, doi: 10.1109/jestpe.2014.2331062.

[10]   J. Vetter, P. Nov, M. R. Wagner, and C. Veit, "Ageing mechanisms in lithium-ion batteries," *J. ofPower Sources*, vol. 147, pp. 269–281, 2005, doi: 10.1016/j.jpowsour.2005.01.006.

[11]   P. Keil and A. Jossen, "Charging protocols for lithium-ion batteries and their impact on cycle life-An experimental study with different 18650 high-power cells," *J. Energy Storage*, vol. 6, pp. 125–141, 2016, doi: 10.1016/j.est.2016.02.005.

[12]   G. Sikha, P. Ramadass, B. S. Haran, R. E. White, and B. N. Popov, "Comparison of the capacity fade of Sony US 18650 cells charged with different protocols," *J. Power Sources*, vol. 122, no. 1, pp. 67–76, 2003, doi: 10.1016/S0378-7753(03)00027-2.

[13]   P. H. L. Notten, J. H. G. O. H. Veld, and J. R. G. Van Beek, "Boostcharging Li-ion batteries: A challenging new charging concept," *J. Power Sources*, vol. 145, no. 1, pp. 89–94, 2005, doi: 10.1016/j.jpowsour.2004.12.038.

[14]   M. Ye, H. Gong, R. Xiong, and H. Mu, "Research on the Battery Charging Strategy with Charging and Temperature Rising Control Awareness," *IEEE Access*, vol. 6, pp. 64193–64201, 2018, doi: 10.1109/ACCESS.2018.2876359.

[15]   C. L. Liu, S. C. Wang, Y. H. Liu, and M. C. Tsai, "An optimum fast charging pattern search for Li-ion batteries using particle swarm optimization," *6th Int. Conf. Soft Comput. Intell. Syst. 13th Int. Symp. Adv. Intell. Syst. SCIS/ISIS 2012*, pp. 727–732, 2012, doi: 10.1109/SCIS-ISIS.2012.6505335.

[16]   S. C. Wang and Y. H. Liu, "A PSO-Based Fuzzy-Controlled Searching for the Optimal Charge Pattern of Li-Ion Batteries," *IEEE Trans. Ind. Electron.*,

vol. 62, no. 5, pp. 2983–2993, 2015, doi: 10.1109/TIE.2014.2363049.

[17] Y. F. Luo, Y. H. Liu, and S. C. Wang, "Search for an optimal rapid-charging pattern for li-ion batteries using the Taguchi approach," *IEEE Trans. Ind. Electron.*, vol. 57, no. 12, pp. 3963–3971, 2010, doi: 10.1109/TIE.2009.2036020.

[18] T. Ikeya *et al.*, "Multi-step constant-current charging method for an electric vehicle nickel/metal hydride battery with high-energy efficiency and long cycle life," *J. Power Sources*, vol. 105, no. 1, pp. 6–12, 2002, doi: 10.1016/S0378-7753(01)00907-7.

[19] R. Velho, M. Beirão, M. Do Rosário Calado, J. Pombo, J. Fermeiro, and S. Mariano, "Management system for large li-ion battery packs with a new adaptive multistage charging method," *Energies*, vol. 10, no. 5, 2017, doi: 10.3390/en10050605.

[20] Y. H. Liu, C. H. Hsieh, and Y. F. Luo, "Search for an optimal five-step charging pattern for li-ion batteries using consecutive orthogonal arrays," *IEEE Trans. Energy Convers.*, vol. 26, no. 2, pp. 654–661, 2011, doi: 10.1109/TEC.2010.2103077.

[21] D. Anseán, M. González, J. C. Viera, V. M. García, C. Blanco, and M. Valledor, "Fast charging technique for high power lithium iron phosphate batteries: A cycle life analysis," *J. Power Sources*, vol. 239, pp. 9–15, 2013, doi: 10.1016/j.jpowsour.2013.03.044.

[22] Y. Ji and C. Y. Wang, "Heating strategies for Li-ion batteries operated from subzero temperatures," *Electrochim. Acta*, vol. 107, pp. 664–674, 2013, doi: 10.1016/j.electacta.2013.03.147.

[23] J. Li, E. Murphy, J. Winnick, and P. A. Kohl, "The effects of pulse charging on cycling characteristics of commercial lithium-ion batteries," *J. Power Sources*, vol. 102, no. 1–2, pp. 302–309, 2001, doi: 10.1016/S0378-7753(01)00820-5.

[24] M. Abdel Monem *et al.*, "Lithium-ion batteries: Evaluation study of different charging methodologies based on aging process," *Appl. Energy*, vol. 152, pp. 143–155, 2015, doi: 10.1016/j.apenergy.2015.02.064.

[25] M. Abdel-Monem, K. Trad, N. Omar, O. Hegazy, P. Van den Bossche, and J. Van Mierlo, "Influence analysis of static and dynamic fast-charging current profiles on ageing performance of commercial lithium-ion batteries," *Energy*, vol. 120, no. 2017, pp. 179–191, 2017, doi: 10.1016/j.energy.2016.12.110.

[26] F. Savoye, P. Venet, M. Millet, and J. Groot, "Impact of Periodic Current Pulses on Li-Ion Battery Performance," *IEEE Trans. Ind. Electron.*, vol. 59, no. 9, pp. 3481–3488, 2012, doi: 10.1109/TIE.2011.2172172.

[27] S. S. Zhang, "The effect of the charging protocol on the cycle life of a Li-ion battery," *J. Power Sources*, vol. 161, no. 2, pp. 1385–1391, Oct. 2006, doi: 10.1016/j.jpowsour.2006.06.040.

[28] L. Patnaik, A. V. J. S. Praneeth, and S. S. Williamson, "A Closed-Loop Constant-Temperature Constant-Voltage Charging Technique to Reduce Charge Time of Lithium-Ion Batteries," *IEEE Trans. Ind. Electron.*, vol. 66, no. 2, pp. 1059–1067, 2019, doi: 10.1109/TIE.2018.2833038.

[29] Z. Guo, B. Y. Liaw, X. Qiu, L. Gao, and C. Zhang, "Optimal charging method for lithium ion batteries using a universal voltage protocol accommodating aging," *J. Power Sources*, vol. 274, pp. 957–964, 2015, doi: 10.1016/j.jpowsour.2014.10.185.

[30] L. R. Chen, "A design of an optimal battery pulse charge system by frequency-varied technique," *IEEE Trans. Ind. Electron.*, vol. 54, no. 1, pp. 398–405, 2007, doi: 10.1109/TIE.2006.888796.

[31] L. R. Chen, "Design of duty-varied voltage pulse charger for improving Li-ion battery-charging response," *IEEE Trans. Ind. Electron.*, vol. 56, no. 2, pp. 480–487, 2009, doi: 10.1109/TIE.2008.2002725.

[32]   U. R. Koleti, T. N. M. Bui, T. Q. Dinh, and J. Marco, "The Development of Optimal Charging Protocols for Lithium-Ion Batteries to Reduce Lithium Plating," *J. Energy Storage*, vol. 39, no. September 2020, 2021, doi: 10.1016/j.est.2021.102573.

[33]   S. Schindler, M. Bauer, H. Cheetamun, and M. A. Danzer, "Fast charging of lithium-ion cells: Identification of aging-minimal current profiles using a design of experiment approach and a mechanistic degradation analysis," *J. Energy Storage*, vol. 19, no. March, pp. 364–378, 2018, doi: 10.1016/j.est.2018.08.002.

[34]   S. Hein and A. Latz, "Influence of local lithium metal deposition in 3D microstructures on local and global behavior of Lithium-ion batteries," *Electrochim. Acta*, vol. 201, pp. 354–365, 2016, doi: 10.1016/j.electacta.2016.01.220.

[35]   S. K. Chung, A. A. Andriiko, A. P. Mon'Ko, and S. H. Lee, "On charge conditions for Li-ion and other secondary lithium batteries with solid intercalation electrodes," *J. Power Sources*, vol. 79, no. 2, pp. 205–211, 1999, doi: 10.1016/S0378-7753(99)00058-0.

[36]   L. R. Chen, S. L. Wu, D. T. Shieh, and T. R. Chen, "Sinusoidal-ripple-current charging strategy and optimal charging frequency study for Li-ion batteries," *IEEE Trans. Ind. Electron.*, vol. 60, no. 1, pp. 88–97, 2013, doi: 10.1109/TIE.2012.2186106.

[37]   N. Noura, L. Boulon, and S. Jemeï, "A Review of Battery State of Health Estimation Methods : Hybrid Electric Vehicle Challenges," *World Electr. Veh. J.*, vol. 11, no. 66, 2020, doi: 10.3390/wevj11040066.

[38]   Y. Zheng, M. Ouyang, X. Han, L. Lu, and J. Li, "Investigating the error sources of the online state of charge estimation methods for lithium-ion batteries in electric vehicles," *J. Power Sources*, vol. 377, no. October 2017, pp. 161–188, 2018, doi: 10.1016/j.jpowsour.2017.11.094.

[39] H. H. Afshari, S. A. Gadsden, and S. Habibi, "Gaussian filters for parameter and state estimation: A general review of theory and recent trends," *Signal Processing*, vol. 135, no. December 2016, pp. 218–238, 2017, doi: 10.1016/j.sigpro.2017.01.001.

[40] C. Vidal, P. Malysz, P. Kollmeyer, and A. Emadi, "Machine Learning Applied to Electrified Vehicle Battery State of Charge and State of Health Estimation: State-of-the-Art," *IEEE Access*, vol. 8, pp. 52796–52814, 2020, doi: 10.1109/ACCESS.2020.2980961.

[41] M. Murnane and A. Ghazel, "A Closer Look at State of Charge (SOC) and State of Health (SOH) Estimation Techniques for Batteries," *Analog devices*, 2017.

[42] W. Wang *et al.*, "Comparison of Kalman Filter-based state of charge estimation strategies for Li-Ion batteries," *2016 IEEE Transp. Electrif. Conf. Expo, ITEC 2016*, pp. 1–6, 2016, doi: 10.1109/ITEC.2016.7520302.

[43] C. J. Goncalves Vidal, "Deep Neural Networks for Improved Terminal Voltage and State-of-Charge Estimation of Lithium-Ion Batteries for Traction Applications," 2020.

[44] Y. Tian, R. Lai, X. Li, L. Xiang, and J. Tian, "A combined method for state-of-charge estimation for lithium-ion batteries using a long short-term memory network and an adaptive cubature Kalman filter," *Appl. Energy*, vol. 265, no. March, p. 114789, 2020, doi: 10.1016/j.apenergy.2020.114789.

[45] I. Jokić, Ž. Zečević, and B. Krstajić, "State-of-charge estimation of lithium-ion batteries using extended Kalman filter and unscented Kalman filter," *2018 23rd Int. Sci. Conf. Inf. Technol. IT 2018*, vol. 2018-Janua, pp. 1–4, 2018, doi: 10.1109/SPIT.2018.8350462.

[46] J. Luo, J. Peng, and H. He, "Lithium-ion battery SOC estimation study based on Cubature Kalman filter," *Energy Procedia*, vol. 158, pp. 3421–3426, 2019, doi: 10.1016/j.egypro.2019.01.933.

[47]   C. Vidal, P. Kollmeyer, E. Chemali, and A. Emadi, "Li-ion Battery State of Charge Estimation Using Long Short-Term Memory Recurrent Neural Network with Transfer Learning," in *2019 IEEE Transportation Electrification Conference and Expo (ITEC)*, 2019, vol. 8, pp. 1–6, doi: doi: 10.1109/ITEC.2019.8790543.

[48]   R. Xiong, H. He, F. Sun, and K. Zhao, "Evaluation on State of Charge estimation of batteries with adaptive extended kalman filter by experiment approach," *IEEE Trans. Veh. Technol.*, vol. 62, no. 1, pp. 108–117, 2013, doi: 10.1109/TVT.2012.2222684.

[49]   R. Xiong, F. Sun, and H. He, "State-of-Charge Estimation of the Lithium-Ion Battery Using an Adaptive Extended Kalman Filter Based on an Improved Thevenin Model Hongwen," *Gaojishu Tongxin/Chinese High Technol. Lett.*, vol. 22, no. 2, pp. 198–204, 2012, doi: 10.3772/j.issn.1002-0470.2012.02.014.

[50]   W. He, N. Williard, C. Chen, and M. Pecht, "State of charge estimation for electric vehicle batteries using unscented kalman filtering," *Microelectron. Reliab.*, vol. 53, no. 6, pp. 840–847, 2013, doi: 10.1016/j.microrel.2012.11.010.

[51]   T. Kim *et al.*, "Model-based condition monitoring for lithium-ion batteries," *J. Power Sources*, vol. 295, pp. 16–27, 2015, doi: 10.1016/j.jpowsour.2015.03.184.

[52]   S. R. H. Mohammed Farag , Mina Attari , S. Andrew Gadsden, "Lithium-Ion Battery State of Charge Estimation Using One State Hysteresis Model with Nonlinear Estimation Strategies," *Int. J. Chem. Mol. Nucl. Mater. Metall. Eng.*, vol. 11, no. 3, pp. 214–218, 2017.

[53]   K. Movassagh, A. Raihan, B. Balasingam, and K. Pattipati, "A Critical Look at Coulomb Counting Approach for State of Charge Estimation in Batteries," *Energies*, vol. 14, no. 1, p. 4074, 2021.

[54] M. Fleckenstein, O. Bohlen, M. A. Roscher, and B. Bäker, "Current density and state of charge inhomogeneities in Li-ion battery cells with LiFePO4 as cathode material due to temperature gradients," *J. Power Sources*, vol. 196, no. 10, pp. 4769–4778, 2011, doi: 10.1016/j.jpowsour.2011.01.043.

[55] R. Zhang *et al.*, "A study on the open circuit voltage and state of charge characterization of high capacity lithium-ion battery under different temperature," *Energies*, vol. 11, no. 9, 2018, doi: 10.3390/en11092408.

[56] Q. Q. Yu, R. Xiong, L. Y. Wang, and C. Lin, "A comparative study on open circuit voltage models for lithium-ion batteries," *Chinese J. Mech. Eng. (English Ed.*, vol. 31, no. 4, pp. 0–7, 2018, doi: 10.1186/s10033-018-0268-8.

[57] M. A. Roscher and D. U. Sauer, "Dynamic electric behavior and open-circuit-voltage modeling of LiFePO 4-based lithium ion secondary batteries," *J. Power Sources*, vol. 196, no. 1, pp. 331–336, 2011, doi: 10.1016/j.jpowsour.2010.06.098.

[58] Y. Zheng *et al.*, "Cell state-of-charge inconsistency estimation for LiFePO4 battery pack in hybrid electric vehicles using mean-difference model," *Appl. Energy*, vol. 111, pp. 571–580, 2013, doi: 10.1016/j.apenergy.2013.05.048.

[59] R. Zhang *et al.*, "State of the art of lithium-ion battery SOC estimation for electrical vehicles," *Energies*, vol. 11, no. 7, 2018, doi: 10.3390/en11071820.

[60] W. He, M. Pecht, D. Flynn, and F. Dinmohammadi, "A Physics-Based Electrochemical Model for Lithium- Ion Battery State-of-Charge Estimation Solved by an Optimised Projection-Based Method and Moving- Window Filtering," *Energies*, vol. 11, pp. 1–24, 2018, doi: 10.3390/en11082120.

[61] S. Nejad, D. T. Gladwin, and D. A. Stone, "A systematic review of lumped-parameter equivalent circuit models for real-time estimation of lithium-ion battery states," *J. Power Sources*, vol. 316, pp. 183–196, 2016, doi:

10.1016/j.jpowsour.2016.03.042.

[62] F. Sun, R. Xiong, and H. He, "A systematic state-of-charge estimation framework for multi-cell battery pack in electric vehicles using bias correction technique," *Appl. Energy*, vol. 162, pp. 1399–1409, 2016, doi: 10.1016/j.apenergy.2014.12.021.

[63] X. Hu, S. Li, and H. Peng, "A comparative study of equivalent circuit models for Li-ion batteries," *J. Power Sources*, vol. 198, no. January, pp. 359–367, 2012, doi: 10.1016/j.jpowsour.2011.10.013.

[64] R. E. Kalman, "A new approach to linear filtering and prediction problems," *J. Basic Eng. Trans. ASME*, vol. 82, no. 1, pp. 35–45, 1960, doi: 10.1115/1.3662552.

[65] S. R. Habibi and R. Burton, "The variable structure filter," *J. Dyn. Syst. Meas. Control. Trans. ASME*, vol. 125, no. 3, pp. 287–293, 2003, doi: 10.1115/1.1590682.

[66] S. A. Gadsden and S. R. Habibi, "A new robust filtering strategy for linear systems," *J. Dyn. Syst. Meas. Control. Trans. ASME*, vol. 135, no. 1, 2013, doi: 10.1115/1.4006628.

[67] S. J. Julier and J. K. Uhlmann, "Unscented Filtering and Nonlinear Estimation," *Proc. IEEE*, vol. 92, no. 12, p. 1958, 2004, doi: 10.1109/JPROC.2004.837637.

[68] I. Arasaratnam and S. Haykin, "Cubature kalman filters," *IEEE Trans. Automat. Contr.*, vol. 54, no. 6, pp. 1254–1269, 2009, doi: 10.1109/TAC.2009.2019800.

[69] I. Arasaratnam, S. Haykin, and R. J. Elliott, "Discrete-time nonlinear filtering algorithms using gauss-hermite quadrature," *Proc. IEEE*, vol. 95, no. 5, pp. 953–977, 2007, doi: 10.1109/JPROC.2007.894705.

[70] S. Sepasi, R. Ghorbani, and B. Y. Liaw, "A novel on-board state-of-charge

estimation method for aged Li-ion batteries based on model adaptive extended Kalman filter," *J. Power Sources*, vol. 245, pp. 337–344, 2014, doi: 10.1016/j.jpowsour.2013.06.108.

[71]   A. Rahimi, K. D. Kumar, and H. Alighanbari, "Enhanced adaptive unscented Kalman filter for reaction wheels," *IEEE Trans. Aerosp. Electron. Syst.*, vol. 51, no. 2, pp. 1568–1575, 2015, doi: 10.1109/TAES.2014.130766.

[72]   Z. Chen, Y. Fu, and C. C. Mi, "State of charge estimation of lithium-ion batteries in electric drive vehicles using extended Kalman filtering," *IEEE Trans. Veh. Technol.*, vol. 62, no. 3, pp. 1020–1030, 2013, doi: 10.1109/TVT.2012.2235474.

[73]   F. Orderud, "Comparison of kalman filter estimation approaches for state space models with nonlinear measurements," *... Scand. Conf. Simul. ...*, vol. 194, no. 7491, pp. 157–162, 2005, doi: 10.1109/ICCME.2010.5558873.

[74]   Z. Cai and D. Zhao, "The Unscented Kalman Filter for Nonlinear Estimation," *Geomatics Inf. Sci. Wuhan Univ.*, vol. 31, no. 2, pp. 180–183, 2006.

[75]   J. T. Ambadan and Y. Tang, "Sigma-point Kalman filter data assimilation methods for strongly nonlinear systems," *J. Atmos. Sci.*, vol. 66, no. 2, pp. 261–285, 2009, doi: 10.1175/2008JAS2681.1.

[76]   S. A. Gadsden, "Smooth Variable Structure Filtering: Theory and Applications," Ph.D dissertation, Dept. of Mech. Eng., McMaster University, Hamilton, ON, 2011.

[77]   S. Habibi, "The extended variable structure filter," *J. Dyn. Syst. Meas. Control. Trans. ASME*, vol. 128, no. 2, pp. 341–351, 2006, doi: 10.1115/1.2194070.

[78]   S. R. Habibi, "The Smooth Variable Structure Filter," *Proc. IEEE*, vol. 95, no. 5, pp. 1026–1059, 2007.

[79] M. S. Farag, R. Ahmed, S. A. Gadsden, S. R. Habibi, and J. Tjong, "A comparative study of Li-ion battery models and nonlinear dual estimation strategies," *2012 IEEE Transp. Electrif. Conf. Expo, ITEC 2012*, 2012, doi: 10.1109/ITEC.2012.6243485.

[80] R. Ahmed, S. Rahimifard, and S. Habibi, "Offline Parameter Identification and SOC Estimation for New and Aged Electric Vehicles Batteries," *ITEC 2019 - 2019 IEEE Transp. Electrif. Conf. Expo*, pp. 31–36, 2019, doi: 10.1109/ITEC.2019.8790474.

[81] M. A. Hannan, M. S. H. Lipu, A. Hussain, and A. Mohamed, "A review of lithium-ion battery state of charge estimation and management system in electric vehicle applications: Challenges and recommendations," *Renew. Sustain. Energy Rev.*, vol. 78, no. August 2016, pp. 834–854, 2017, doi: 10.1016/j.rser.2017.05.001.

[82] G. Zames, "Feedback and Optimal Sensitivity: Model Reference Transformations, Multiplicative Seminorms, and Approximate Inverses," *IEEE Trans. Automat. Contr.*, vol. 26, no. 2, pp. 301–320, 1981, doi: 10.1109/TAC.1981.1102603.

[83] T. R. B. Grandjean, J. Groenewald, A. McGordon, W. D. Widanage, and J. Marco, "Accelerated internal resistance measurements of lithium-ion cells to support future end-of-life strategies for electric vehicles," *Batteries*, vol. 4, no. 49, 2018, doi: 10.3390/batteries4040049.

[84] D. Strickland, L. Chittock, D. A. Stone, M. P. Foster, and B. Price, "Estimation of transportation battery second life for use in electricity grid systems," *IEEE Trans. Sustain. Energy*, vol. 5, no. 3, pp. 795–803, 2014, doi: 10.1109/TSTE.2014.2303572.

[85] M. Chen *et al.*, "Recycling End-of-Life Electric Vehicle Lithium-Ion Batteries," *Joule*, vol. 3, no. 11, pp. 2622–2646, 2019, doi: 10.1016/j.joule.2019.09.014.

[86] K. Yang, Y. Tang, and Z. Zhang, "Parameter identification and state-of-charge estimation for lithium-ion batteries using separated time scales and extended kalman filter," *Energies*, vol. 14, no. 4, 2021, doi: 10.3390/en14041054.

[87] L. Rozaqi, E. Rijanto, and S. Kanarachos, "Comparison between RLS-GA and RLS-PSO for Li-ion battery SOC and SOH estimation: a simulation study," *J. Mechatronics, Electr. Power, Veh. Technol.*, vol. 8, no. 1, pp. 40–49, 2017, doi: 10.14203/j.mev.2017.v8.40-49.

[88] E. Rijanto, L. Rozaqi, A. Nugroho, and S. Kanarachos, "RLS with Optimum Multiple Adaptive Forgetting Factors for SoC and SoH Estimation of Li-Ion Battery," *Proc. 2017 5th Int. Conf. Instrumentation, Control. Autom. ICA 2017*, pp. 73–77, 2017, doi: 10.1109/ICA.2017.8068416.

[89] S. Rahimifard, S. Habibi, and J. Tjong, "Dual Estimation Strategy for New and Aged Electric Vehicles Batteries," pp. 579–583, 2020, doi: 10.1109/itec48692.2020.9161556.

[90] H. He, R. Xiong, H. Guo, and S. Li, "Comparison study on the battery models used for the energy management of batteries in electric vehicles," *Energy Convers. Manag.*, vol. 64, pp. 113–121, 2012, doi: 10.1016/j.enconman.2012.04.014.

[91] X. Sun, J. Ji, B. Ren, C. Xie, and D. Yan, "Adaptive forgetting factor recursive least square algorithm for online identification of equivalent circuit model parameters of a lithium-ion battery," *Energies*, vol. 12, no. 11, 2019, doi: 10.3390/en12122242.

[92] N. Wassiliadis *et al.*, "Revisiting the dual extended Kalman filter for battery state-of-charge and state-of-health estimation: A use-case life cycle analysis," *J. Energy Storage*, vol. 19, no. June, pp. 73–87, 2018, doi: 10.1016/j.est.2018.07.006.

[93] Y. Zheng, F. He, and W. Wang, "SOC Estimation of Lithium Battery Based

on Dual Adaptive Extended Kalman Filter," *IOP Conf. Ser. Mater. Sci. Eng.*, vol. 677, no. 3, 2019, doi: 10.1088/1757-899X/677/3/032077.

[94] S. Yang *et al.*, "A parameter adaptive method for state of charge estimation of lithium-ion batteries with an improved extended Kalman filter," *Sci. Rep.*, vol. 11, no. 1, pp. 1–15, 2021, doi: 10.1038/s41598-021-84729-1.

[95] L. Fang, J. Li, and B. Peng, "Online estimation and error analysis of both SOC and SOH of lithium-ion battery based on DEKF method," *Energy Procedia*, vol. 158, pp. 3008–3013, 2019, doi: 10.1016/j.egypro.2019.01.974.

[96] H. H. Afshari, M. Attari, R. Ahmed, A. Delbari, S. Habibi, and T. Shoa, "Reliable state of charge and state of health estimation using the smooth variable structure filter," *Control Eng. Pract.*, vol. 77, pp. 1–14, 2018, doi: 10.1016/j.conengprac.2018.04.015.

[97] S.-H. Jeong, "Specification of product for Lithium-ion rechargeable cell Model name : INR21700-30T," 2017.

[98] U. S. D. of E. V. T. Program, "United States Advanced Battery Consortium Battery Test Manual For Electric Vehicles," *Contract*, no. June, 2015, doi: uscar.org/commands/files_download. php?files_id=405.

[99] A. Shafiei, A. Momeni, and S. S. Williamson, "Battery modeling approaches and management techniques for plug-in hybrid electric vehicles," *2011 IEEE Veh. Power Propuls. Conf. VPPC 2011*, pp. 1–5, 2011, doi: 10.1109/VPPC.2011.6043191.

[100] M. S. Farag, "Lithium-Ion Batteries: Modelling and State of Charge Estimation," M.S. thesis, Dept. of Mech. Eng., McMaster University, Hamilton, ON, 2013.

[101] J. Gazzarri, "Battery Modeling," 2021. [Online]. Available: https://www.mathworks.com/matlabcentral/fileexchange/36019-battery-modeling. [Accessed: 08-Oct-2021].

[102] P. Kollmeyer and M. Skells, "Samsung INR21700 30T 3Ah Li-ion Battery Data," *Mendeley Data*, 2020, doi: 10.17632/9xyvy2njj3.1.

[103] C. R. Birkl, M. R. Roberts, E. Mcturk, P. G. Bruce, and D. A. Howey, "Degradation diagnostics for lithium ion cells," *J. Power Sources*, vol. 341, pp. 373–386, 2017, doi: 10.1016/j.jpowsour.2016.12.011.

[104] C. Weng, Y. Cui, J. Sun, and H. Peng, "On-board state of health monitoring of lithium-ion batteries using incremental capacity analysis with support vector regression," *J. Power Sources*, vol. 235, pp. 36–44, 2013, doi: 10.1016/j.jpowsour.2013.02.012.

[105] A. Hauser and R. Kuhn, "High-voltage battery management systems (BMS) for electric vehicles," in *Advances in Battery Technologies for Electric Vehicles*, Elsevier Ltd., 2015, pp. 265–282.

[106] S. Li *et al.*, "Effects of pulse charging on the performances of lithium-ion batteries," *Nano Energy*, vol. 56, no. 30, pp. 555–562, 2019, doi: 10.1016/j.nanoen.2018.11.070.

[107] M. Klett *et al.*, "Non-uniform aging of cycled commercial LiFePO4//graphite cylindrical cells revealed by post-mortem analysis," *J. Power Sources*, vol. 257, pp. 126–137, 2014, doi: 10.1016/j.jpowsour.2014.01.105.

[108] S. F. Schuster *et al.*, "Nonlinear aging characteristics of lithium-ion cells under different operational conditions," *J. Energy Storage*, vol. 1, no. 1, pp. 44–53, 2015, doi: 10.1016/j.est.2015.05.003.